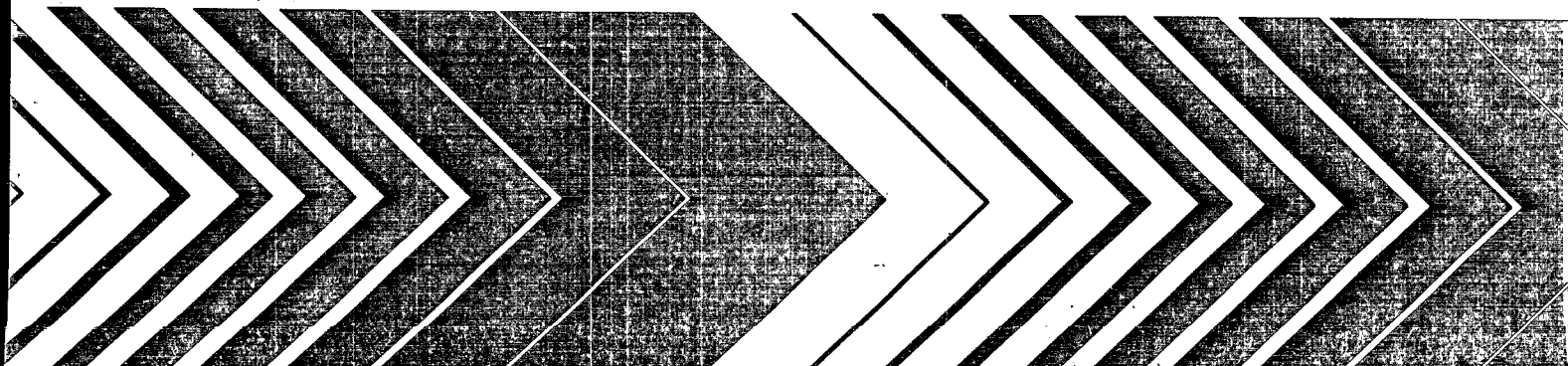




Preparation and Evaluation of Powdered Activated Carbon from Lignocellulosic Materials



RESEARCH REPORTING SERIES

Research reports of the Office of Research and Development, U.S. Environmental Protection Agency, have been grouped into nine series. These nine broad categories were established to facilitate further development and application of environmental technology. Elimination of traditional grouping was consciously planned to foster technology transfer and a maximum interface in related fields. The nine series are:

1. Environmental Health Effects Research
2. Environmental Protection Technology
3. Ecological Research
4. Environmental Monitoring
5. Socioeconomic Environmental Studies
6. Scientific and Technical Assessment Reports (STAR)
7. Interagency Energy-Environment Research and Development
8. "Special" Reports
9. Miscellaneous Reports

This report has been assigned to the ENVIRONMENTAL PROTECTION TECHNOLOGY series. This series describes research performed to develop and demonstrate instrumentation, equipment, and methodology to repair or prevent environmental degradation from point and non-point sources of pollution. This work provides the new or improved technology required for the control and treatment of pollution sources to meet environmental quality standards.

EPA-600/2-80-123
August 1980

PREPARATION AND EVALUATION OF POWDERED ACTIVATED CARBON
FROM LIGNOCELLULOSIC MATERIALS

by

Paul V. Roberts, Douglas M. Mackay, and Fred S. Cannon
Department of Civil Engineering
Stanford University
Stanford, California 94305

Grant No. EPA-R-803188

Project Officer

Richard Dobbs
Wastewater Research Division
Municipal Environmental Research Laboratory
Cincinnati, Ohio 45268

MUNICIPAL ENVIRONMENTAL RESEARCH LABORATORY
OFFICE OF RESEARCH AND DEVELOPMENT
U.S. ENVIRONMENTAL PROTECTION AGENCY
CINCINNATI, OHIO 45268

DISCLAIMER

This report has been reviewed by the Municipal Environmental Research Laboratory, U.S. Environmental Protection Agency, and approved for publication. Approval does not signify that the contents necessarily reflect the views and policies of the U.S. Environmental Protection Agency, nor does mention of trade names or commercial products constitute endorsement or recommendation for use.

FOREWORD

The U.S. Environmental Protection Agency was created because of increasing public and government concern about the dangers of pollution to the health and welfare of the American people. Noxious air, foul water, and spoiled land are tragic testimonies to the deterioration of our natural environment. The complexity of that environment and the interplay of its components require a concentrated and integrated attack on the problem.

Research and development is that necessary first step in problem solution; it involves defining the problem, measuring its impact, and searching for solutions. The Municipal Environmental Research Laboratory develops new and improved technology and systems to prevent, treat, and manage wastewater and solid and hazardous waste pollutant discharges from municipal and community sources, to preserve and treat public drinking water supplies, and to minimize the adverse economic, social, health, and aesthetic effects of pollution. This publication is one of the products of that research and provides a most vital communications link between the researcher and the user community.

The project reported here evaluated the technical feasibility of converting a solid waste (prune pits) into adsorbents suitable for wastewater treatment.

Francis T. Mayo, Director
Municipal Environmental Research
Laboratory

ABSTRACT

This research project was conceived as a preliminary evaluation of the technical feasibility of converting solid wastes into adsorbents suitable for wastewater treatment. The work emphasized the pyrolysis of solid wastes rich in organic constituents, mainly agricultural wastes. The char prepared from one of these materials (prune pits) was subsequently activated for comparison with activated carbons that are widely used in water and wastewater treatment. Experiments were conducted in laboratory equipment using milligram quantities of solids.

The char yield from pyrolysis depends on educt composition, temperature and heating rate. For a given pyrolysis temperature, maximum char yield is attained with educts of high lignin content and low heating rates.

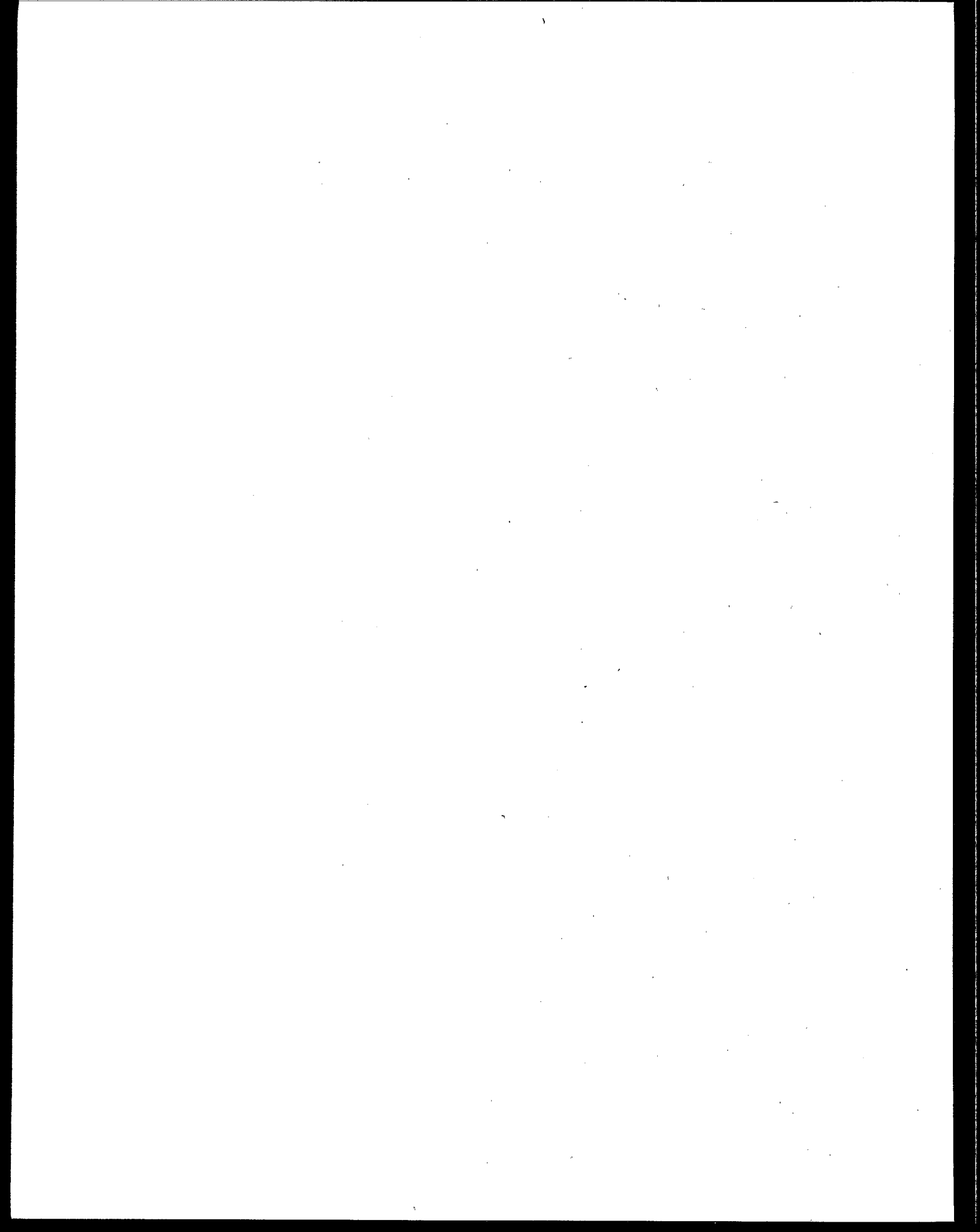
The chars so prepared showed specific surface areas of 300 to 650 m²/g, measured by CO₂ adsorption (195K), but the pores were so small that the solids were penetrated only slowly by N₂. Activation with CO₂ at 900°C for 30 to 60 min greatly increased the specific surface area, the pore volume, and the size of pores. Activated carbon prepared by exposing prune pit chars to an atmosphere of CO₂ at 900°C for 30, 42, and 60 min had surface areas of 930, 1180, and 1690 m²/g (N₂, 77K), respectively.

The activated carbons made from prune pits demonstrated favorable adsorption performance when compared with an activated carbon widely used in water and wastewater treatment. The prune pit char activated at 60 min demonstrated a higher adsorption capacity and superior adsorption kinetics than did a ground commercial product (Filtrisorb 400), when judged according to the uptake of dissolved organic carbon (DOC) from secondary effluent. An adsorbent made by activation of prune pit char for 42 min was approximately equivalent to Filtrisorb 400 in every respect: specific surface, pore size distribution, adsorption capacity, and adsorption rate.

The uptake of DOC from secondary effluent by powdered activated carbon behaved according to a model that assumes linear equilibrium and rate control by pore diffusion. The apparent diffusivities estimated from the uptake rate were in the range of 1×10^{-10} to 3×10^{-10} m²/s, conforming to expectations based on molecular diffusion of organic substances of the sort expected in secondary effluent.

Samples of refuse-derived fuel (a shredded, organic-rich fraction of municipal solid waste) were pyrolyzed and activated under the same conditions as for prune pits. The specific surface area of the activated material from refuse-derived fuel was only one-fourth that of the corresponding material from prune pits.

This report was submitted in fulfillment of Grant No. R-803188 by the Department of Civil Engineering, Stanford University, under the sponsorship of the U.S. Environmental Protection Agency. This report covers the period 1 November 1976 to 29 October 1979, and work was completed 29 October 1979.



CONTENTS

Foreword	iii
Abstract	iv
Figures	ix
Tables	xi
Acknowledgments	xiii
 1. Introduction	 1
Statement of the Problem	1
Objectives	1
Research Approach	2
2. Conclusions	3
3. Recommendations	5
4. Physical Characterization and Preparation of Activated Carbon . .	7
Physical characterization	7
Pyrolysis	13
Activation	15
5. Measures of Sorption Performance	18
Equilibrium isotherms	18
Kinetics of adsorption	20
Adsorption of organics from wastewater effluent	22
6. Materials and Methods	24
Cellulose	24
Lignocellulosic materials	24
Refuse-derived fuel	25
Materials preparation	25

CONTENTS (continued)

6. (cont.)	
Raw materials analysis	26
Pyrolysis	29
Activation	31
Characterization of char and activated carbon	33
Measuring adsorption of organics from wastewater	34
7. Results and Discussion	37
Pyrolysis of lignocellulosics and refuse-derived fuel	37
Activation of lignocellulosics and refuse-derived fuel	56
Sorption properties of activated lignocellulosics	76
Summary	92
References	93
Appendices	
A. Use of Linear Regressions for Data Plotting	101
B. Mercury Porosimetry Measurements	107
C. DOC Rate of Adsorption Experiments	115
D. Freundlich Isotherm Coefficients	118
E. Linear Isotherms for F400 for Various Experiments	119
F. Roots of $\tan q_n$ in Analytic Solution to Diffusivity	121
G. Computation of Diffusion Coefficients	122

FIGURES

<u>Number</u>		<u>Page</u>
1	Schematic of pyrolysis equipment	30
2	Schematic of activation equipment	32
3	Measured yield versus yield predicted by char yield model for pyrolysis at 15°C/min to 500°C	43
4	Ash-free char yield versus final temperature: low and medium heating rates	49
5	Ash-free char yield versus final temperature: high heating rates .	50
6	Carbon yield versus final temperature	51
7	Ash-free yield versus heating rate	53
8	Surface area of char versus final temperature	57
9	Surface area per gram carbon versus final temperature	58
10	Surface area per gram educt versus final temperature	59
11	Mass loss versus activation time for prune pit char	61
12	Nitrogen isotherms for 60M, 42M, 30M, 15M, and F400	63
13	Nitrogen isotherms for F400, F100, and AN-A	64
14	N ₂ -BET specific surface area versus percent mass loss for activated prune pit chars	67
15	Mercury porosimetry: cumulative penetration volume versus pore diameter for 60M	68
16	Mercury porosimetry: relative cumulative pore volume of mercury penetration versus equivalent pore radius for 60M, 42M, 30M, 15M and CHAR	69
17	Mercury porosimetry: relative cumulative pore volume of mercury penetration versus equivalent pore radius for F400, F100, and AN-A	71
18	Pore volume versus pore radius as determined by N ₂ -adsorption isotherms and mercury porosimetry for 60M, 42M, 30M, 15M, and F400	72
19	Pore volume versus pore radius as determined by N ₂ -adsorption isotherms and mercury porosimetry for F400, F100, and AN-A . . .	73
20	Kinetics of DOC adsorption for F400, F100, and AN-A (run 2) . . .	78

FIGURES (continued)

<u>Number</u>		<u>Page</u>
21	Kinetics of DOC adsorption for 60M, 42M, 30M, and F400 (average of runs 4 and 11)	79
22	DOC adsorption isotherms for 60M, 42M, 30M, and F400 (run 8) . . .	81
23	Γ_e versus C_e for DOC adsorption for 60M, 42M, 30M, and F400 (run 8)	84
24	Pore diffusion model for kinetics of DOC adsorption by 60M, 42M, 30M, and F400	89
A-1	Ash-free char yield versus final temperature: low and medium heating rates	102
A-2	Ash-free char yield versus final temperature: high heating rates .	103
A-3	Linearity of the plots of ash-free yield versus final temperature for pyrolysis at 15°C/min	104
A-4	Linearity of the plots of ash-free yield versus final temperature for pyrolysis at 1°C/min	105
B-1	Mercury porosimetry: cumulative penetration volume for 42M . . .	108
B-2	Mercury porosimetry: cumulative penetration volume for 30M . . .	109
B-3	Mercury porosimetry: cumulative penetration volume for 15M . . .	110
B-4	Mercury porosimetry: cumulative penetration volume for CHAR . . .	111
B-5	Mercury porosimetry: cumulative penetration volume for F400 . . .	112
B-6	Mercury porosimetry: cumulative penetration volume for F100 . . .	113
B-7	Mercury porosimetry: cumulative penetration volume for AN-A . . .	114
C-1	Kinetics of DOC adsorption for 60M, 42M, 30M, and F400 (run 4) . .	116
C-2	Kinetics of DOC adsorption for 60M, 42M, 30M, and F400 (run 11) .	117
E-1	Linear DOC adsorption isotherms for F400 for runs 6 and 8	120

TABLES

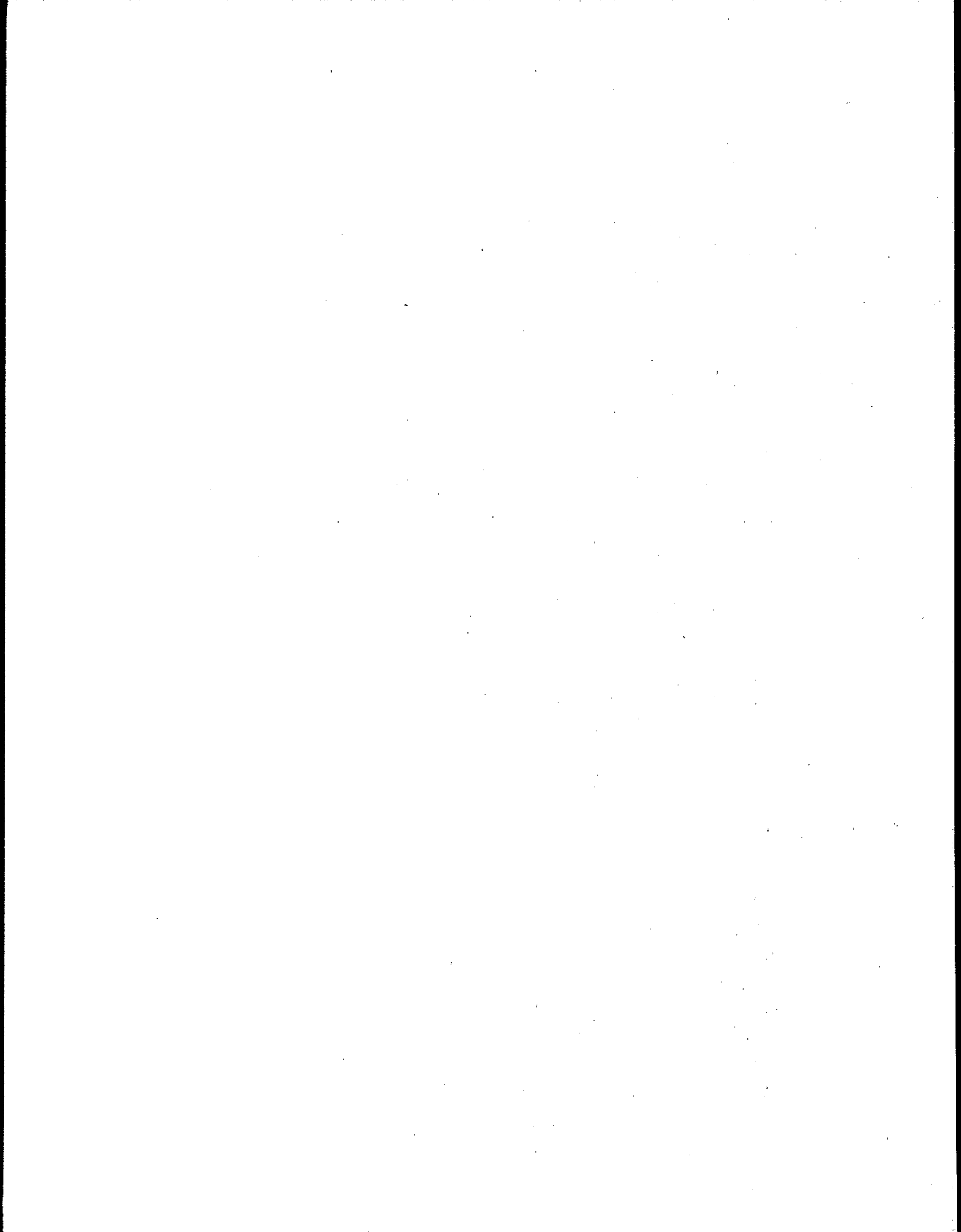
<u>Number</u>		<u>Page</u>
1	Summary of Lignocellulosic Composition and Char Yield Pyrolysis Conducted at 15°C/Min to 500°C	38
2	Summary of Results of Multiple Regressions Varying the Data Utilized and the Inorganic Parameter in the Power Function . . .	40
3	Composition and Char Yield of Refuse-Derived Fuel (RDF)	42
4	Summary of Pyrolysis of Selected Lignocellulosics for Varying Pyrolysis Conditions	45
5	Dependence of Ash Content Observed upon Ignition to Varying Final Temperatures	47
6	Carbon Content and Carbon Yield for Varying Pyrolysis Conditions	48
7	Linear Regressions of Ash-Free Char Yield versus Heating Rate or ln(Heating Rate) for Pyrolysis to Final Temperature T_F	52
8	Summary of Surface Area Analyses on Selected Lignocellulosic Chars	55
9	Physical Properties of Activated Prune Pit Char and Several Commercial Activated Carbons	62
10	Relation Between Surface Area and Burnoff for Chars Activated for 15 Min	65
11	Comparison of Pore Volumes Determined by N_2 -Isotherms and Mercury Porosimetry for 60M, 42M, 30M, 15M, and F400	70
12	Comparison of Activation of Prune Pit Char and RDF Char	75
13	Linear Adsorption Isotherm Coefficients	82
14	Estimation of the Partition Parameter R	87
15	Median Diffusion Coefficient and Pore Volume	90
16	Estimated Diffusion Coefficients	91

TABLES (continued)

<u>Number</u>		<u>Page</u>
A-1	Summary of Linear Regressions of Ash-Free Char Yield versus Final Pyrolysis Temperature for Selected Lignocellulosics . . .	106
A-2	Summary of Linear Regressions of Carbon Yield versus Final Pyrolysis Temperature for Selected Lignocellulosics	106
D-1	Freundlich Isotherm Coefficients	118
F-1	Roots of $\tan q_n = 3q_n / (3 + \alpha q_n^2)$	121
G-1	Computation of Diffusion Coefficients for 60M, 42M, 30M, F400 . .	122
G-2	Computation for Pore Diffusion Model Based on an Assumed Median D for 60M, 42M, 30M, F400	123

ACKNOWLEDGMENTS

The authors are grateful to Dr. Paul H. Brunner, who provided valuable guidance on pyrolysis and on the use of gas adsorption techniques to characterize porous solids. Sam Luoma, U.S. Geological Survey, Menlo Park, Calif., kindly permitted the use of a carbon analyzer in his laboratory. Professor James O. Leckie of Stanford University was instrumental in establishing the project's direction at the outset.



SECTION 1

INTRODUCTION

STATEMENT OF THE PROBLEM

Solid waste management has become a national problem of prodigious proportions. Historically the primary objective of solid waste management has been disposal, while minimizing damage to the environment. However, the cost of traditional disposal methods is now rising rapidly, while satisfactory disposal sites are becoming more scarce. Thus there is widespread interest in methods of solid waste management that will result in volume reduction, reuse of materials, or both.

Agricultural wastes, some industrial wastes, and the major organic fraction of municipal solid waste are composed of natural or modified plant tissue (lignocellulose). Awareness of the large potential of such materials as a source of energy and raw materials has aroused interest in the physical and chemical processing of lignocellulosic wastes. Pyrolytic processes, in particular, appear to offer the combined benefits of reducing the solid waste volume, minimizing pollutant emissions, and producing valuable products such as gaseous and liquid fuels and a solid, carbonaceous char.

Recently such pyrolytic chars have been considered as possible source materials for production of adsorbents for water and wastewater treatment. The economic viability of powdered activated carbon processes for municipal wastewater treatment may depend on the availability of an inexpensive, one-use adsorbent. Additionally, the proposed Environmental Protection Agency regulations for water quality control regarding organic pollutants encourage the use of adsorption processes to meet these standards, thereby creating a large need for activated carbon or similar adsorbents. Conceivably, this potential market could be supplied by the conversion of abundant lignocellulosic wastes into inexpensive activated carbon with suitable adsorptive properties.

OBJECTIVES

The objectives of this study were to:

1. Determine the effect of lignocellulosic composition and pyrolysis conditions on the yield and surface physical properties of pyrolytic char.
2. Ascertain the yield and properties of activated carbon prepared by activation of a lignocellulosic char.

3. Determine the usefulness of data obtained from experiments with lignocellulosic substances for understanding the pyrolysis and activation of municipal solid waste.
4. Compare activated carbons prepared from lignocellulosic waste with commercially available activated carbons according to surface physical characteristics (e.g. surface area), sorptive capacity, and the kinetics of the uptake of organic carbon from secondary effluent.

RESEARCH APPROACH

The study of pyrolysis was conducted with a wide range of materials representative of solid wastes of agricultural, forest product, industrial, and municipal waste origin. The activation studies were performed on a char prepared from a specific lignocellulosic material (prune pits), as well as classified municipal solid waste. Pyrolysis and activation were performed in small-scale laboratory equipment to ensure controllable, well-defined conditions.

The adsorption comparisons of waste-derived and commercial activated carbons were conducted in small-scale laboratory apparatus using filter-sterilized, unchlorinated secondary effluent from a local municipal wastewater treatment facility. Comparisons were made on the basis of adsorption equilibrium capacity for and kinetics of removal of dissolved organic carbon (DOC). Results of these adsorption experiments were interpreted in terms of simple models for adsorption and transport.

SECTION 2

CONCLUSIONS

The yield of char from pyrolysis of lignocellulosic materials (agricultural wastes, paper, and modified cellulose) can be correlated with the initial composition. Data analysis by multiple linear regression reveals that the yield can be expressed as a linear combination of the contributions from the holocellulose, lignin, extractive, and ash fractions, with a correlation coefficient exceeding 0.99.

The char yield (mass basis) from lignin (50 to 55%) is higher than that from the other organic fractions: holocellulose (19%) and extractives (35 to 45%). The ash fraction appears to behave as an inert material during pyrolysis. No significant catalytic effect due to ash constituents was observed in pyrolysis of natural lignocellulosic materials.

The measured char yield from refuse-derived fuel (RDF, an air-classified, shredded municipal solid waste fraction) was 10% lower than the value predicted for its composition, based on the yield correlation for lignocellulosic materials (34.2% compared to a predicted value of 37.5% under the conditions studied). Adjustment for the plastic content of RDF reduced the difference between the measured and predicted values to less than 4%.

The char yield decreased approximately in linear dependence on the pyrolysis temperature (above 500°C) and on the logarithm of the heating rate.

The specific surface areas (CO_2 -BET, 195K) of chars from lignocellulosic materials ranged from 300 to 650 m^2 per g char. The specific surface of chars prepared from representative plant wastes, a paper product, and a purified cellulose were similar in magnitude and showed a similar dependence on pyrolysis temperature. After adjustment for carbon content, the values of specific surface (m^2 per gram carbon) for five lignocellulose-derived chars agreed within $\pm 15\%$. The specific surface of the char increased markedly (20 to 30%), when the pyrolysis temperature was raised from 500 to 700°C, but generally was not significantly higher at 900°C than at 700°C.

Activated carbon prepared by CO_2 activation of a char obtained from a representative lignocellulosic material (prune pits) had a specific surface area in the range commonly found for commercially available activated carbon products. The specific surface of activated carbon derived from prune pits was 660 to 1700 m^2/g (N_2 -BET, 77K) depending on the time of activation at 900°C (15 to 60 min).

Activation of the prune pit char for 42 to 60 min at 900°C resulted in an activated carbon with an N_2 -BET surface area greater than that of ground Filtrasorb 400, an activated carbon widely used for treatment of water and wastewater. The volumes and size distributions of pores in the range of 3 to 300 nm were virtually indistinguishable, when a highly activated carbon of lignocellulose origin (60 min activation time) was compared with the ground commercial product, Filtrasorb 400. Activation of prune pit char for 30 min at 900°C resulted in a product with surface area and pore size characteristics similar to Aqua-Nuchar A, a low-cost powdered activated carbon used in water treatment, but inferior to Filtrasorb 400.

Activated carbon prepared from refuse-derived fuel (RDF) had a specific surface less than half that of activated carbons derived from prune pits under similar conditions. This is largely explained by the high inorganic content of RDF.

Activated carbons derived from prune pits adsorbed substantial quantities of organic constituents (measured as DOC) from secondary effluent. The equilibrium adsorption capacity of prune-pit activated carbon depended strongly on the activation time; the DOC uptake capacity after 60 min activation was approximately 2.5 times greater than that after 42 min, and five times greater than after 30 min. The equilibrium capacity of Filtrasorb 400 was intermediate between those of prune pit carbons that had been activated for 42 and 60 min.

The adsorption equilibrium isotherms for DOC uptake from secondary effluent were approximately linear, after adjustment was made for a non-adsorbable fraction. The resulting partition coefficients lie in the range of 20,000 to 100,000 g DOC adsorbed per g DOC in solution within the adsorbent grains.

The apparent pore diffusion coefficients estimated for the prune-pit activated carbons were in the range of $1.1 \times 10^{-10} \text{ m}^2/\text{s}$ (30 min activation) to $3.2 \times 10^{-10} \text{ m}^2/\text{s}$ (60 min activation). The corresponding value for Filtrasorb 400— $1.4 \times 10^{-10} \text{ m}^2/\text{s}$ —fell within that range. The diffusion coefficients estimated from experimental data agree in order of magnitude with expectations based on molecular diffusivities. Accordingly, a simple pore diffusion model appears to explain the observed DOC uptake rates.

Powdered activated carbon prepared from lignocellulosic waste material (prune pits) compares favorably with commercially available activated carbon products as an adsorbent for removal of dissolved organic carbon from secondary effluent. In view of the similar properties and yields of chars prepared from a broad spectrum of lignocellulosic materials, it is possible that adsorbents useful for water and wastewater treatment could be produced from any of a wide variety of lignocellulosic solid wastes from agriculture and the forest products industry. Municipal solid waste appears less suitable as a raw material for activated carbon manufacture than are agricultural and wood wastes.

SECTION 3

RECOMMENDATIONS

In this work it has been shown that activated carbons prepared from an agricultural waste material can perform as effectively in removing organic constituents from wastewater effluent as do presently used, commercial activated carbon products. Hence, it seems justified to conduct further research and development directed toward: identifying and characterizing candidate raw materials, evaluating their availability, optimizing the conditions of pyrolysis and activation, understanding the effects of physical and surface chemical characteristics on adsorbent performance, verifying the validity of laboratory tests of adsorbent performance, and comparing the efficiency of waste-derived and conventional activated carbons for the removal of organic priority pollutants from water and wastewater.

Agricultural wastes constitute a solid waste management problem, but also a resource of lignocellulosic materials of high carbon content. If agricultural products such as grain are to be converted to liquid fuels using fermentation, large quantities of lignocellulosic wastes will result. The utilization of these solid wastes as pyrolysis feedstocks ought to be investigated. Activated carbon production is one promising pyrolysis alternative. The logistics and economics of such operations deserve evaluation.

Additional work is required to optimize the overall sequence of pyrolysis and activation. The approach in this study has been to optimize pyrolysis with the objective of maximizing the micropore volume of the char, while maintaining an acceptable char yield. In activation, only one activating atmosphere and one temperature were used. A parametric study of activation temperature and atmosphere may result in significant improvement in the yield and properties of activated carbon from solid wastes. Also, it is possible that the overall yield and the product properties could be improved by pyrolyzing under conditions less severe than needed to prepare a char having a maximum micropore volume. This approach merits further research.

The relation between an adsorbent's physical and chemical properties and its adsorption performance must be better understood if adsorbents prepared from a great number of candidate solid waste raw materials are to be screened intelligently. Basic questions relating to the interpretation of data from gas penetration and mercury porosimetry measurements need to be clarified before such information can be used with confidence.

From this work, it appears that a simple approach based on linear adsorption equilibrium, coupled with a transport model incorporating pore diffusion in spherical geometry, is sufficient to simulate the extent and rate of uptake

of dissolved organic carbon (DOC) from secondary effluent, if biodegradation is excluded. Because of the convenience afforded by this simple model, its general applicability to water and wastewater treatment should be investigated. If verified, the model would facilitate the computation of DOC removal in treatment processes.

In the light of increased concern about hazardous organic contaminants, solid-waste-derived activated carbons should be tested to ascertain their efficacy for adsorbing selected organic priority pollutants. Also, the leaching of priority pollutants (both inorganic and organic) from waste-derived activated carbons should be compared to that from currently marketed products.

SECTION 4

PHYSICAL CHARACTERIZATION AND PREPARATION OF ACTIVATED CARBON

Activated carbon is generally produced by a two-step process consisting of pyrolyzing (carbonizing) the source material under appropriate conditions and then activating the resultant pyrolytic char by oxidation in a controlled environment (1). The purpose of these processes is to yield a final product with extensive porosity and high adsorptive capacity. In this chapter we discuss pyrolysis, activation, and methods of characterization of the extent of porosity. Physical characterization will be discussed first to allow definition of terms used in subsequent sections.

PHYSICAL CHARACTERIZATION

The pores in chars and activated carbons vary in size from remnants of the tissue structure in the case of lignocellulosics (cell diameters range from 10-100 μm) to apertures which are inaccessible even to helium at room temperature (2,3,4). The volume which constitutes the internal pores of an adsorbent and is accessible from the exterior of the adsorbent particle is of prime interest in studies of sorptive capacity and behavior. A large pore volume does not necessarily imply a large pore surface area, because the specific surface area is dependent on the distribution of pore sizes (4); a preponderance of small pores is necessary to assure a large specific surface area. For porous adsorbents, the following classification of pore sizes is common (4,5):

Micropores	diameter < 2nm
Transitional-Pores	2 nm < diameter < 20nm
Macropores	20 nm < diameter

The methods used in this study to characterize the internal pore structure of chars and activated carbons are based on adsorption of gases and mercury penetration, discussed in detail below.

Gas Adsorption

Gas adsorption is a common technique for the estimation of surface area of porous materials and can also be used to estimate pore size distribution, at least for micro- and some transitional-porosity.

The gas adsorption analysis entails admitting the adsorbate gas to a sample of known weight, which has previously been completely freed of all adsorbed gases and vapors during an outgassing period (elevated temperature and high vacuum). In practice the gas is admitted in known incremental amounts, determined by allowing the gas to come to equilibrium in the

instrument manifold (known volume and temperature) and measuring the pressure. The number of moles of gas present is estimated by means of the ideal gas law. The gas is then allowed to expand into the previously evacuated sample container (the volume and temperature of the sample container are known). Some portion of the gas adsorbs onto the sample and eventually a new equilibrium pressure is reached. A material balance on the adsorbate using the gas law, with corrections for nonideality due to low sample temperature, allows the determination by difference of the number of moles of gas adsorbed by the solid sample. The procedure is repeated for increasing equilibrium pressures, generating the adsorption isotherm, or the amount of gas adsorbed (expressed as cm³ of gas (STP) per gram sample) as a function of equilibrium pressure.

The resultant adsorption isotherm must then be interpreted to yield estimates of sample surface area, pore size, and pore volume. The interpretive methods in common use are discussed separately below, followed by a discussion of two very important details of the analytical procedure: outgassing conditions and equilibrium time.

BET Surface Area--

This method is applicable to adsorption data from nitrogen at 77K and carbon dioxide at 195K. The method assumes layer-by-layer filling of the pores with the adsorbate gas. The sample surface area is calculated by determining the number of molecules of adsorbate necessary to produce a monomolecular layer on the sample, and multiplying that number by the cross sectional area assumed to be occupied by the adsorbed gas. The monolayer capacity is conventionally determined by the Brunauer-Emmett-Teller (BET) equation (4,6), used in the following form:

$$\frac{p}{V(p_s - p)} = \frac{1}{V_m C} + \frac{(C - 1)}{V_m C} \cdot \frac{p}{p_s} \quad (1)$$

where V = the volume adsorbed at equilibrium pressure p ,

p_s = the saturation pressure of the adsorbate at the adsorption temperature,

V_m = the monolayer capacity, and

C = a constant.

A plot of $p/V(p_s - p)$ versus p/p_s therefore should yield a straight line of slope $(C - 1)/V_m C$ and intercept $1/V_m C$. The range of relative pressure for which the plot is linear will vary with the material being analyzed (4); in general the linear range is $(0.05 < p/p_s < 0.35)$ (7).

The monolayer capacity is thus:

$$V_m = \frac{1}{\text{slope} + \text{intercept}} \quad (2)$$

Sample surface area is therefore given by the following expression

$$S = \frac{V_m N_A \sigma_a}{V^0} \quad (3)$$

where S = sample surface area (m^2/g),

V_m = monolayer volume at STP (cm^3/g sample),

σ_a = cross sectional area of adsorbed molecule ($\text{m}^2/\text{molecule}$),

V^0 = ideal gas molar volume at STP (cm^3/mole), and

N_A = Avogadro's number (molecules/mole).

The BET method was originally derived for non-porous or large-pore adsorbents. The method assumes that the surface is covered with energetically uniform sites, that only one molecule of adsorbate is adsorbed to each site, and that there is no interaction between adsorbed molecules (7). There is general agreement that these assumptions may not be valid for some adsorbate-adsorbent systems (4,5,7). In particular, the assumption of layer-by-layer adsorption is thought to be inapplicable to microporous adsorbents, such as pyrolytic chars and activated carbons, because the diameters of the pores (< 2 nm) are in the same order of magnitude as those of the adsorbing gas (e.g., about 0.5 nm for N_2 at 77K) (5,7,8). Dubinin (5) states that due to an adsorption force field in the entire volume of micropores, adsorption results in volume filling in the pores. Since this results in larger volumes of adsorbed gas for a given pressure than would be the case for monolayer adsorption, the BET method will calculate erroneously high values of "monolayer volume" and "surface area" (4,5,9,10). The theoretical maximum surface area of pure graphite is $2680 \text{ m}^2/\text{g}$, assuming adsorption on both sides of the graphite plane (9). Thus, surface areas calculated by the BET method which are greater than $1000\text{--}1300 \text{ m}^2/\text{g}$ must be erroneous (9,11).

The reporting of surface areas for microporous adsorbents is therefore open to criticism. The situation is compounded by the ambiguity inherent in assigning a value for the cross-sectional area of the adsorbed molecule (4,7). Due to geometric and energetic characteristics which are unique to each adsorbate-adsorbent system, the monolayer packing density and thus the effective cross-sectional area of an adsorbate may vary with the adsorbent (7). Since it is impossible to allow for these considerations in general, it is common to assign cross-sectional areas of adsorbates based on comparative adsorption experiments on well-characterized adsorbents; the adsorbate generally used as the standard is N_2 at 77K (7).

In summary, there are substantial uncertainties in the calculation of BET surface area for microporous materials such as pyrolytic chars and activated carbons. Moreover, the very concept of a "surface" is questionable for pores whose dimensions in such materials, often < 0.6 nm (8), approach the carbon-carbon bond lengths (~ 0.14 nm) in a graphitic structure. Nonetheless, provided the ambiguity of the concept and calculation technique is recognized,

BET surface areas are useful comparative measures of porosity in chars and activated carbons, and are commonly reported for lack of a more accurate method of characterization.

Pore Size Distribution--

The pore radius (r_p) corresponding to the given point on the adsorption isotherm (i.e., a given value of relative pressure) may be calculated from the modified Kelvin equation (4):

$$r_p = r_k + t = \frac{(2 \times 10^{-7}) \sigma V \cos \theta}{RT \ln(p_s/p)} + t \quad (4)$$

where r_k = Kelvin radius (nm),

σ = surface tension of the liquid adsorbate (N/m),

V = molar volume of the liquid adsorbate (m^3/mole),

θ = contact angle between the liquid and pore wall,

p_s = saturation vapor pressure (Pa),

p = equilibrium pressure (Pa),

R = gas constant ($\text{J/K}\cdot\text{mole}$),

T = absolute temperature (K), and

t = layer thickness, discussed below, (nm).

It is commonly assumed that θ equals zero, i.e., that the liquid adsorbate wets the pore walls (4). Use of the Kelvin equation assumes filling of the pores by capillary condensation. Before capillary condensation occurs, however, one or more adsorbed layers may form on the pore walls (at least for pores > 2 nm diameter). Thus the actual pore radius (r_p) will be the Kelvin radius plus the thickness of the already adsorbed layers. Various methods have been used to estimate the layer thickness; in this study we used the method of Cranston and Inkley (12).

For nitrogen adsorption at 77K, equation (4) reduces to

$$r_p = \frac{0.96}{\ln(p_s/p)} + t \quad (5)$$

The range of pore sizes that can be determined with reasonable accuracy by this approach is approximately $2 \text{ nm} < \text{diameter} < 50 \text{ nm}$ (7). The upper limit is determined by the shape of the isotherm near saturation and the precision of gas measurement and temperature control. The lower limit is due to the inappropriateness of assuming the existence of a liquid meniscus and

bulk liquid properties for capillary "condensates" in pores whose diameters correspond to a few adsorbate molecular diameters.

There is some controversy regarding whether to use the adsorption or the desorption branch of the isotherm to calculate pore size. Although use of the desorption branch is customary, for materials with "ink bottle" type pores (narrow neck, larger pore beyond), analysis of the adsorption branch yields a more nearly correct interpretation of the porosity (7). Many chars are thought to contain such "ink-bottle" pores (13).

Pore Volume--

Combination of the basic adsorption data with the Kelvin equation theoretically can be used to estimate the pore volume for pores smaller than a given diameter or to calculate the complete pore volume distribution (14). Cranston and Inkley (12) describe a method for the determination of pore volume distribution which takes into account the fact that the volume determined in the adsorption experiment includes both that which fills the pores with radius less than r_p plus that which is adsorbed on the walls of pores with radius greater than r_p . The raw adsorption data, however, are expressed as volume (at STP) of adsorbate gas adsorbed in the pores. To convert this to an estimate of the absolute volume of the pores, the density of the adsorbed gas must be known. As discussed previously, this may depend on the particular adsorbate-adsorbent system. Although there is general agreement on the use of bulk liquid density for N_2 at 77K, the appropriate density for CO_2 at 195K is still an unresolved question (9).

Outgassing Conditions--

Gas adsorption data obtained from microporous chars and activated carbons are very sensitive to the heat treatment and outgassing conditions used to prepare the material for analysis (4). The materials are thought to chemisorb oxygen on exposure to air at room temperature, e.g., during storage. Since chars contain "ink bottle" pores, the chemisorbed oxygen may reduce the size of the "bottleneck" to such an extent that the adsorbate cannot enter, resulting in lower surface area and pore volume values. It has been shown (4) that apparent surface area increases as outgassing conditions become more severe (higher temperature or longer evacuation). Thus, to ensure absolute and repeatable data, very severe conditions are recommended, such as evacuation at a temperature close to but lower than the temperature at which the char was prepared (4). Unfortunately, such outgassing may, itself, alter the char pore structure (15).

Equilibration Time--

In the analysis of microporous adsorbents, the time to reach adsorption equilibrium can be quite long due to activated diffusion, i.e., diffusion of the adsorbate through pores only a few times the adsorbate's diameter (4, 16). For this reason the so-called equilibrium pressure is generally noted after a fixed arbitrary time, depending on the adsorbate, or noted when the rate of decrease of pressure reaches some fixed level. If equilibrium times are very

long there is a danger of error caused by the leak rate characteristic of the analytical apparatus.

Comparison of Adsorbates and Adsorption Temperatures--

Due to the size of the nitrogen molecule, some microporosity, especially in chars, may not be accessible to it during the adsorption analysis (4). Accordingly, the estimate of surface area based on the adsorption of N_2 at 77K is considered to exclude the area of the smaller micropores, diameter approximately 0.6 nm or less (4). Adsorption of CO_2 at 195K is thought to measure essentially the total surface of microporous chars and carbons (4).

Mercury Porosimetry

Mercury porosimetry is used to measure the macro- and transitional-pore volume distribution of porous materials including carbonaceous adsorbents (4, 17). In practice mercury is forced into the pores of the material at increasingly higher pressures. The volume of mercury penetration is measured as a function of the applied pressure (p). The value of the pore radius (r) corresponding to (p) is calculated using the Washburn equation (18):

$$r = \frac{-(2\gamma \cos \theta)}{p} \quad (6)$$

where γ is the surface tension of mercury and θ is the contact angle between mercury and the pore wall.

The analysis is conducted by adding a known weight of sample to the penetrometer followed by sample evacuation. Next mercury is admitted to the evacuated chamber and the pressure-penetration measurements are made. Pressures as high as 420 MPa (60,000 psi) are possible with commercially available equipment, which theoretically implies an ability to measure pore sizes down to 1.8 nm. However, Mahajan and Walker (4) state that pore size information for high pressures may be faulty due to particle breakdown and/or opening of previously closed pores. Dickinson (19) reports that mercury intrusion can cause such damage to graphite for pressures above 2000-3000 psi, corresponding to 50-35 nm pore radii.

The Washburn equation assumes cylindrical pores. Chars, however, are known to have "ink-bottle" (or aperture-cavity) type porosity (4); for such pores, the pore volume distribution results will be subject to error because for a given pressure the pore radius will be determined by the aperture, while the intruded volume will be determined by the cavity.

Other limitations are discussed by Mahajan and Walker (4), including the possible dependence of surface tension on pore radius for radii < 50 nm.

Finally, for powdered samples mercury porosimetry results cannot distinguish between the small interparticle voids and macroporosity in the particles themselves. In this case the data must be analyzed carefully to avoid misinterpretation.

Thus, as was the case for the other methods of physical characterization of chars and activated carbons, interpretation of mercury porosimetry results is subject to a number of limitations. However, if the limitations are acknowledged, the technique is useful for the comparison of materials.

PYROLYSIS

Pyrolysis is strictly defined as chemical decomposition by heat. As a step in activated carbon preparation, pyrolysis is generally conducted at temperatures in the range 400°-1000°C and in the absence of air (1). Research on pyrolysis of carbonaceous materials, especially with respect to char properties, has been largely limited to coal and model compounds such as cellulose. The focus of this study is utilization of cellulosic and lignocellulosics waste materials. Pertinent concepts of pyrolysis of pure cellulose and lignocellulosics in general are discussed below.

Pyrolysis of Cellulose

Cellulose is the main structural component in the cell walls and fibrous and woody tissues of plants. It is a linear polymer of D-glucose in $\beta 1 \rightarrow 4$ linkage, usually represented by the chemical formulas $(C_6H_{10}O_5)_n$. Naturally occurring cellulose polymers contain 300 to 15,000 glucose monomer units and are organized in bundles of parallel chains to form fibrils (20).

Despite the fact that the pyrolysis of cellulose is a well-examined process (21), no definite scheme of reaction mechanism has been established. This is due to the highly complex nature of the thermal decomposition of cellulose, which consists of many interrelated reactions with a great number of reactants, intermediates, and reaction products. Tang and Bacon (22,23) have presented a model for the pyrolysis of cellulosic fibers, which is in agreement with most of the work done by others (21). Based on carbonization experiments and subsequent elemental analysis, x-ray, infrared, and thermal analyses, they conclude that pyrolysis starts with the physical desorption of water ($< 150^\circ\text{C}$), followed by dehydration ($150^\circ\text{--}240^\circ\text{C}$) and cleavage of the $1 \rightarrow 4$ glycosidic linkages ($> 240^\circ\text{C}$). According to Tang and Bacon, the final polymeric char is made up of four-carbon building blocks, which originate directly from the initial cellulose. Thus the maximum char yield is expected to be 29.5%. The dehydration reactions below 240°C appear to be slow when compared to the depolymerization and scission of C-O and C-C bonds above 240°C .

The reaction kinetics of the thermal decomposition of cellulose has been widely studied in the context of fire research and flame retardants (21,24,25). Tang and Neill (25) found that the pyrolysis reactions are best separated into two groups: a pseudo-zero-order reaction below 310°C with an activation energy of ≈ 34 kcal/mol, and a pseudo-first-order reaction above 310°C with a higher activation energy of 54 kcal/mol. Flame retardants and some inorganic contaminants (such as Lewis acids) have been shown to decrease the activation energies as well as the DTA maxima and usually to increase char yield (21,25-28).

The yield and properties of low-temperature ($< 1000^{\circ}\text{C}$) pyrolytic chars have not been as well examined as the pyrolysis reaction itself. In a study of cellulose pyrolysis and activation (26), Brunner found a log-linear dependence of char yield on the rate of heating to the final pyrolysis temperature. Slow heating (e.g., $< 1^{\circ}\text{C}/\text{min}$) was found to result in considerably increased char yields. This was thought to result from the longer exposure of the cellulose to temperatures below 240°C , in which range the dehydration reactions predominate. The more completely dehydrated polymer, due to the presence of carbon-carbon double bonds, is thought to be less susceptible to cleavage at temperatures above 240°C , resulting in the observed higher char yields.

It has also been shown (29) that, when cellulose was pyrolyzed at a slow heating rate, there was not significant weight loss above approximately 700°C , whereas rapidly charred cellulose continued to lose weight at least up to 1000°C . Furthermore, slow heating resulted in lower oxygen content of the char.

The surface area and micropore volume of cellulose char is reported to increase with temperature up to a maximum (700° – 1000°C), beyond which they begin to decrease (26,29,30). This effect, also observed for pyrolysis of coal products, is thought to be due to progressive development of micropores up to 1000°C followed by rapid closure of the micropore entrances (4,11,30,31). Constriction of the micropores is detectable by gas adsorption methods as low as 700° – 800°C (11,29). Furthermore, it has been observed that low heating rates result in a higher maximum surface area, somewhat larger micropore openings, and a less pronounced decrease of surface area at higher temperatures (26,29).

Finally, pore development in pyrolyzed cellulose is limited to small micropores whose diameters are on the order of magnitude of the molecular sizes of nitrogen and carbon dioxide (29), approximately 0.4 nm or less (7,16). Mercury porosimetry of cellulose chars heated at various rates to a range of final temperatures (500° – 1000°C) revealed no development of transitional- or macroporosity (29).

Pyrolysis of Lignocellulosics.

Plant tissue, or lignocellulose, is a matrix of three main components: lignin, cellulose and hemicellulose. Cellulose, as mentioned previously, is present in long fibrils, while the other two components fill the interfibrillar spaces and serve to cement the matrix together (20). Lignin is a high molecular weight (10^3 – 10^6) three-dimensional polymer of aromatic alcohols (32). Hemicellulose refers to branched polysaccharides composed primarily of pentoses with lesser amounts of hexoses (20). Both the hemicellulose and lignin fractions vary chemically with the parent lignocellulosic and are difficult or virtually impossible to isolate unaltered (20,32). Compared to the substantial body of research on cellulose pyrolysis, considerably less is known about the pyrolysis of the other two components and very little about pyrolysis of the lignocellulosic matrix in general.

Shafizadeh and McGinnis (33) found that the thermal behavior of wood reflects the sum of the thermal responses of its three major components,

cellulose, hemicellulose, and lignin. The data indicate, as discussed by Shafizadeh and Chin (34), that the components are initially dried on heating at 50°-100°C. Hemicellulose is the least stable component, decomposing at 225°-325°C. Lignin decomposes gradually within the wide range of 250°-500°C, with a much higher percent char yield than the other components. They conclude further that since the pyrolysis products of wood reflect the sum of the products from the major components, there is no major interaction between the components during pyrolysis.

Philpot (35), however, in a study of a variety of plant materials, found that minerals present in the plant tissue appeared to increase the yield of char from the lignocellulose, much as fire retardants and certain inorganics had been shown to affect cellulose pyrolysis (21,25-28). He found, further, that the char yield was even better correlated to silica-free ash, a measure of the mineral content of the plant tissue excluding silica. The explanation offered for this correlation was that silica, unlike the other ash components, is effectively inert and incapable of affecting pyrolysis of the organic fraction.

Philpot and others (35,36) have shown for pyrolysis of plant materials that the effect of inorganics on char yield levels off for ash contents between 5-7%. Also it has been observed (34) that the effect of inorganics on hemicellulose pyrolysis is similar to the effect on cellulose. Little is known about the effect of inorganics on char yield from lignin, although strong acid treatment of lignin is known to increase its char yield slightly (32,33).

Rothermel (37), using data derived from other studies (36,38), developed an empirical model for lignocellulosic char yield (pyrolysis at 15°C/min to 400°C) as a function of composition. The model calculated the total char yield as the sum of the char yields of the components, and assumed the components did not interact, except that the holocellulose (cellulose plus hemicellulose) yield increased with silica-free ash content. The catalytic effect of the silica-free ash was included as a power function to account for leveling off of the effect at increasing ash contents.

There has been little reported research on surface area and pore volume development in lignocellulosic chars, only studies specific to one material and set of pyrolysis conditions (e.g., olive stones (2), and plum stones (3)). Based on these limited studies, it appears that lignocellulosic chars develop only microporosity.

There has been no systematic research reported on the effect of pyrolysis heating rate or final temperature on the yield, surface area or micropore volume of lignocellulosics in general.

ACTIVATION

Activation refers to processes which increase the adsorptive capacity of chars, usually by increasing the extent of porosity (surface area and micropore volume). Many commercial processes entail reacting the char with

oxidizing gases (e.g., steam, carbon dioxide, oxygen or air) at elevated temperatures (600-1000°C)(1). In general, the adsorptive capacity developed is determined by the nature and concentration of the oxidizing gas, the temperature of the reaction, the extent of oxidation (measured for example as weight loss, or "burn-off"), and the amount and kind of mineral ingredients in the char (1). It is also generally accepted (1,39,40) that the results of activation depend on the nature of the starting char, its processing history and to some degree its parent material.

There does appear to be some agreement (4,41-44) that gasification (activation by oxidizing gases) may involve any or all of three basic phenomena: widening of porosity existing in the char, opening of previously blocked micropores and, possibly, creation of or elongation of micropores. Thus, as activation proceeds, both the total number of pores and their average radius is increased, resulting in an increase in specific pore volume and specific surface area (i.e. per gram remaining material) (4). At some point, however, depending on the structure of the char, walls between existing pores are gasified away, resulting in a decrease in the total number of open pores (4,43). While this leads to a continuous increase in specific pore volume, specific surface eventually reaches a maximum and declines thereafter (4,45). One study, (46) for example, reports such maxima in the range 60-80% weight loss in activation for coal chars. Brunner (26), however, in a study of cellulose char activation, found a continuous increase of surface area with increasing oxidation up to weight losses of 60-80%.

The choice of oxidizing gas also affects the porosity developed during activation. Carbon dioxide activation has been observed to produce only micropores for burn-offs less than 30-35% in studies of cellulose, cellulose triacetate and sucrose chars (26,41,47). Steam activation has been found to result in more pronounced transitional-porosity (42,48). Tomkow, et al. (48) compared O₂, CO₂ and H₂O activation of brown coal chars and found the effect of the gas varied with the burnoff. At low burnoff (1-8%), oxygen activation resulted in higher surface areas than carbon dioxide or steam. At high burnoff (70%), the reverse was found. For oxygen activation, total pore volume leveled off at only 25% burnoff, whereas total pore volume increased steadily for steam and carbon dioxide activation. Carbon dioxide activation yielded the highest total pore volume at high burnoff.

Both the partial pressure and flowrate of the oxidizing gas has been observed to influence the rate and effect of gasification. Carbon monoxide, a product of carbon dioxide activation, is known to have a pronounced retarding effect on the gasification rate (49,50,51). At low flow rates of CO₂, the CO retained at the carbon surface is thought to inhibit gasification of the particle exterior and result in greater development of microporosity (50). Also, dilution of carbon dioxide with inert gases (e.g. Xe, N₂, Ar) has been observed to result in higher gasification rates (52).

Activation temperature also profoundly affects the rate of gasification. Brunner (26) found that the time for 40% burnoff of cellulose char in CO₂ increased twofold and threefold as temperature was lowered from 960°C to 915°C and 880°C, respectively. Similarly, the rate of development of surface area increased with activation temperature.

Finally, the rate of gasification is known to increase in the presence of almost any inorganic impurity, even in trace amounts (51). It is thought that inorganic impurities in the char agglomerate as reduced metals during activation (53) and migrate to the char surface (51). Catalysis occurs only in the vicinity of the metal agglomerate (53,54) and results in development of macro- and transitional-pores with little change in microporosity (53). Catalysis is thought to continue until the metal is oxidized (53). However, the same activation products that normally inhibit uncatalyzed gasification (i.e., CO, H₂) may serve as accelerators in that their presence in sufficient amounts maintains the catalyst in a more reduced and active state.

SECTION 5

MEASURES OF SORPTION PERFORMANCE

Sorption performance measurements include kinetic studies and equilibrium isotherms. Kinetic studies relate to the rate at which solute diffuses into activated carbon grains and is adsorbed onto the surface of the activated carbon; equilibrium isotherms measure the partitioning of solute between that which adsorbs and that which remains in solution at equilibrium conditions.

EQUILIBRIUM ISOTHERMS

Several models have been proposed to describe adsorption isotherms: the Langmuir, Brunauer-Emmett-Teller (BET), Freundlich, Linear, and Simplified Ideal Adsorbed Solution (IAS) models.

The Langmuir isotherm (55) was derived in much the same way that chemical equilibrium equations have been derived, assuming a four-component system of adsorbed solvent, solute in solution, adsorbed solute, and solvent in solution (56). The Langmuir isotherm is of the form:

$$q_e = \frac{Q^0 b C_e}{1 + b C_e} \quad (8)$$

where q_e is grams of solute adsorbed per gram of activated carbon, and Q^0 is the grams of solute adsorbed per gram of carbon at complete monolayer coverage of the carbon. C_e is the concentration of solute in bulk solution, and b is a constant related to the net enthalpy, ΔH , of adsorption.

The Langmuir model occasionally has been used to describe adsorption onto activated carbon from a liquid phase with some success (57,58). The Langmuir equation is based on the following assumptions: The maximum adsorption that can ever occur corresponds to a saturated monolayer of solute molecules on the adsorbent surface; the energy of adsorption is constant; and no surface diffusion occurs (59). In general, those conditions are not fulfilled in most solute/activated carbon systems. Since adsorption forces pervade the micropores of carbon (5), volume filling may occur instead of monolayer coverage. Secondly, the surface of activated carbon is composed of many types of functional groups (60), which exhibit a broad spectrum of adsorption energies. Thirdly, surface diffusion is believed to occur (13,61).

The BET model is an extension of the Langmuir model. It is based on the assumption that a number of layers of adsorbate form on the surface of a solid

and that for each of these layers, the Langmuir equation applies. The BET model is used to describe the behavior of gases adsorbing onto a solid when the gas is at temperatures close to those required for condensation of the gas. Section 4 of this report discusses the BET model in more detail.

The Freundlich isotherm (62) makes allowances for heterogeneous surface energies and is of the form

$$q_e = K_f C_e^{1/n} \quad (9)$$

where K_f is a constant related to sorption capacity, and $1/n$ is related to the favorability of adsorption. If $n > 1$, favorable adsorption is indicated. If $n < 1$, adsorption is unfavorable. If $n = 1$, the isotherm is linear, i.e., the amount of solute adsorbed is directly proportional to the amount of solute present.

The Freundlich isotherm has been used extensively in both a theoretical and empirical context, and often successfully describes the adsorption behavior of a wide range of organic compounds from solution phase onto activated carbon. Sontheimer (63) has found the Freundlich isotherms more useful than Langmuir relations to characterize the adsorption of a wide range of compounds; Dobbs et al. (64) have presented a collection of Freundlich isotherms for 143 organic compounds.

The linear isotherm is of the form:

$$q_e = RC_e$$

It is a special case of the Langmuir equation (equation 8) where

$$Q^0b = R \quad (10)$$

and $bC_e \ll 1$, or of the Freundlich equation (equation 9) where $1/n = 1$.

The ideal adsorbed solution model (IAS) was developed for bi-solute systems by Radke and Prausnitz (65). This was later applied and simplified by Fritz and Schlünder (66). Radke and Prausnitz (65) proposed from thermodynamic principles that the adsorbed phase could be considered as an ideal two-dimensional solution; it could therefore be described by equations in two dimensions similar to those for bulk solution in three dimensions. Further, if it is assumed that the spreading pressure, π , of each of several solutes in mono-solute experiments is equal to the spreading pressure of the mixtures of these solutes in bi-solute or multi-solute experiments, then the data from the former can be used to predict the adsorption behavior of various compounds in multi-solute experiments. The spreading pressure π is an integral function of bulk and solid concentrations; in principle, it can be determined for each component independently of the other components by mono-solute isotherms.

Fritz and Schlunder (66) simplified the IAS model by assuming that the adsorption of each individual component could be modeled by the Freundlich isotherm. This simplified the integral for π found in Radke and Prausnitz to a more useful form:

$$\frac{Y_1^0}{b_{1,k}} - C_{1,k} = \pi(Y_1^0) = \pi(Y_2^0) = \frac{Y_2^0}{b_{2,k}} - C_{2,k} \quad (11a)$$

$$X_1 = X_1^0(z_1) \quad (11b)$$

$$X_2 = X_2^0(1 - z_1) \quad (11c)$$

$$\frac{Y_1}{Y_1^0} + \frac{Y_2}{Y_2^0} = 1 \quad (11d)$$

where Y_1^0 and Y_2^0 are adsorbed concentrations of component 1 and 2, respectively, determined in independently determined mono-solute experiments; X_1 and Y_1 are the equilibrium bulk and adsorbed concentrations of component 1 in the bi-solute system and b and C are constants as described in (66). The value z_1 is the mole fraction of component 1, excluding the solvent (water). Fritz and Schlunder reported good agreement between experimental data and this model.

The IAS model was simplified by DiGiano et al. (67) into what has been called the simplified competitive adsorption model (SCAM).

KINETICS OF ADSORPTION

The rate of adsorption is regulated by three steps: (i) transport of the adsorbate from the bulk solution to the activated carbon particle (film diffusion), (ii) diffusion of the adsorbate through the internal macro- and transitional-pores of the carbon particle (internal diffusion), and (iii) adsorption of the solute onto the carbon's internal surface (59). Within a well-mixed batch reactor, internal diffusion is generally found to be rate-limiting. The rate of internal diffusion may be determined by one of two parallel mechanisms: molecular diffusion through the fluid that fills the internal pores (pore diffusion) or diffusion of adsorbed solute along the pore walls (surface diffusion). The overall rate of internal diffusion is given by the sum of the rates of transport by the two mechanisms. If the rates are widely different, the overall transport is given approximately by the rate of the faster of the two parallel processes.

Pore diffusion into a sphere, if it is assumed that diffusion occurs radially inward, is characterized by the continuity equation (68):

$$\frac{\partial C}{\partial t} = D \left(\frac{\partial^2 C}{\partial r^2} + \frac{2}{r} \frac{\partial C}{\partial r} \right) \quad (12)$$

where C is the concentration at any radius r for a given time t. The diffusion coefficient D is assumed to be constant. If adsorption occurs, then equation 12 must be modified to the form:

$$\frac{\partial C}{\partial t} = D \left(\frac{\partial^2 C}{\partial r^2} + \frac{2}{r} \frac{\partial C}{\partial r} \right) - \frac{\partial S}{\partial t} \quad (13)$$

If it is assumed that adsorption is instantaneous and is further governed by a linear isotherm of the form $S = RC$, (S = adsorbed concentration, R = partition factor), then the quantity $[D/(1 + R)]$ can be substituted for D in equation 12. This means that when adsorption occurs, for each amount of solute present in the solution enclosed by a pore, there is R times that amount adsorbed along the surface of that same pore. In its adsorbed state, the solute would not directly contribute to a driving force for diffusion in the bulk phase of the pores. So the amount adsorbed (R), according to this reasoning, would not be involved in establishing a concentration gradient. Consequently, it would require $(R + 1)$ amount of solute to achieve the same concentration gradient that it took one amount of solute to achieve without adsorption (18). Equation 12 then becomes

$$\frac{\partial C}{\partial t} = \left(\frac{D}{1 + R} \right) \left(\frac{\partial^2 C}{\partial r^2} + \frac{2}{r} \frac{\partial C}{\partial r} \right) \quad (14)$$

This expression has been solved analytically (68) for the case where the total amount of solute in the sphere after time t is compared to the total amount adsorbed at equilibrium. This method, which will be used in Section 7 of this report, has also been used by Roberts (69). Roberts successfully employed this and other related equations to compare two dimensionless parameters: the fractional approach to equilibrium, $f = (C_o - C_t)/(C_o - C_\infty)$ versus dimensionless time, $\tau = Dt/a^2$. Using these two parameters, he was able to model the rate at which a synthetic zeolite adsorbent adsorbed normal paraffins from binary liquid solutions.

The diffusion equation (equation 12) has been discussed by Walker et al. (13) in relation to the diffusion of gases into zeolite and carbon molecular sieves. Walker et al. suggest two models to account for the effect of adsorption. In the first, the gas held by the solid would be considered to be in an occluded state. As such it would not behave as a free gas following ideal gas laws. Rather, it would be affected by force fields which are significant throughout the cross section of the micropores. Such an occluded gas would not be so firmly fixed in one position that it could not diffuse through the system. Rather, it would undergo activated (hindered) diffusion, and its driving force, $\partial C/\partial x$, would be in units such as gram-mole/cm³ pores/cm distance.

In a second model, conceived by Walker et al. (13), it is assumed that the gas within the adsorbent is partitioned into two phases: (i) those molecules occupying the open porosity of the solid which would be relatively free to diffuse (pore diffusion); and (ii) those molecules adsorbed in a layer on the internal walls of the solid, which would be relatively non-mobile. Walker

suggested that the Langmuir isotherm could be used to determine partitioning between adsorbed and non-adsorbed gas within the pore matrix.

The first of these models, Walker suggested, would be more useful in describing the behavior of molecular-sieve materials. However, the second could be useful with porous carbons, if consideration were to be given to both pore and surface diffusion. Walker further stated that when pores are of near-molecular dimensions, the two models are physically identical.

Both pore and surface diffusion were considered by Fritz, Merk, and Schlunder (61) in their model of competitive adsorption of two dissolved organics onto activated carbon. They found remarkable agreement between experimental and theoretical kinetics data when they considered

$$n_{i,k} = \gamma_{i,p} \frac{\partial x_i}{\partial r} + \rho_k \gamma_{i,s} \frac{\partial S_i}{\partial r} \quad (14)$$

where $n_{i,k}$ is the flux of component i , $\gamma_{i,p}$ is the pore diffusion coefficient of component k which at radius r has a pore concentration of x_i , $\gamma_{i,s}$ is the surface diffusion coefficient of component i which has a surface concentration S within a grain with particle density ρ_k .

Surface diffusion was proposed to be the predominant intraparticle mass transfer process by Crittenden (70,71) in his model for the design of fixed-bed adsorbers. He therefore based his diffusion equation on the surface phase concentration, essentially the last term in Eq. 14. He based the numerical solution for his differential equation on the solutions given by Crank (68).

Kinetic studies have also been presented by others, notably in the early work of Weber and Morris (72), who experimentally evaluated the rate of adsorption of several single solutes. In this article, they developed no theoretical models to describe the data, but rather calculated a "rate coefficient," k , in units of moles solute adsorbed per gram carbon per square root of hours.

ADSORPTION OF ORGANICS FROM WASTEWATER EFFLUENT

Considerations Regarding Composition

Real waters and wastewaters are complex in composition: they contain a multitude of organic compounds, which differ greatly with respect to molecular weight, chemical composition, functional groups, polarity, adsorbability, and diffusivity. The presence and concentration of a limited number of these organic compounds can be determined through advanced analytical procedures. Only a small fraction of the organic material in natural waters and wastewaters can be identified specifically as single substances with currently available techniques.

The molecular weight distribution of the soluble organic compounds in secondary effluents, as determined by DeWalle and Chian (73), included 36% with a molecular weight less than 100, 21% with molecular weight between 100 and 500, 28% with molecular weight of 500 to 5000, and 15% with molecular weight greater than 5000. Activated carbon treatment removed 57% of those compounds with molecular weight < 100, 82% of those compounds with molecular weight of 100-500, and 90% of those compounds with molecular weight > 500. Many of the compounds of molecular weight less than 100 were polar. The high molecular weight compounds consisted of carbohydrates, proteins, and humic acids. Similar molecular weight distributions were found by Parkin (74) and Keller (75) for effluent from wastewater treatment plants, notably the Palo Alto Water Quality Control Plant.

Wastewater Effluent Adsorption Behavior

Most fundamental kinetic and isotherm studies have been conducted on single solutes or on a few well-characterized model compounds. Real systems found at water and wastewater treatment plants have been predominantly studied in an empirical way (76,77), i.e., data from these facilities have shown how much of various compounds have been removed from the solution phase. Although such articles have been useful, they have not usually been developed sufficiently to offer fundamental, quantitative understanding of the behavior of competing solutes.

Because of the complexity of real waters and wastewaters, those who study their adsorption choose to use collective parameters such as total organic carbon (TOC), dissolved organic carbon (DOC), or total organic chlorine (TOCL); settle for data on only a few important compounds; or resort to a combination of these approaches.

Such an attempt was made by Frick (78). He applied the simplified competitive adsorption model (65) to unknown mixtures by idealizing the mixed solutes as a semi-defined system having a smaller number of pseudo components. He achieved this by adding a specific amount of a tracer substance to the unquantified mixture. By watching the adsorption behavior of the added compound in the presence of the unknown organic compounds, he felt that it was possible to obtain information on the single-solute data and on the concentration of key components within this mixture.

Secondary effluent, characterized by TOC, was used by Hsieh (79) for kinetic experiments over time periods up to 270 hours for a number of ratios of activated carbon to wastewater volume. After 48 hours, the control concentration in these experiments experienced a gradual but significant reduction, probably due to bacterial decomposition. Clearly, caution must be exercised in adsorption rate experiments to avoid the complication of biodegradation phenomena being superimposed on adsorption phenomena.

SECTION 6

MATERIALS AND METHODS

CELLULOSE

Two reagent grade celluloses were used in this study. Cellulose M is a microcrystalline cellulose prepared for column chromatography by EM Laboratories, Inc. of Elmsford, New York. The ash content of cellulose M is 65 ppm (parts per million) (26). Cellulose Σ is alpha cellulose fiber (α -cellulose) distributed by the Sigma Chemical Company, St. Louis, Missouri. The ash content of cellulose Σ is 0.19% (method described below).

LIGNOCELLULOSIC MATERIALS

Twenty lignocellulosic materials were selected for experimentation, representing the three major taxonomic groups of terrestrial plants (softwood trees, hardwood trees, and grasses), as well as three types of paper, several varieties of fruit pits and shells, steer manure, and two types of decayed woods (pecky cedar and cubic brown rot from a lodgepole pine). Table 1 (see Section 7) lists the materials selected along with their composition, determined as described below. The materials were chosen with a view to obtain a variety of lignocellulosics with widely ranging fractions of the tissue components (lignin, holocellulose, extractives and ash). Table 1 indicates this criterion was satisfied. Thus we expect our experimental results could be applied to virtually any natural lignocellulosic material and even, perhaps, to man-made waste materials composed largely of natural or modified lignocellulosics.

Pecky cedar, a waste product from cedar milling, was donated by California Cedar Products, Stockton, California. Cubic brown rot was collected in the Sierra Nevada from fallen lodgepole pine. The peat sample was supplied by Dynatech R/D Co., Cambridge, Massachusetts; the peat had originated from Minnesota and thus was likely to be the decay product of arborescent plants. Steer manure was a commercially available garden supplement distributed by Sequoia Chemical Corporation, Chino, California. Prune pits were donated by a local fruit processing facility. Walnut shells were gathered locally from English walnut trees. Coconut shells were separated by hand from store-bought coconuts. Newsprint paper was taken from roll ends purchased from a local newspaper and was free of print. White fir wood was donated by the Forest Products Research Laboratory, University of California at Berkeley. The other wood samples were derived from naturally dried branches (free of bark), except for walnut which had been kiln-dried. Computer paper was taken from waste bins at the Stanford Center for Information Processing. The kraft paper

sample was prepared from standard cardboard boxes used for shipping. Some of the agricultural samples were provided courtesy of Lawrence Berkeley Laboratory, Berkeley, California while the others were obtained from various agricultural sources in California.

REFUSE-DERIVED FUEL (RDF)

Refuse-derived fuel refers to the fraction of municipal solid waste remaining after the raw waste is classified to remove metals, glass and other inorganics. A sample of RDF was provided by the Occidental Research Corporation, LaVerne, California. The RDF was produced from municipal solid waste from San Diego, California, at the Environmental Protection Agency sponsored demonstration classification and flash pyrolysis plant in El Cajon, California. The complete classification scheme used at the plant is described in detail elsewhere (80); briefly, it consists of pre-shredding, air classification, drying and final screening. The RDF sample used in this work was dry, relatively odorless, and visibly heterogeneous. Particles varied in size and type from powdery inorganic grit to one to two inch pieces of paper and minor amounts of plastic. The presence of relatively large amounts of grit indicates the RDF did not receive final screening. Also visible were small pieces of twigs and stalks, cloth, string, yarn, aluminum foil and aluminum metal.

The RDF was prepared for experimentation by grinding, as described below. The ash content of the ground RDF was approximately 16%. However, the RDF was then sieved prior to experimentation, resulting in a final ash content of approximately 12% and a particle size range of 74-500 μm . Klumb and Brendel (81) report air classified solid waste analyses for over 650 samples which indicate an average ash content of 19.2% (53.8% maximum, 7.6% minimum). Hence, the prepared RDF sample used in this work may be considered representative of relatively efficient, but not atypical, commercial classification technology.

MATERIALS PREPARATION

Cellulose M and cellulose Σ were used as supplied. All other materials were ground and sieved prior to use.

Preparation for Grinding

All lignocellulosics except prune pits and steer manure were air-dried and cut or broken into small (1 inch) pieces prior to grinding. Prune pits, which were taken directly from the food processing facility, had large amounts of the fruit flesh adhering to them. The flesh and kernel were separated from the pit coat by blending in hot water in a large, stainless steel blender. Both the flesh and kernel were thus washed away and the pit coat broken to small pieces. This was necessary to yield a relatively high lignin material, which was desirable for our experimental purposes, and to ensure sample homogeneity. The steer manure was also blended briefly in cold water and then placed in a No. 30 (U.S. Standard) sieve (0.595 mm openings) and rinsed

repeatedly with cold water to remove dirt and grit and thus reduce the ash content. Both prune pits and steer manure were air-dried prior to grinding.

Grinding

All lignocellulosics were ground in a Wiley mill to pass a 0.5-mm screen. The mill operates by a shearing action between rotating and stationary steel knives. All materials except coconut shells, walnut shells and prune pits ground very rapidly. The shells and pits, however, were very resistant to grinding and caused the mill to heat up. To avoid thermal alteration of the lignocellulosic, the mill was operated cyclically, to provide cool-down periods and insure the temperature never exceeded 50-80°C.

Sieving

The ground samples were air-dried by placing them in direct sunlight to speed the sieving process. Sieves were shaken for 10 to 20 min depending on the type of sample. The fraction of the lignocellulosic sample passing U.S. Standard sieve No. 45 (0.354 mm openings) and retained on U.S. Standard sieve No. 200 (0.074 mm openings) was retained for analysis and experimentation. This fraction is nominally composed of particles in the size range 74-354 μm . This size fraction was selected as a compromise between the need for sample homogeneity, the resistance of some materials to grinding, and the requirements of the analytical procedures discussed below.

Preparation of Subsamples

The last step in materials preparation was the production of 10-20 gram subsamples of the 45-200 mesh fraction using a standard riffle sampler. Riffle samplers are designed to yield subsamples which are representative of the sample as a whole (i.e., having the same particle size distribution and overall composition). This step thus insures that the analyses of one subsample yield data applicable to the subsamples used in the pyrolysis experiments, and further that replicate pyrolysis experiments are performed with the same starting material.

RAW MATERIALS ANALYSIS

All lignocellulosics were analyzed using the methods described below to determine their composition in terms of the basic cell wall constituents: lignin, holocellulose, extractives and inorganics. Additionally all materials, including the reagent celluloses, were analyzed as described below for their carbon content.

Ash

The ash content is a measure of the inorganics present in the lignocellulosic material, but is not necessarily quantitatively equivalent, due to volatilization of some of the organics during the ashing procedure. The method used in this study is an adaption of the method described by the U.S. Forest Products Laboratory for determination of ash in wood (82). The

procedure yields the percent residue (dry weight basis) upon ignition at 600°C to constant weight. The analysis is carried out using porcelain crucibles, 3- to 5-gram samples, and carbonization of the sample over a bunsen burner, followed by ignition at 600°C in a muffle furnace overnight (10 hours or more). Analyses were conducted in triplicate. Standard deviations for the analysis varied from less than 1% of the mean for homogeneous materials to 5-7% of the mean for very low ash or nonhomogeneous materials.

Silica-Free Ash

Silica-free ash is a measure of inorganics other than silica present in a lignocellulosic material. The analysis was performed by Ultrachem Corporation, Walnut Creek, California. Weighed portions of the sample ash (residue upon ignition at 600°C overnight) were treated with sulfuric and hydrofluoric acids, muffled at 1200°C to volatilize the silica, dessicated and weighed. The acid treatment and volatilization were repeated until constant residue weight was achieved. Residue is defined as silica-free ash, but other compounds not volatilized at 600°C could be volatilized under the acidic and higher temperature conditions of this analysis. Standard deviation on replicate analyses was approximately 2%.

Extractives

Extractives in lignocellulosics consist of materials soluble in neutral solvents but not part of the lignocellulose matrix itself. Such materials are resins, tannins, waxes, gums, fats, and phenolics. The method used is an adaption of the Forest Product Laboratory's determination of extractives in wood (82). Three to five grams of air-dried sample is accurately weighed into a fritted glass extraction thimble. The sample is also weighed into a pair of glass weighing bottles for separate drying and determination of sample moisture content. The thimble is placed in a soxhlet extraction apparatus and extracted with a 2:1 benzene-ethanol azeotrope at a rate of not less than four siphonings per hour for 8 hours. The thimble is then placed in a crucible holder attached to a vacuum flask and rinsed 4-5 times with ethanol, allowing a minimum 5-min soak time in ethanol between vacuum rinses. The sample is then rinsed twice with anhydrous ether to aid drying. The thimble is placed in a vacuum oven at 100°C for approximately 36 hours and reweighed. Weight loss corrected for original moisture content is reported as percent extractives. Analyses are run in triplicate. The standard deviation for the analyses varies from 20% of the mean for a material with a very low extractive content to less than 1% of the mean for extractive-rich materials. Most sample standard deviations lie between 1% and 10% of the mean.

Lignin

Lignin is a high molecular weight polymer of aromatic alcohols which interpenetrates the cellulose fibrils and hemicellulose polymers and in essence cements the lignocellulose matrix together. The method used is that known as the acid-insoluble lignin - modified hydrolysis method (82). Extractive-free sample is subjected to sulfuric acid hydrolysis in two steps to hydrolyze the carbohydrates, leaving the acid-insoluble lignin as a solid residue to be captured on a filter and measured gravimetrically. Only air-

dried, extracted sample is used since oven drying has been observed to increase the apparent lignin content, due to alteration of the carbohydrates, part of which are thus transformed into acid-insoluble form. The first hydrolysis step is accomplished in 72% H_2SO_4 for one hour at 30°C (achieved by placing the vials containing the samples in a water bath). The sample/acid mixture is stirred three times during this period. The sample/acid mixture is then diluted to a 4% H_2SO_4 solution for secondary hydrolysis, which is accomplished by autoclaving for one hour at 121°C . The autoclave is allowed to exhaust slowly enough to avoid boiling and evaporation of the liquid. The acid insoluble lignin is then filtered onto glass fiber filters placed in filtering crucibles. Crucibles are then dried, weighed, ignited overnight, and reweighed. The weight loss upon ignition is defined as acid-insoluble lignin. Analyses are performed in duplicate with standard deviations for lignin as percent of extractive-free sample generally less than 1% of the mean. This value is then corrected, using the extractives content as described above, to lignin as percent (dry weight basis) of the raw sample.

Holocellulose

Holocellulose is defined as the total carbohydrate content of the lignocellulosic, which is composed of cellulose and hemicellulose. For the purposes of this study, we found it sufficient to determine percent holocellulose (α_{cell}) by difference (i.e., $\alpha_{\text{cell}} = 100 - \alpha_{\text{lig}} - \alpha_{\text{ext}} - \alpha_{\text{ash}}$). This may result in a positive bias of the estimate of the holocellulose content, especially if there is a substantial portion of the native lignin which is acid soluble and thus not measured in the lignin analysis. For example, up to 15% of hardwood lignin may be acid-soluble (32), which, for a typical hardwood of 20% lignin, 75% holocellulose, and 5% extractives (negligible ash), would result in an experimental estimate of holocellulose (by difference) which was only approximately 4% too high (78% versus 75%).

Percent Carbon

The percent carbon (dry weight basis) of raw materials (and chars as described below) was determined using a WR-12 Carbon Determinator, Model 761-100, made by Leco Corporation, St. Joseph, Michigan. Approximately 75 mg of dry sample (40 mg for chars) was accurately weighed (± 0.5 mg for samples, ± 0.1 mg for chars) into a special crucible and then covered with copper catalyst and iron chips. The crucible was then purged with pure O_2 and ignited in an induction furnace for 70 seconds. The combustion gases were dried, passed over a catalyst to convert all CO to CO_2 , and through a molecular sieve to retain CO_2 . The sieve was next heated to release the CO_2 which passed through a thermal conductivity detector. The integrated result for a sample was compared to a standard curve derived from standards supplied by Leco. Analyses were generally performed in triplicate. Standard deviations were between 1% and 2% of the mean for raw materials, and between 1% and 4% of the mean for chars.

PYROLYSIS

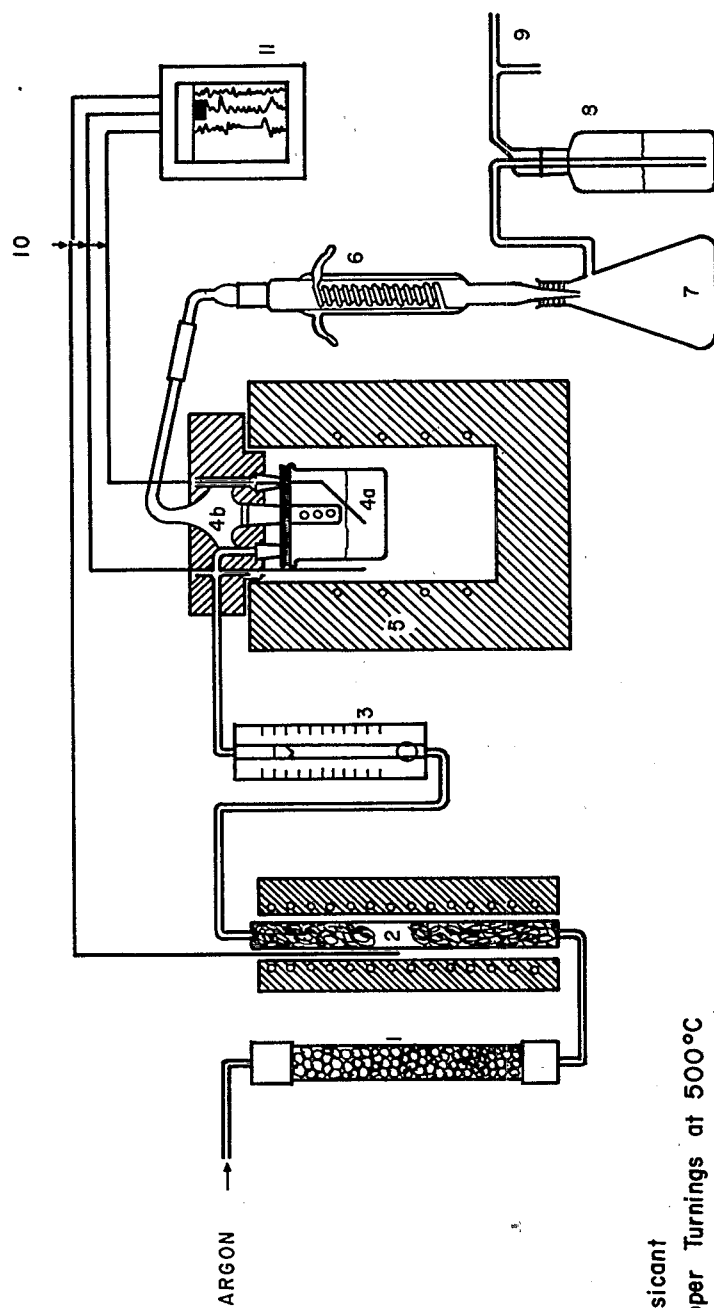
The equipment used in the pyrolysis experiments is schematically illustrated in Figure 1. Ten to twenty gram dry samples were accurately weighed and placed in either a 275-ml or 750-ml quartz glass reactor (previously tared). The reactor top was sealed to the reactor bottom using high-temperature silicone grease and metal clamps. The entire reactor assembly was suspended over the furnace, which could be raised around the reactor or lowered with a heavy duty laboratory jack. The reactor assembly was attached to the argon purge gas system and the tar and condensable by-product traps with silicone rubber tubing.

The argon purge gas system consisted of research grade argon (99.998%) supplied through a two-stage regulator. The argon was first passed through a 12-inch column of silica gel to ensure dryness and then over copper filings contained in a tube heated to 500°C to remove oxygen. Argon flow was regulated by a Nupro "J" series miniature valve and measured with a rotameter (Matheson Gas Products, Tube 600). The argon was introduced to the reactor through a ground glass fitting in the reactor top.

The furnace (5-inch I.D. x 6 inches deep) was constructed from cylindrical half section elements supplied by Thermcraft, Incorporated, Winston-Salem, North Carolina. The furnace temperature was regulated with a temperature programming subsystem consisting of a commercial furnace controller (Model 72-1, Love Controls Corporation, Wheeling, Illinois) and a voltage generator made at Stanford University. The programming system allowed controlled, linear furnace-heating rates from 0.03 to 25 °C/min.

Temperature was monitored in the reactor and furnace by 1/16-inch diameter inconel-sheathed, grounded-junction Type K (chromel-alumel) thermocouples. The tip of the sample thermocouple was positioned approximately in the center of the sample. Temperatures were recorded with a Leeds and Northrup Speedomax 250 multipoint recorder, calibrated for Type K thermocouples. The recorder could monitor up to 10 signals simultaneously with time between successive readings of 1 second. Chart speed could be varied from 1/4 inch/hour to 15 cm/hour, selection being made on the basis of the expected heating rate.

Heating rates reported in this study were determined as the slope of the temperature-time plot produced by the recorder. For the slowest heating rates (~ 1°C/min) the sample temperature followed the programmed furnace temperature very closely, and sample heating rate was linear throughout the experiment. However, both the medium (~ 15°C/min) and high (> 100°C/min) rate experiments resulted in non-linear sample temperature versus time plots, with higher rates at lower temperatures (between 200-350°C). Since it is within that temperature range that the pyrolytic reactions of dehydration and depolymerization begin, it is probable that the heating rate estimated for that temperature range would be more closely related to char yield than would the average sample heating rate estimated over the entire range (20°C to $T_f > 500^\circ\text{C}$) or any other portion of the temperature-time plot. Thus, the heating rates reported herein are taken from the plots between 200-350°C for the medium rate experiments and below 350°C for the high rate experiments. Note also that the maximum controlled heating rate achievable with the furnaces used in this



- 1 Dessicant
- 2 Copper Turnings at 500°C
- 3 Rotameter
- 4a Reaction Flask
- 4b Top with tar trap
- 5 Furnace
- 6 Condenser
- 7 Condensibles Trap
- 8 Water Seal
- 9 Aspirator
- 10 Thermocouples
- 11 Recorder

Figure 1. Schematic of pyrolysis equipment.

study was approximately 25°C/min. Consequently, to achieve very high heating rates (> 100°C/min), it was necessary to immerse the reactor into the preheated furnace. Hence, the maximum sample heating rate increased with the final pyrolysis temperature.

The reactor top contained an integral tar trap which collected easily condensable materials. The remainder of the gaseous and condensable by-products and argon purge gas were routed via silicone rubber tubing to a water-cooled condensor and condensate trap, through a water seal to prevent inadvertent entrance of atmospheric oxygen, and finally to an aspirator discharging to the sewer.

Before a pyrolysis experiment began, the sealed reactor containing the sample was purged with argon (> 250 ml/min) for a minimum of one half hour to remove atmospheric oxygen. The argon flow was then lowered to approximately 50 ml/min for the duration of the pyrolysis experiment. The sample was held at the desired final temperature (500-900°C) for 1 hour, after which the furnace was lowered rapidly from around the reactor and the reactor allowed to cool. Argon flow was increased during the cooling phase to approximately 150 ml/min. When the sample temperature dropped below 100°C, the reactor bottom and char were transferred to a dessicator. Char was weighed in the reactor bottom and the yield of char calculated on a dry-weight basis. Preliminary experiments with lignocellulosics indicated for triplicate pyrolyses a standard deviation for char yield of 0.5-1% of the mean. Later experiments to elucidate char yield of lignocellulosics were run in duplicate with the same low standard deviation.

ACTIVATION

The equipment used in the activation experiments is schematically illustrated in Figure 2. Accurately weighed 1- to 3-gram char samples were placed on the frit of the quartz-glass, gas preheating assembly and the 750-ml quartz-glass activation chamber was fitted over the sample by means of a ground joint. The activation chamber had a frit at the top to allow gases to escape while retaining the char under activation and a ground joint to allow introduction of a thermocouple (identical to those described previously) for activation temperature measurement.

The entire activation assembly was connected via silicone rubber tubing to the purge and activation gas system. The argon system described previously was used to supply the inert purge gas. Carbon dioxide (99.9%) was used as the activating (oxidizing) gas with no further treatment. A three-way valve allowed virtually instant switching from argon to carbon dioxide and vice-versa. Gas flow was measured with rotameters (Matheson Gas Products, Tubes 600 and 603).

The activation chamber assembly could be lowered into and removed rapidly from the activation furnace (2-5 seconds). The activation furnace (5-inch I.D. x 12 inches deep) was constructed in the same manner as the pyrolysis furnace. Temperature was controlled within $\pm 5^\circ\text{C}$ with a Love Model 72-1 temperature controller. Furnace temperature was sensed with a Type K

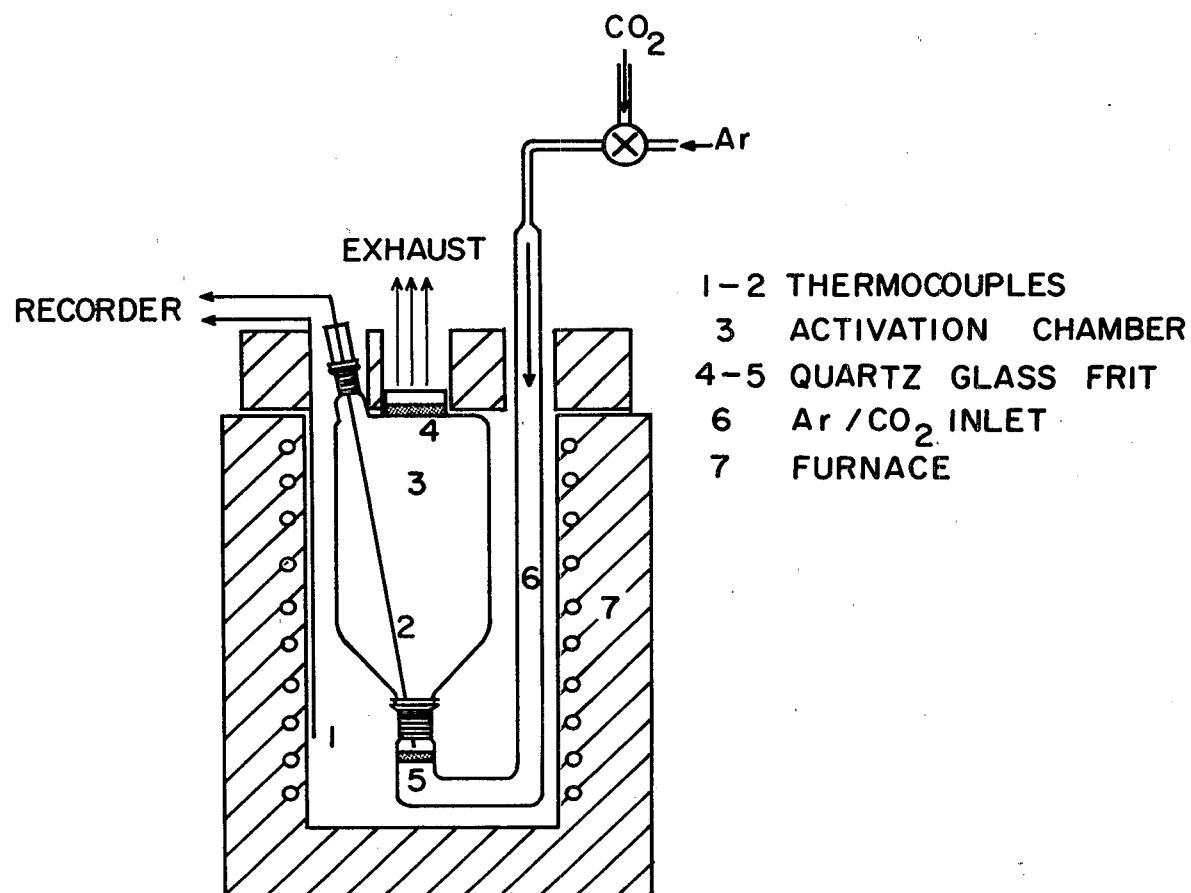


Figure 2. Schematic of activation equipment.

thermocouple (identical to those described above) and activation chamber and furnace temperature were recorded on the Leeds and Northrup multipoint recorder described previously.

Activation experiments were conducted by purging the preweighed char sample in the activation chamber for 20 min with argon while the entire assembly was outside the preheated furnace. The assembly was then lowered quickly into the preheated furnace; purging with argon continued until the desired temperature was reached within the activation chamber. At this point the gas valve was switched to admit carbon dioxide to the activation chamber and timing by stopwatch was begun. The gas flow rate for both argon and carbon dioxide were previously determined in trial runs to assure fluidization of the char samples at the activation temperature. The flow rate, of course, depended on the particle size and density of the char. For prune pit char activation, a CO_2 flow rate of 580 ml/min was used, whereas for RDF char a flow rate of greater than 3 l/min was necessary to achieve marginally acceptable homogeneity of fluidization, due to the clumping tendency of the RDF. At the end of the desired activation time (determined by iteration, since percent burnoff is of greater interest in this work than is activation time), the gas flow was switched to argon and the reactor quickly removed from the furnace and allowed to cool. When the interior temperature reached 100°C the activation assembly was opened and the char transferred to a weighing bottle or boat. Complete recovery was not possible, because some char visibly remained either on the top frit or side walls of the activation chamber. Nevertheless, percent burnoff for prune pit char had a standard deviation of only approximately 4% of the mean for three activation replications.

CHARACTERIZATION OF CHAR AND ACTIVATED CARBON

Percent Carbon

The percent carbon (dry-weight basis) of lignocellulosic chars was determined as described above under "Raw Materials Analysis."

Surface Area and Micropore Volume

The surface and pore characteristics of the chars and carbons were derived from gas adsorption isotherms determined with a Orr Model 2100 surface area and pore volume analyzer (Micromeritics Instrument Corporation, Norcross, Georgia). The adsorbate gases and adsorption temperatures used in this study were nitrogen at 77K, and carbon dioxide at 195K. For most chars, adsorption equilibrium was reached quickly ($\Delta p/\Delta t < 1.33$ Pa/min in 15 min), while for some others, adsorption was not completed after 18 hours. Adsorption equilibrium in activated carbon analysis was generally reached within 30 min. Only isotherms of experiments in which equilibrium was reached quickly (within 30-60 min) were evaluated quantitatively. The slower adsorption experiments were used to infer qualitative results only.

Adsorption isotherms were interpreted using the Brunauer-Emmett-Teller (BET) equation (Eq. 1) discussed earlier. In most experiments, the BET plot was linear within a fairly narrow range of relative pressures ($0.01 < p/p_s <$

0.10) and the data within that range were analyzed by linear regression for the calculation of surface area. Cross sectional areas of the adsorbed gases were taken as follows: $16.2 \times 10^{-20} \text{ m}^2$ for N_2 at 77K and $21.8 \times 10^{-20} \text{ m}^2$ for CO_2 at 195K (4). Saturation vapor pressures for the adsorbates were taken as 104 kPa (780 torr) and 105 kPa (787 torr) for N_2 at 77 K (14) and CO_2 at 195 K (83), respectively.

Pore size distributions were calculated from N_2 (77K) adsorption isotherms using the Kelvin equation (Eq. 4) and the method of Cranston and Inkley (12). This approach was quite useful for the activated carbons with a range of pore sizes. However, the chars, with porosity largely limited to micropores, did not adsorb much additional gas for $p/p_s > 0.4$, which corresponds to a pore radius of approximately 18 Å for N_2 adsorption at 77K. Consequently, for chars we do not report pore size distribution.

For use in the modified Kelvin equation, we assumed the following values for the constants applicable for nitrogen adsorption at 77K: surface tension of 8.9 dyne/cm, monolayer thickness of 0.43 nm and a molar volume of the liquid adsorbate of $34.9 \text{ cm}^3/\text{mole}$ (14).

Macro- and Transitional-Pore Volume

Macro- and transitional-pore volume was determined by mercury porosimetry by the American Instrument Corporation. Powdered char samples (50-100 mg) were analyzed in an Amingo mercury porosimeter and subjected to pressures up to 60,000 psi ($4.14 \times 10^8 \text{ Pa}$). Absolute pressure and volume of mercury were recorded simultaneously. Pore radii were calculated from intrusion pressure using the Washburn equation (Eq. 6). Mercury-carbon contact angle was assumed to be 130° . Results were corrected by the American Instrument Company for temperature and for compression of mercury by subtracting the mercury penetration previously measured in the identical sample flask without porous solid sample. No correction was made for compression or collapse of the sample. Estimates of pore volume based on mercury penetration data to 60,000 psi do not take into account closed porosity or volume in open pores less than 3 nm in diameter.

MEASURING ADSORPTION OF ORGANICS FROM WASTEWATER EFFLUENT

Determination of Organic Carbon

The dissolved organic carbon (DOC) of effluent samples was determined by placing 3 to 10 ml of sample into an ampule, along with make-up water, $\text{K}_2\text{S}_2\text{O}_8$ and 10% phosphoric acid reagents. In the presence of the acid, inorganic carbon in the sample was converted to CO_2 at room temperature. This inorganic carbon was removed by purging the ampule contents with hydrocarbon-free oxygen. The ampule mouths were then melted shut by an Oceanography International ampule sealer. The sealed ampules were next autoclaved at 121°C for 4 hours, during which time the organic matter in the sample was decomposed to CO_2 .

To determine the CO_2 present, the sealed mouth of the ampule was crushed within a closed space that was connected by Teflon tubing to a Dohrmann D-52

analyzer. The CO_2 was stripped from the ampule and delivered to the analyzer by a stream of inert carrier gas. Within the instrument, the CO_2 was catalytically converted to CH_4 , and the CH_4 subsequently carried to a Flame Ionization Detector; the ions were then collected by an electrode surrounding the flame. The electrical impulse was amplified and detected by an electrometer. By comparing the digital readout of an unknown sample with the readout from known standards, one could determine the organic carbon content of the unknown samples (84).

DOC Uptake Rate Experiments

Both adsorption rate experiments and the adsorption equilibrium isotherm experiments were conducted with unchlorinated secondary effluent which was collected from the Palo Alto Regional Water Quality Control Plant. This effluent was first vacuum-filtered through a 0.45- μm millipore filter. Such filtration effectively excluded any bacteria from the secondary effluent, thus minimizing the risk of biological degradation during sorption experiments. If not used immediately, the filtered effluent was stored at 4°C. The sample was always used within 24 hours so that biodegradation would be minimized.

The isotherm tests were performed in a series of 250-ml erlenmeyer flasks, one flask for each time interval analyzed (e.g., 1 min, 2 min, etc.). One set of flasks was used for each kind of carbon. Into each of these flasks was placed a known amount of activated carbon together with 10 ml. of organic-free water (prepared with a Milli-Q™ water purification system). The activated carbon samples were then degassed in a vacuum chamber for 30 min to ensure that the internal pores of the carbon were completely wetted with the organic-free water. This step was taken to ensure that the rate of solute uptake during adsorption rate experiments would not be affected by the simultaneous penetration of the internal porosity by the solvent (water).

Next 100 ml of filtered effluent was added, and the flasks covered and shaken on a shaker table at room temperature (20 to 25°C) for the specified time. A wastewater sample without any activated carbon was included as a control.

Immediately after the specified time of adsorption, the wastewater sample was forced through a rinsed 0.45- μm millipore filter to separate the activated carbon from the wastewater. This step was included to ensure that the adsorption process would cease at the intended time and also that the activated carbon would not be collected into the DOC ampule and contribute to the DOC measurement. The pressure was applied to the water sample above the filter by a syringe system (Luer-Lok, Becton-Dickinson and Company). It was found that the millipore filter pads consistently leached 1.78 ± 0.11 mg DOC into these samples; therefore, the pads were rinsed four times before use to minimize contamination. The DOC of the water samples was determined in triplicate by the method described above.

DOC Adsorption Equilibrium Experiments

DOC adsorption isotherm experiments were conducted with materials and procedures much like those used for the adsorption rate experiments.

Unchlorinated secondary effluent was filtered, then introduced into erlenmeyer reaction flasks together with a known quantity of pre-wetted activated carbon. The contents were shaken for a period of 24 hours at 20-25°C. Samples were collected and prepared in ampules as described above and analyzed on the Dorhmann DC-52 instrument.

However, in these experiments, the parameter of concern was the ratio of activated carbon to volume of wastewater, rather than time. Moreover, for the equilibrium isotherm experiments, reaction flasks were shaken for 24 hours to assure that equilibrium conditions had been established. If longer equilibrium times had been chosen, biological or photochemical decomposition might have played a significant role. System controls without activated carbon were run to permit evaluation of the extent of DOC concentration decrease not attributable to the presence of the adsorbent.

Ideally in adsorption isotherm experiments, the equilibrium concentration of the adsorbate is varied over several orders of magnitude (66). However, in our case this was not feasible. The upper limit for our experiments was established by the concentration of DOC in real secondary effluent (10 to 14 mg/l); the practical lower limit was a result of the fact that between 0.5 and 1.0 mg/l of the initial DOC was unadsorbable. These constraints limited to one order of magnitude the range of concentration data which could be obtained.

SECTION 7

RESULTS AND DISCUSSION

PYROLYSIS AND ACTIVATION OF LIGNOCELLULOSICS AND REFUSE-DERIVED FUEL

Introduction

A wide range of both virgin and waste materials has been studied for the production of activated carbon (1). However, much of the research has been conducted by activated carbon manufacturers and is therefore proprietary and unavailable to the public. The published research on pyrolysis and activation for activated carbon production is mainly confined to coal and coal products. There are some published results for pyrolysis and activation of lignocellulosics (e.g., 2,3,85,86,87), but they are generally confined to specific educts or sets of pyrolysis conditions. In general it appears that the results of activation depend to some degree on the nature of the educt, its processing history (carbonization) and the characteristics of the char (1,39,40). The purpose of this section is to examine a wide range of lignocellulosics to develop an understanding of the dependence of char yield and physical characteristics on the educt composition and pyrolysis conditions. Additionally we examine the activation of one lignocellulosic material in some detail. Finally, refuse-derived fuel (RDF), prepared by classification of municipal solid waste, is pyrolyzed and activated for comparison with results obtained with the model lignocellulosics.

Char Yield as a Function of Lignocellulosic Composition

Representative subsamples of the 22 materials selected for this program were prepared for analysis and experimentation as described in Section 6. The 44 pyrolysis experiments (duplicates for each material) were performed in random order to avoid bias. Table 1 lists the results of the educt analyses and pyrolysis experiments. The pyrolysis temperature was raised at approximately 15°C/min to 500°C, then held for 1 hour at that final value. The heating rate was selected to allow comparison with the results of published thermogravimetric studies of cellulose and lignocellulosics, generally conducted at 15°C/min (33,35,38). The final temperature was selected as the lowest temperature at which the majority of pyrolytic decomposition and weight loss would be complete and significant porosity would have developed, based on published results on cellulose and lignocellulosics (26,33).

As discussed previously, there is reason to expect (10,11) that char yield could be predicted for a given set of pyrolysis conditions with an equation of the following form

TABLE 1. SUMMARY OF LIGNOCELLULOSIC COMPOSITION AND CHAR YIELD PYROLYSIS CONDUCTED AT 15°C/MIN TO 500°C

	Composition, % ^a						Char Yield, %			
	α_{ash}	α_{sfa}	α_{ext}	α_{lig}	α_{cell}	Exp.#1	Exp.#2	Average Yield	S ^b	Ash-Free ^c Yield
1 Pecky Cedar	0.88	nd ^d	13.05	70.26	15.81	48.94	49.50	49.22	0.4	48.77
2 Peat	14.72	10.75	3.56	55.30	26.42	51.60	49.91	50.76	1.2	42.26
3 CBR	0.49	nd	10.96	46.59	41.96	40.27	38.55	39.41	1.2	39.11
4 Prune Pits	0.62	nd	5.87	35.72	57.79	30.67	30.37	30.52	0.2	30.09
5 Walnut Shells	1.65	nd	5.20	30.68	62.47	32.51	33.31	32.91	0.6	31.78
6 Steer Manure	17.85	12.32	2.75	31.49	47.91	46.68	45.32	46.00	1.0	34.27
7 Coconut	0.92	nd	2.50	35.04	61.54	33.89	33.42	33.66	0.3	33.04
8 Newsprint	0.27	nd	1.41	20.05	78.27	25.32	25.77	25.55	0.3	25.36
9 White Fir	0.25	nd	1.16	29.27	69.32	27.53	27.91	27.72	0.3	27.54
10 Redwood	0.15	nd	11.95	34.45	53.45	33.23	34.10	33.67	0.6	33.57
11 Walnut Wood	0.41	nd	8.02	21.93	69.64	27.64	27.48	27.56	0.1	27.26
12 Wheat Straw	8.16	3.59	5.74	18.83	67.27	34.78	35.11	34.95	0.2	29.17
13 Barley Straw	10.09	5.25	8.13	14.80	66.98	35.47	35.01	35.24	0.3	27.97
14 Bean Straw	7.90	7.90	8.92	13.53	69.65	31.44	31.15	31.30	0.2	25.41
15 Rice Straw	11.61	2.79	5.12	11.02	72.25	34.83	34.57	34.70	0.2	26.12
16 Corn Stover	5.90	4.13	9.92	12.97	71.21	31.56	31.36	31.46	0.1	27.16
17 Bagasse	3.54	2.87	2.97	19.83	73.66	31.50	31.15	31.33	0.3	28.81
18 Red Oak	0.25	nd	4.33	19.33	76.09	25.34	26.36	25.85	0.7	25.66
19 Kraft Paper	1.01	nd	1.18	13.76	84.05	24.82	25.26	25.04	0.3	24.28
20 Computer Paper	6.66	3.00	0.81	0.97	91.56	27.14	26.91	27.02	0.2	21.81
21 Cellulose, EM	0.0065 ^e	nd	0	0	~ 100	21.96	21.28	21.62	0.5	21.61
22 Cellulose, Sigma	0.19	nd	0	0	99.81	19.40	18.61	19.01	0.6	18.86

^a α_{ash} = % ash, α_{sfa} = % silica-free ash, α_{ext} = % benzene-ethanol extractives, α_{lig} = % lignin, and α_{cell} = % holocellulose (i.e., total carbohydrate or hemicellulose + cellulose) which is determined by difference: $\alpha_{\text{cell}} = 100 - \alpha_{\text{ash}} - \alpha_{\text{ext}} - \alpha_{\text{lig}}$.

^bStandard deviation of char yields.

^cAsh-free yield = [(average yield - α_{ash})100]/[100 - α_{ash}], which assumes no change of weight in ash during pyrolysis.

^dnd = not determined. ^eSource: P. Brunner, 1976. Original datum from EM technical pamphlet.

$$Y = (c_0 + c_1(\alpha_{sfa})^x) \alpha_{cell} + c_2 \alpha_{lig} + c_3 \alpha_{ext} + c_4 \alpha_{ash} \quad (15)$$

where

c_0, c_1, \dots, c_4 = coefficients determined by multiple regression,

x = exponent to account for the increased char yield from holocellulose believed to be caused by inorganics ($x < 1$), and

$\alpha_{cell}, \alpha_{lig}, \alpha_{ext}, \alpha_{ash}, \alpha_{sfa}$ = fractions of holocellulose, lignin, extractives, ash, and silica-free ash in the starting material.

The model assumes that the overall char yield is simply a sum of the char yields of the components and that there is no interaction between the components during pyrolysis, except that certain inorganics (represented here by silica-free ash) increase the char yield of the holocellulose fraction in a way that can be modeled as a power function. This is the approach supported by the work of Rothermel (37) who developed a model for char yield as follows:

$$Y = [0.0917 + 0.5(\alpha_{sfa})^{0.462}] \alpha_{cell} + 0.624 \alpha_{lig} + 0.285 \alpha_{ext} + \alpha_{ash} \quad (16)$$

Pyrolysis was accomplished in Rothermel's experiments in thermogravimetric equipment at 15°C/min to 400°C. However, their model was developed in a statistically unconvincing way. Furthermore, certain coefficients seemed suspect based on our work with pure cellulose and reported values for lignin char yield (32). Specifically, we expected the value of c_0 in equation 15 to be approximately 0.20 rather than 0.0917 and the value of c_2 to be approximately 0.55 instead of 0.624.

Subsets of our lignocellulosic composition and char yield data were analyzed by computerized multiple regression techniques. The results of these analyses are listed in Table 2. Regressions were performed using either ash or silica-free ash in the power function to test the hypothesis that silica-free ash is more fundamentally related to catalysis of holocellulose char yield. For materials for which silica-free ash had not been determined (i.e., those with ash contents lower than 2%), we assumed silica-free ash to be equal to ash content for the purposes of the regression analysis. The decision to limit the silica-free ash data was based on the high cost of commercial analysis. Initial regression analysis with incomplete silica-free ash values were expected to indicate whether, in fact, using silica-free ash in the power function resulted in a better fit of the model to the experimental data. Had this been true, additional silica-free ash analyses would have been warranted. As discussed below, however, this was not the case.

The multiple regressions summarized in Table 2 all set the power function exponent equal to 0.462, a value taken from the work of Rothermel and others (36,37) on the effect of fire-retardant additives on cellulose char yield. This assumption was made to allow initial analysis of the data by standard linear multiple regression techniques.

TABLE 2. SUMMARY OF RESULTS OF MULTIPLE REGRESSIONS VARYING THE DATA UTILIZED AND THE INORGANIC PARAMETER IN THE POWER FUNCTION

Code	Materials Included in Analysis	Parameter Used in Power Function	Regression Coefficients ^a					Multiple Correlation Coefficient (r ²) ^b
			c ₀	c ₁	c ₂	c ₃	c ₄	
Ia	All 22	α _{ash}	0.185	0.0722	0.540	0.411	0.97	0.9982
Ib		α _{sfa}	0.192	-0.0001	0.529	0.456	1.06	0.9981
Ic		None	0.192	set = 0	0.529	0.456	1.06	0.9981

Materials with								
IIa	α _{ash} < 11.61 & α _{sfa} < 7.90	α _{ash}	0.188	-0.0025	0.551	0.368	1.16	0.9978
IIb		α _{sfa}	0.192	-0.0613	0.551	0.374	1.24	0.9978

Materials with								
III	α _{sfa} < 5.25	α _{sfa}	0.188	0.0059	0.542	0.411	1.17	0.9979

Materials with								
IV	α _{sfa} < 4.13	α _{sfa}	0.188	0.0059	0.541	0.419	1.19	0.9978

^aExperimental data is fit by multiple regression to a model of the following form

$$\text{Char Yield} = \{c_0 + c_1(\text{inorganic parameter})^{0.462}\} \alpha_{cell} + c_2 \alpha_{lig} + c_3 \alpha_{ext} + c_4 \alpha_{ash}$$

where α is expressed as a fraction (i.e., $\alpha < 1$).

^bAnalysis of variance allows computation of the multiple correlation coefficient (r^2), adjusted for the sample size.

All materials were included in the regressions coded Ia and Ib in Table 2. It is apparent from the values of r^2 listed in the table that, for the full set of materials, using either α_{ash} or α_{sfa} in the power function results in a very good fit of the model to the data ($r^2 > 0.99$). Furthermore, use of α_{sfa} in the power function results in a value of c_1 which is statistically indistinguishable from zero (confidence limits contain zero). This result is particularly interesting in light of the expectation that silica-free ash would be a better indicator of inorganic catalysis of carbohydrate pyrolysis than total ash content. Had this expectation been correct we would have anticipated $c_1 > 0.0722$, the coefficient derived when total ash content was used in the power function. Thus it appears that the model could be simplified to a simple linear additive form without any loss in predictive ability (i.e., eliminate the power function altogether). The analysis coded Ic in Table 2 is a separate regression for this simple linear model (setting $c_1 = 0$) which verifies this conclusion.

There are two possible reasons for the apparent negligible effect of inorganics on carbohydrate char yield: 1) the catalytic effect is thought to saturate at relatively low ash contents (5-7% or lower) (35,36), whereas some of our materials have ash contents as high as 17.9%; and 2) the assumed power function exponent (0.462) may be too high.

Regressions IIA, IIb, III, and IV (Table 2) were performed to examine the possibility that the effect of inorganic catalysis was underestimated due to the inclusion of materials with high ash contents. By restricting our analysis to materials of successively lower ash contents as in II, III, and IV, we might expect the catalytic effect to become more observable as evidenced by an increase in coefficient c_1 determined by the regression. This, however, was not observed. In fact, due to the large standard deviations of coefficient c_1 as determined in analyses II through IV, statistically the coefficients cannot be distinguished from zero (confidence limits for c_1 contain zero).

To examine the possibility that the assumed power function exponent was too high, we analyzed the full set of data with a nonlinear multiple regression technique to generate a new estimate for the exponent. This resulted in a slightly higher estimate (~ 0.48) than originally assumed, while confidence limits for c_1 again contained zero.

These results favor the acceptance of the char yield model Ic in Table 2, which assumes no detectable effect of inorganics on holocellulose char yield. Examination of the other coefficients lends additional support to the model. Coefficient c_0 indicates a holocellulose char yield for pyrolysis at 15°C/min to 500°C of 19.2% which is consistent with Brunner's results for pure cellulose in similar experimental equipment (26). Coefficient c_2 indicates a lignin char yield of 52.9%, which is within the range of Särkanen's observations (32) and thermogravimetric results of Shafizadeh and McGinnis (33). Coefficient $c_4 = 1.06$ indicates that slightly more inorganics are recovered in the pyrolytic char than are measured by the standard ash analysis (ignition overnight at 600°C). Considering that the ash analysis is carried out at a higher temperature, for a longer time, and in the presence of atmospheric oxygen, it is quite reasonable that ash by ignition would underestimate inorganic recovery in a char pyrolyzed in an inert atmosphere to 500°C.

Coefficient $c_3 = 0.456$ indicates the char yield from extractives to be higher than that predicted by Rothermel's model (0.285). Rothermel's value was derived from work by others (38) on thermogravimetric analysis of extractives from six lignocellulosic "fuels" (generally wood, stems, and leaves). A possible problem is that the compounds measured by the extraction process vary widely with the plant material and include oils, waxes, resins, tannins, gums, phenolics, and terpenes. It is likely these compounds vary somewhat in their pyrolytic char yield and therefore we might expect coefficient c_4 to be sensitive to the materials used in its derivation. Since our data base includes a much larger sample of lignocellulosics, it is reasonable to assume that our value is more generally applicable.

In conclusion, the results presented here suggest that lignocellulosic char yield for pyrolysis at 15°C/min to 500°C can be predicted satisfactorily with the model listed in Table 2 as Code Ic. The fit of the model's

predictions to the experimental char yield data is displayed graphically in Figure 3. The spread of the measured values around the predicted values is small, and the variance appears to be independent of the predicted yield. There is no evidence of deviation for low-lignin, high-cellulose materials (low predicted yields), nor for high-lignin, low-cellulose materials (high predicted yields)

As a test of the ability of the above model to predict char yield, we performed duplicate pyrolysis experiments on refuse-derived fuel (RDF). RDF is prepared from municipal solid waste and therefore would be expected to be quite heterogeneous, as confirmed in Section 6. These complications notwithstanding, the RDF was subjected to exactly the same composition analysis and pyrolysis conditions as were the materials used to derive the char yield model.

Table 3 lists the results of the composition analysis and the pyrolysis experiments. Also listed is the char yield predicted by the model on the basis of the composition. The model thus appears to overestimate the yield. However, the 95% confidence interval for the model's prediction is [40.5, 34.4] compared to the experimental value of 34.2%, whose 95% confidence limits are [35.3, 33.1]. Thus there is reasonable agreement of experimental and predicted yields, considering the assumption that RDF could be treated like a natural lignocellulosic material.

In fact, RDF contains plastic, which is not taken into account in the above prediction. Because plastics are not soluble in neutral solvents or subject to acidic hydrolysis, the plastic content of RDF will be measured as lignin in the composition analysis. By hand-sorting of a 100-gram subsample of unground RDF, its plastic content was estimated to be approximately 4.9% (dry weight basis), which is within the range expected for glass and metal-free refuse (88). The pyrolytic yield of plastics or synthetic polymers is known to vary with the polymer structure (89); e.g., polystyrene and polyethylene are almost entirely volatilized, PVC (polyvinyl chloride) char yield is on the order of 25%, and some polymers used as binders in pelletized activated carbon manufacture have yields as high as 50-60%.

If we assume that the true lignin content of RDF lignin is given by the measured value (15.75%) less the 4.9% plastic content, then the best estimate of RDF's lignin content is $15.75 - 4.9 = 10.85\%$ lignin. Further assuming that

TABLE 3. COMPOSITION AND CHAR YIELD OF REFUSE-DERIVED FUEL (RDF)

Composition (%)				Char Yield Pyrolysis at 15°C/min to 500°C		
α_{cell}	α_{lig}	α_{ext}	α_{ash}	Predicted by Model	Experimental	
					Mean	Std. Dev.
61.91	15.75	10.66	11.68	37.46	34.18	0.12

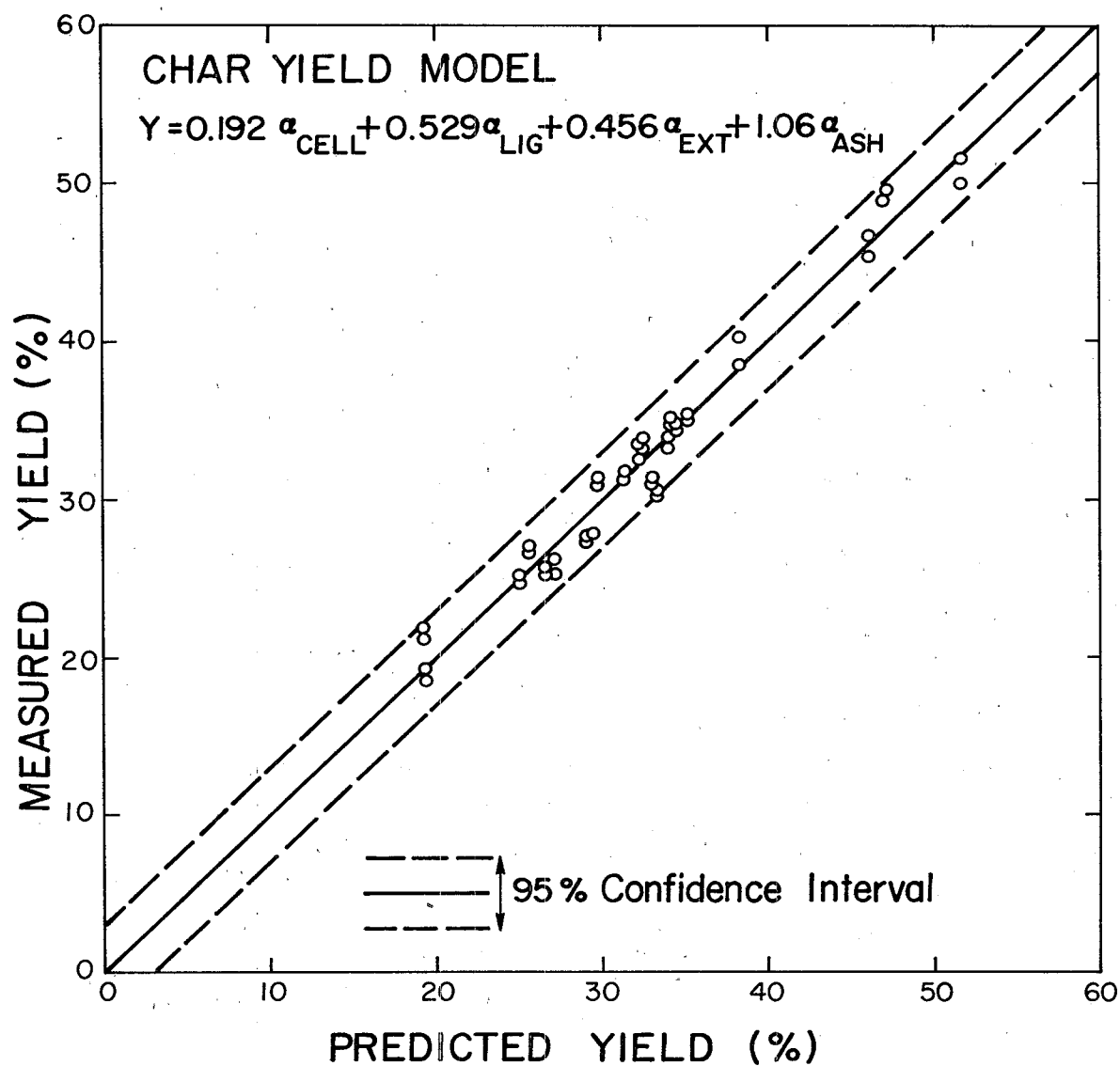


Figure 3. Measured yield versus yield predicted by char yield model for pyrolysis at 15°C/min to 500°C

the plastic is equally divided between polyethylene and PVC-type plastics, our char yield prediction is revised to approximately 35.46% for RDF, which agrees well with the measured value of 34.2%. This further supports the predictive ability and wide applicability of the char yield model as presented.

Char Yield as a Function of Pyrolysis Conditions

To evaluate the dependence of char yield on pyrolysis conditions, a series of experiments was performed with a small subset of lignocellulosics, chosen to represent the full range of compositions encountered. Pecky cedar was selected as a very high-lignin, low-ash material. Redwood served as a moderately high-lignin, low-ash sample, representative of softwoods. Corn stover was included as representative of agricultural wastes, having a relatively low-lignin, high-ash composition. Computer paper was selected as representative of finished paper products and also because it is composed almost entirely of cellulose and inorganics. Thus the subset of lignocellulosics used in this portion of the study included the extremes of composition likely to be encountered in waste materials, as well as samples of more common composition. This approach was taken to highlight any effect that educt composition might exert on the relationship between pyrolysis conditions and char yield (also char physical characteristics as discussed later).

The pyrolysis conditions varied in this experimental program were heating rate (ϕ) and final pyrolysis temperature (T_F). The heating rates studied were 1°C/min, 15°C/min and the maximum heating rate achievable with our equipment ($> 100^\circ\text{C}/\text{min}$ and dependent on T_F as discussed in Section 6). Pyrolysis was conducted at each of the heating rates to final pyrolysis temperatures of 500°, 700°, and 900°C. Additional pyrolysis experiments to 600°C were conducted at 15°C/min.

Results of the pyrolysis experiments under varying conditions are listed in Table 4. Standard deviations of the yield for duplicate experiments were again on the order of 1 to 2% of the mean. To allow comparisons between the materials using the original volatile solids content as a measure of potentially pyrolyzable organic material, ash-free yields were calculated as indicated in Table 4. Ash-free yield is simply a comparison of the oxidizable mass present before and after pyrolysis and is calculated using ash data derived in a separate set of analyses reported in Table 5. Ash contents were determined by ignition in a muffle furnace to the indicated temperature. For materials with α_{ash} less than 1% (600°C), we assumed α_{ash} at higher temperatures to be unchanged. For such low ash contents the correction from yield on total weight basis to ash-free yield is small enough such that refinement of α_{ash} values at $T > 600^\circ\text{C}$ would have insignificant effect on the calculation.

As an alternative method of comparing pyrolytic behavior of the materials, the yield of carbon was calculated using the results of percent carbon analyses of the educts and chars. The results of the analyses and the calculated carbon yields are presented in Table 6. Percent carbon data were not obtained for the high heating rate chars. Neither percent carbon data nor carbon yields are adjusted to account for the carbon which may be present in the inorganic fraction of the educts, e.g., as carbonates, and possibly lost during pyrolysis (e.g.,

TABLE 4. SUMMARY OF PYROLYSIS OF SELECTED LIGNOCELLULOSICS FOR VARYING PYROLYSIS CONDITIONS

Material	Final Temp. °C T _F	Heat Rate ^a (°C/min), ϕ		Yield %				Ash-Free Yield, % ^b	
		Exp.1	Exp.2	Exp.1	Exp.2	Ave.	s	Ave.	s ^c
A. Low Heating Rate									
Redwood	500	0.99	0.91	37.93	37.46	37.70	0.33	37.60	2.53
	700	0.95	0.98	32.58	32.45	32.52	0.09	32.41	2.16
	900	0.97	0.99	30.38	30.28	30.33	0.07	30.23	2.02
Corn Stover	500	0.99	0.98	33.84	33.64	33.74	0.14	29.58	0.24
	700	0.96	0.99	30.82	30.59	30.71	0.16	26.50	0.40
	900	0.98	1.00	28.63	28.21	28.42	0.30	24.47	0.84
Computer Paper	500	0.96	0.96	33.58	33.45	33.52	0.09	28.77	0.15
	700	0.98	—	29.86	—	29.86	—	24.88	—
	900	0.97	1.01	27.05	26.83	26.94	0.16	21.84	0.21
Pecky Cedar	500	1.06	—	50.38	—	50.38	—	49.94	—
	700	0.99	—	43.51	—	43.51	—	43.01	—
	770	1.02	—	41.96	—	41.96	—	41.44	—
	900	0.98	—	40.10	—	40.10	—	39.57	—
Sigma Cellulose	700	0.99	—	24.63	—	24.63	—	24.48	—
B. Intermediate Heating Rate									
Redwood	500	16.5	16.8	33.23	34.10	33.67	0.62	33.57	2.32
	600	15.2	—	29.39	—	29.39	—	29.28	—
	700	18.5	19.2	28.01	27.97	27.99	0.03	27.88	1.86
	900	18.3	17.5	27.16	27.02	27.09	0.10	26.98	1.80
Corn Stover	500	15.9	17.7	31.56	31.36	31.46	0.14	27.17	0.22
	600	15.9	—	29.71	—	29.71	—	25.30	—
	700	19.0	18.2	28.62	28.74	28.68	0.08	24.35	0.35
	900	18.5	17.9	27.94	28.13	28.04	0.13	24.06	0.79
Computer Paper	500	16.0	15.7	27.14	26.91	27.03	0.16	21.82	0.16
	600	15.9	—	24.92	—	24.92	—	19.56	—
	700	17.7	17.3	24.25	24.43	24.34	0.13	18.97	0.11
	900	15.5	15.0	23.50	23.45	23.48	0.04	18.13	0.14
Pecky	500	17.5	17.8	48.94	49.50	49.22	0.40	48.77	0.68
	700	18.3	18.4	42.25	42.27	42.26	0.01	41.75	0.47
	900	17.0	17.2	40.42	40.59	40.51	0.12	39.98	0.47
Sigma Cellulose	700	14.3	—	17.94	—	17.94	—	17.78	—

TABLE 4 cont.

TABLE 4 cont.

Material	Final Temp. °C T _F	Heat Rate ^a (°C/min), φ		Yield ^d %				Ash-Free Yield, % ^b	
		Exp.1	Exp.2	Exp.1	Exp.2	Ave.	s	Ave.	s ^b
C. High Heating Rate									
Redwood	500	105	105	28.18	27.95	28.07	0.16	27.96	1.87
	700	200	270	22.24	22.25	22.25	0.01	22.13	1.48
	900	333	--	20.68	--	20.68	--	20.56	--
Corn Stover	500	96	110	29.56	29.13	29.35	0.30	24.91	0.30
	700	228	235	26.58	26.33	26.46	0.18	22.00	0.34
	900	405	--	25.35	--	25.35	--	21.23	--
Computer Paper	500	115	105	22.68	22.80	22.74	0.08	17.23	0.10
	700	280	d	19.52	18.99	19.26	0.37	13.53	0.26
	900	425	375	17.50	17.20	17.35	0.21	11.58	0.17
Sigma Cellulose	700	183	--	12.17	--	12.17	--	12.00	--

^aSee discussion in text.

^bAsh-free yield = $\frac{(\% \text{ Yield} - \alpha_{\text{ash}}^T)100}{(100 - \alpha_{\text{ash}}^T)}$, where α_{ash}^T = % ash of raw material

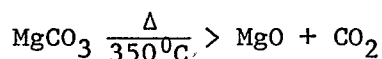
as measured by ignition to T°C. See discussion in text.

^cStandard deviation of ash-free yield estimated by the following expression:

$$S_{\text{AFY}} = Y_{\text{AF}}[(S_Y/Y)^2 + (S_A/\alpha_{\text{ash}})^2]^{1/2}$$

where Y_{AF} = average ash-free yield (%), Y = average yield (%), S_Y = standard deviation of yield (%), α_{ash} = average percent ash of educt (%), and S_A = standard deviation of ash (%).

^dHeating rate unknown since sample thermocouple was accidentally disconnected from recorder for first portion of experiment (< 400°C).



(90)). Calculations which assumed the entire change in ash weight (Table 5) was due to carbonate volatilization indicated that the necessary correction to carbon yield was less than 1% of the uncorrected carbon yield and therefore justifiably ignored.

Figure 4 displays ash-free yield as a function of final pyrolysis temperature (T_F) for the low and medium heating rates. Linear regressions of the data are used, since the plotted data had been shown to be statistically indistinguishable from the linear regressions (Appendix A). Similarly, Figure 5 displays ash-free yield as a function of T_F for the high heating rates,

TABLE 5. DEPENDENCE OF ASH CONTENT OBSERVED UPON IGNITION
TO VARYING FINAL TEMPERATURES

Material	Ash Content (α_{ash}^T)								
	T = 600°C			T = 700°C			T = 900°C		
	Ave. %	n ^a	s ^b	Ave. %	n	s	Ave. %	n	s
Computer Paper	6.66	3	0.03	6.63	4	0.01	6.53	4	0.05
Corn Stover	5.90	3	0.04	5.72	4	0.08	5.23	4	0.17
Redwood	0.15	3	0.01	--			--		
Pecky Cedar	0.88	3	0.01	--			--		
Sigma Cellulose	0.19	3	0.02	--			--		

^an = number of analyses.

^bs = standard deviation in same units as average.

which are influenced by T_F for reasons described in Section 6. Figure 6 shows carbon yield as a function of T_F , again using linear regressions of the data for the same reason (Appendix A). It should be noted that the "regression" of pecky cedar data ($\phi = 1^\circ\text{C}/\text{min}$) contains only two points, but is included nonetheless for purposes of comparison.

Figures 4 and 6 indicate that for a given heating rate, the slope of the yield versus T_F plots ($T_F > 500^\circ\text{C}$) are essentially the same for the range of lignocellulosics studied. Thus it appears that char yield for pyrolysis of any lignocellulosic is largely determined at temperatures below 500°C , the weight loss above 500°C being relatively independent of educt composition, at least for a given heating rate. This is consistent, of course, with the fact that the major pyrolytic weight loss occurs in the range $225\text{--}500^\circ\text{C}$ for each of the major lignocellulosic components (34).

Somewhat surprising is the observation that the slope of the plots is steeper for the lowest heating rate, both for ash-free and carbon yields. Thus the char yield improvement resulting from slow pyrolysis below 500°C is somewhat eroded by continuing the slow heating rate to higher temperatures. This is particularly evident in the case of corn stover which, despite the increased char yield (ash-free or carbon) for slow pyrolysis to 500°C , has virtually identical yield for pyrolysis at medium and low heating rates to 900°C . A similar effect is seen for pecky cedar (ash-free yield) and computer paper (carbon yield). This effect may be due simply to the greatly increased time of exposure to the higher temperatures for the low-rate pyrolysis. The results suggest, furthermore, that maximization of char yield for lignocellulosic pyrolysis may involve heating at different rates through different temperature ranges: low rate below 500°C followed by more rapid heating to the final desired temperature.

TABLE 6. CARBON CONTENT AND CARBON YIELD FOR VARYING PYROLYSIS CONDITIONS

Material	ϕ/T_F °C/min °C	Percent Carbon				Percent Yield			
		Educt (C_O)		Char (C_C)		Gross Wt. (Y)		Carbon (Y_C) ^a	
		Ave.	s_O	Ave.	s_C	Ave.	S_Y	Ave.	s^b
Redwood	1/500	53.69	0.38	87.94	0.65	37.70	0.33	61.75	0.83
	1/700	"	"	93.50	0.71	32.52	0.09	56.63	0.61
	1/900	"	"	99.05	0.81	30.33	0.07	55.95	0.62
Redwood	15/500	53.69	0.38	86.96	1.93	33.67	0.62	54.53	1.62
	15/600	"	"	93.05	0.89	29.39 ^c	--	50.94	0.61 ^d
	15/700	"	"	97.47	1.44	27.99	0.03	50.81	0.83
	15/900	"	"	98.68	1.06	27.09	0.10	49.79	0.67
Corn Stover	1/500	45.03	0.99	74.79	0.64	33.74	0.14	56.04	1.34
	1/700	"	"	76.65	1.15	30.71	0.16	52.27	1.42
	1/900	"	"	75.07	1.23	28.42	0.29	47.38	1.39
Corn Stover	15/500	45.03	0.99	70.62	1.17	31.46	0.14	49.34	1.38
	15/600	"	"	72.73	1.24	29.71 ^c	--	47.99	1.34 ^d
	15/700	"	"	75.45	2.81	28.68	0.09	48.05	2.08
	15/900	"	"	76.15	1.19	28.04	0.13	47.42	1.30
Computer Paper	1/500	40.39	0.41	69.39	1.26	33.52	0.10	57.59	1.21
	1/700	"	"	75.04	1.11	29.86 ^c	--	55.48	1.00 ^d
	1/900	"	"	72.82	0.93	26.94	0.16	48.57	0.84
Computer Paper	15/500	40.39	0.41	65.53	0.73	27.02	0.16	43.84	0.71
	15/600	"	"	70.87 ^c	--	24.92 ^c	--	43.73	0.44 ^d
	15/700	"	"	70.94 ^c	--	24.34	0.13	42.75	0.49 ^d
	15/900	"	"	68.00 ^c	--	23.48	0.04	39.53	0.41 ^d
Pecky Cedar	1/500	58.32	0.35	86.55	2.06	50.38 ^c	--	74.77	1.84 ^d
	1/700	"	"	94.49	1.06	43.51 ^c	--	70.49	0.90 ^d
	1/900	"	"	--	--	40.10 ^c	--	--	--
Pecky Cedar	15/500	58.32	0.35	84.00	1.63	49.22	0.40	70.89	1.55
	15/700	"	"	92.29	0.04	42.26	0.02	66.88	0.40
	15/900	"	"	96.75	1.95	40.51	0.12	67.20	1.43
RDF	15/500	45.27	0.04	61.72	0.47	34.18	0.12	46.60	0.39
	15/900	"	"	65.07	2.11	30.60	0.24	43.98	1.47

^aPercent Carbon Yield = $Y_C = C_C/C_O(\bar{Y})$.^bStandard deviation of Y_C estimated by

$$s = Y_C [(S_O/C_O)^2 + (S_C/C_C)^2 + (S_Y/Y)^2]^{1/2}.$$

^cOnly one experimental value.^dEstimated by setting missing s values (s) = 0.

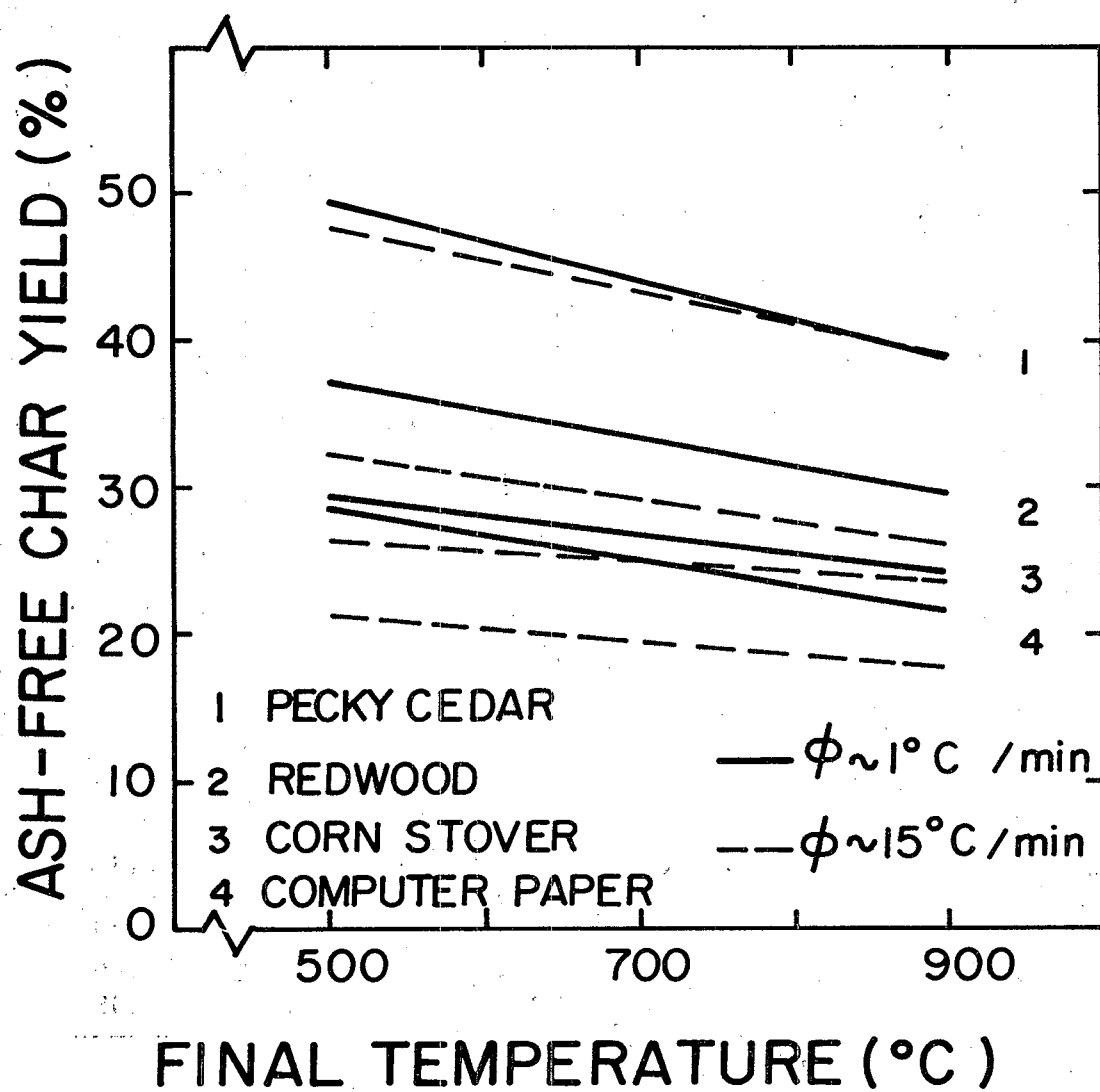


Figure 4. Ash-free char yield versus final temperature: low and medium heating rates

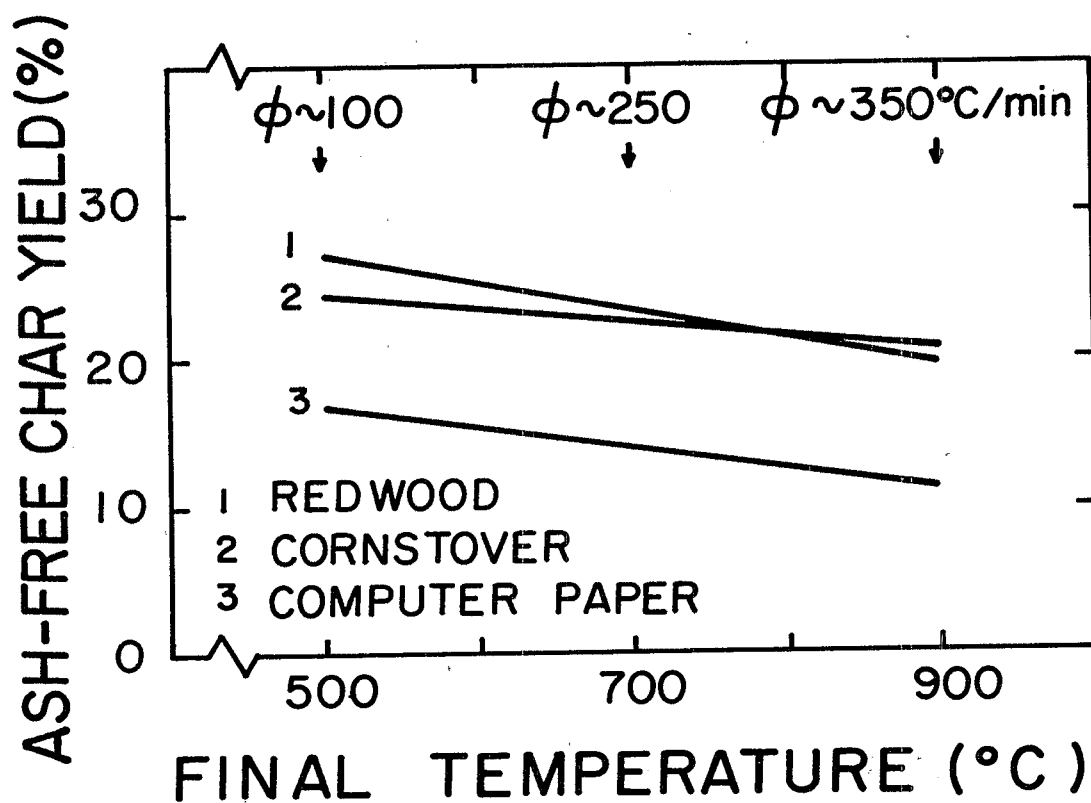


Figure 5. Ash-free char yield versus final temperature: high heating rates.

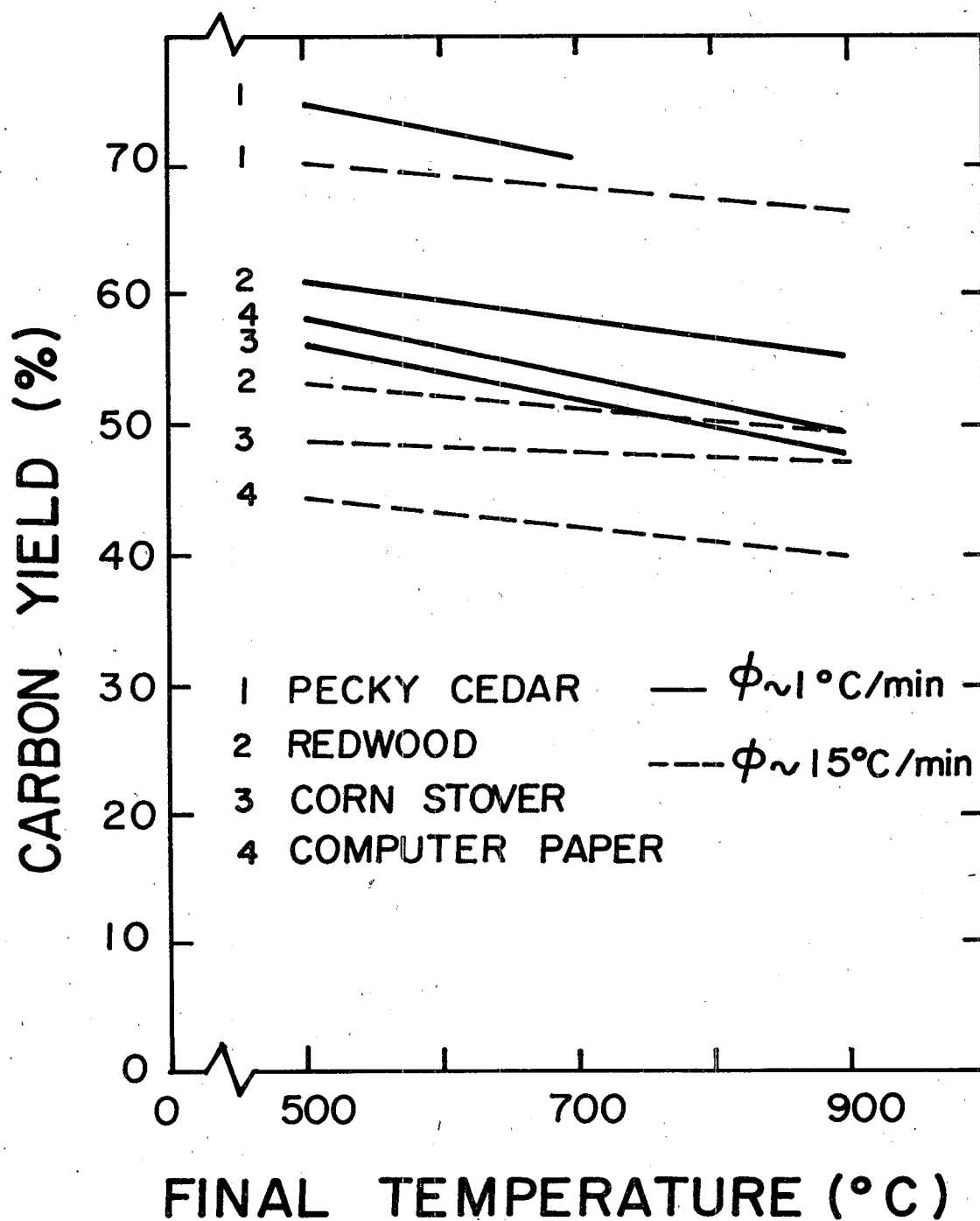


Figure 6. Carbon yield versus final temperature.

The plots in Figure 5 illustrate a similar point. The slopes are similar to the medium heating rate while the absolute yields are much lower. Thus the extremely high heating rates seem to exert their prime effect in depressing char yield at temperatures below 500°C. This effect is even more pronounced when it is considered that the experimental heating rates also increase with the final pyrolysis temperature, as described previously.

Figure 7 presents ash-free yield as a function of the logarithm of the heating rate. The data are represented as log-linear regressions for the same reasons cited previously and also to allow comparison with Brunner's establishment of a log-linear dependence of cellulose char yield on heating rate (26). The data were analyzed both by linear and log-linear regression, the results of which are included in Table 7. Figure 7 presents the log-linear regressions for the lignocellulosics examined in this section of the study, as well as Brunner's results for Cellulose M, given by the following (26):

$$\text{Yield} = a_1 \ln \phi + a_0$$

where

$$a_1 = 2.4,$$

TABLE 7. LINEAR REGRESSIONS OF ASH-FREE CHAR YIELD VERSUS HEATING RATE OR $\ln(\text{HEATING RATE})$ FOR PYROLYSIS TO FINAL TEMPERATURE T_F

Material	T_F (°C)	Linear Regression Constants ^a			Log-Linear Regression Constants ^b		
		a_1	a_0	r^2	a_1	a_0	r^2
Redwood	500	-0.08	36.4	0.913	-1.99	38.0	0.947
	700	-0.04	30.5	0.828	-1.86	32.7	0.985
	900	-0.03	28.9	0.872	-1.58	30.7	0.954
Corn Stover	500	-0.03	27.9	0.719	-0.99	29.7	0.985
	700	-0.02	25.6	0.827	-0.82	26.6	0.992
	900	-0.01	24.3	0.975	-0.49	24.8	0.784
Computer Paper	500	-0.09	26.2	0.755	-2.44	28.6	0.999
	700	-0.03	21.3	0.676	-1.96	24.7	0.999
	900	-0.02	20.2	0.884	-1.72	22.2	0.987
Sigma Cellulose	700	-0.05	21.7	0.770	-2.39	24.4	0.999

^aModel format: Ash-free char yield (%) = $a_1\phi + a_0$, where ϕ is expressed in °C/min.

^bModel format: Ash-free char yield (%) = $a_1(\ln \phi) + a_0$, where ϕ is expressed in °C/min.

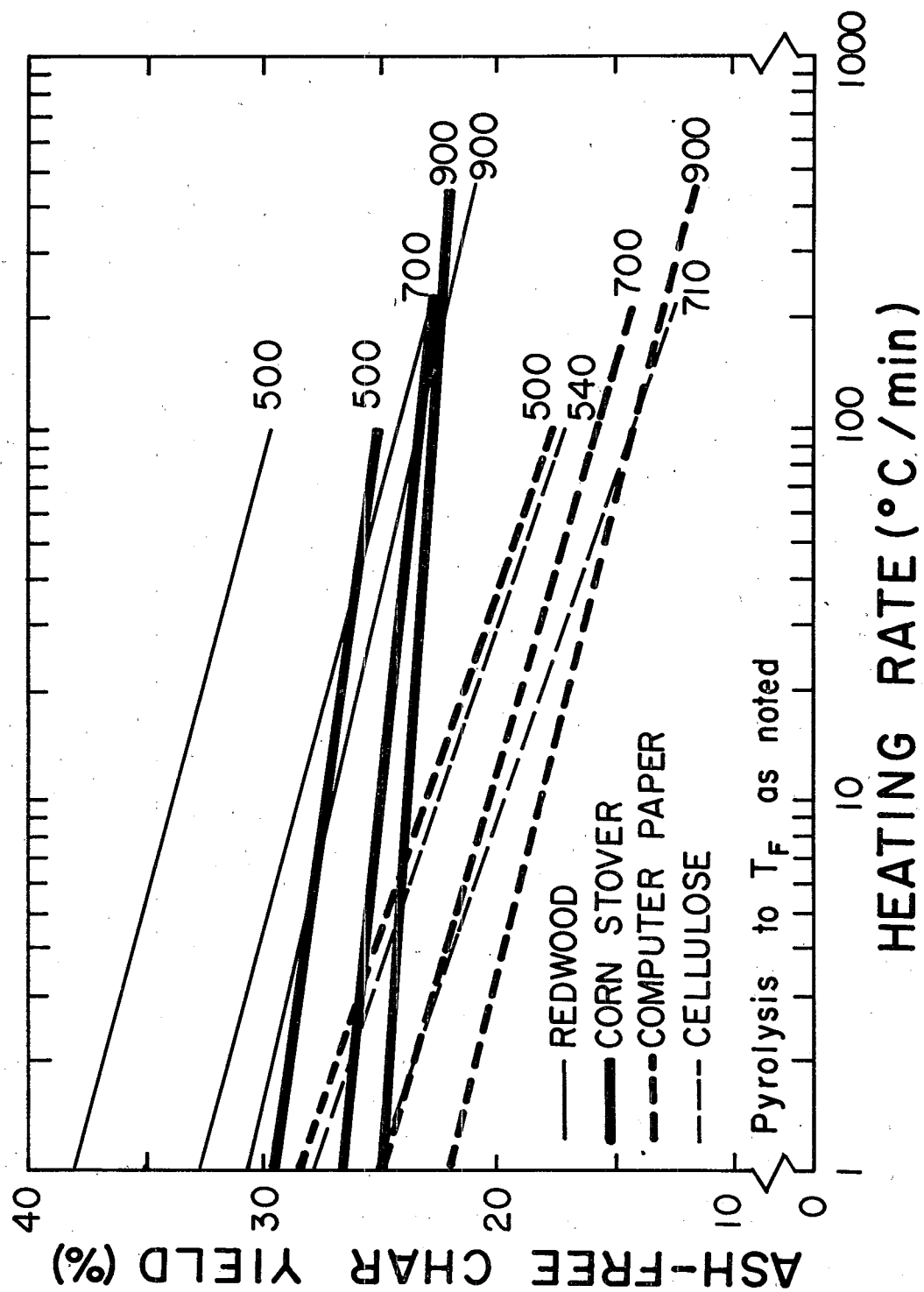


Figure 7. Ash-free yield versus heating rate.

a_0 = empirical constant = $f(\text{educt}, T_F)$

= 27.9 for Cellulose M pyrolyzed to 540°C

= 25.3 for Cellulose M pyrolyzed to 710°C

and no correction to ash-free yield is necessary since the ash content is low (65 ppm).

Comparing Brunner's cellulose results with the lignocellulosic results in Figure 7 and Table 7, we can make the following observations. As expected, lower heating rates result in higher char yields for all materials investigated. Most materials behave qualitatively similarly to cellulose, in that there seems to be a log-linear dependence of ash-free char yield on heating rate. However, slopes of the log-linear regressions vary widely (-0.5 to -2.4) and in general, indicate a less marked dependence of lignocellulosic char yield on heating rate compared to the cellulose results. In some cases (redwood to 500°C, corn stover to 900°C), the data are not well suited to a log-linear model. In fact, corn stover pyrolyzed to 900°C is better described by a simple linear model.

The behavior of computer paper warrants discussion. Computer paper is composed almost entirely of holocellulose and ash (α_{lig} and α_{ext} both less than 1%). The plot of ash-free char yield (500°C) versus ϕ for computer paper agrees closely with that of pure cellulose (540°C) in Figure 7. The higher temperature of the cellulose data could explain the somewhat lower yields observed and thus, the similarity of the computer paper and cellulose results is even more striking. This is somewhat surprising in light of the hypothesis that ash content catalyzes dehydration below ~ 240°C prior to the onset of rapid depolymerization, which results in higher char yields. If ash constituents have the same effect, then cellulose in the presence of ash (e.g., computer paper) would be expected to have a reduced dependence of yield upon ϕ (i.e., a lower slope). For computer paper pyrolyzed to 500°C, this does not appear to be the case, although such behavior is observed for computer paper pyrolyzed to higher temperatures. The behavior of computer paper pyrolyzed to 500°C suggests either that its inorganic fraction does not contain any compounds capable of catalyzing char yield of the cellulose or that the cellulose present in the paper is not susceptible to chemical catalysis, perhaps due to modification during the papermaking process (e.g., delignification and bleaching). Why the effect of heating rate decreases with increasing final pyrolysis temperature, however, remains unclear.

Corn stover exhibits the most unusual behavior in Figure 7, having a significantly lower dependence of char yield on heating rate for all final temperatures. This same behavior was also evident in Figure 5 and reflected in Figures 4 and 6. This behavior may be an indication of the catalytic effect of inorganics on pyrolytic char yield. Corn stover is a high carbohydrate material (71% holocellulose) with relatively high contents of ash (5.9%) and silica-free ash (4.1%), and thus might be expected to exhibit such an effect. As was the case with computer paper, the effect of heating rate declines with increasing T_F .

Lignocellulosic Char Properties

Surface areas of lignocellulosic chars produced under varying pyrolysis conditions were determined by carbon dioxide adsorption at 195K using the BET equation (Eq. 1). The results of the analyses are presented in Table 8, along with calculated values for surface area expressed per gram of carbon and per gram of educt. Surface area of high heating rate chars were not determined since low values had previously been observed for cellulose pyrolyzed at such rates. Most surface area data listed in Table 7 are based on a single determination. Replicate analyses were performed on certain chars, as noted in Table 8, resulting in standard deviations in general of 1 to 2.5% of the mean, except for redwood pyrolyzed at 15°C/min to 500°C for which the standard deviation was much larger (14%).

TABLE 8. SUMMARY OF SURFACE AREA ANALYSES ON SELECTED LIGNOCELLULOSIC CHARS

Material	ϕ °C/min	T_F °C	Surface Area on Basis of		
			Char ^a (m ² /g)	Carbon ^b (m ² /g C)	Educt ^c (m ² /g educt)
Pecky Cedar	15	500	380	452	187
	15	700	486	527	205
	15	900	539	557	218
Redwood	1	500	449 ^d	511	169
	1	700	534 ^d	571	186
	1	900	650 ^e	656	197
	15	500	305 ^e	350	118
	15	600	463	498	136
	15	700	489	502	137
	15	900	500	507	135
	15	900	500	507	135
Corn Stover	1	500	296	396	100
	1	700	394	514	121
	1	900	465	620	132
Computer Paper	1	500	353	509	118
	1	700	421	561	126
	1	900	385	529	104

^aSurface area determined from CO₂ adsorption isotherms (195K) using BET equation; one determination except as noted.

^bSurface area per gram carbon = $\frac{100(\text{surface area per gram char})}{(\text{carbon content of char in \%})}$.

^cSurface area per gram educt = $\frac{(\text{surface area per g char})(\text{char yield in \%})}{100}$.

^d4 replicate analyses: standard deviation = 10 for redwood 1/500, 13 for redwood 1/700.

^e2 replicate analyses: standard deviation = 4 for redwood 1/900, 42 for redwood 15/500.

Specific surface areas expressed as m^2 per gram char, gram carbon, or gram educt are presented as a function of final pyrolysis temperature in Figures 8, 9, and 10, respectively. The shaded areas in these figures represent the surface area observed in Cellulose M chars pyrolyzed at heating rates between $0.03^\circ\text{C}/\text{min}$ and $11^\circ\text{C}/\text{min}$, as found by Brunner and Roberts (29).

Figure 8 indicates that for redwood lower heating rates result in higher surface area for a given final temperature, much as was found for cellulose. Comparing the redwood plots with the shaded area representing cellulose, it is apparent that redwood heated at $1^\circ\text{C}/\text{min}$ has a surface area generally equal to or greater than cellulose heated at $0.03^\circ\text{C}/\text{min}$. This indicates that there may be a critical low heating rate below which little gain in surface area is realized. Further work would be necessary to verify this, however.

As might be expected, Figure 8 shows lower surface areas on a total weight basis for the higher ash materials, corn stover and computer paper. This is at least partly explained by the high content of ash in the chars ($\sim 25\%$ in computer paper pyrolyzed to 900°C) which would contribute little to the measured surface area (91). To isolate the surface area development in the carbonaceous fraction of the chars, surface area based on carbon is displayed in Figure 9. When compared with Figure 8, the carbon-specific areas (Figure 9) exhibit a narrower range of surface areas observed for the widely varying lignocellulosics, especially for $T_F = 700^\circ\text{C}$, at which surface areas for all materials and heating rates studied fall within $\pm 10\%$ of the median value. Assuming that the standard deviations observed for surface areas of redwood chars pyrolyzed at $1^\circ\text{C}/\text{min}$ apply to the other materials, the plots of surface area per gram carbon are statistically indistinguishable (95% confidence intervals overlap).

The results of this study of surface development upon pyrolysis of lignocellulosics indicate that, in general, surface area per gram of carbon varies relatively little with heating rate or educt. Therefore, when compared on the basis of surface area produced per gram of educt (Figure 10), the higher yield materials (e.g., those with higher lignin contents) exhibit a substantially higher production of surface area.

In conclusion it appears that at least on the basis of surface area as determined by CO_2 adsorption at 195K , a wide range of lignocellulosics could serve as starting materials for activated-carbon production, provided the ash content of the chars or activated carbons could be reduced sufficiently. Commercially this is accomplished, especially for ash reduction of the final activated product, by washing with water and/or mineral acid solutions (1). Also, ash reduction of chars prepared from municipal refuse has been shown to be feasible by air classification (92).

ACTIVATION OF LIGNOCELLULOSICS AND REFUSE-DERIVED FUEL

Introduction

The purpose of this section of the study was to investigate the effect of extent of activation on the porous structure of lignocellulosic chars, and

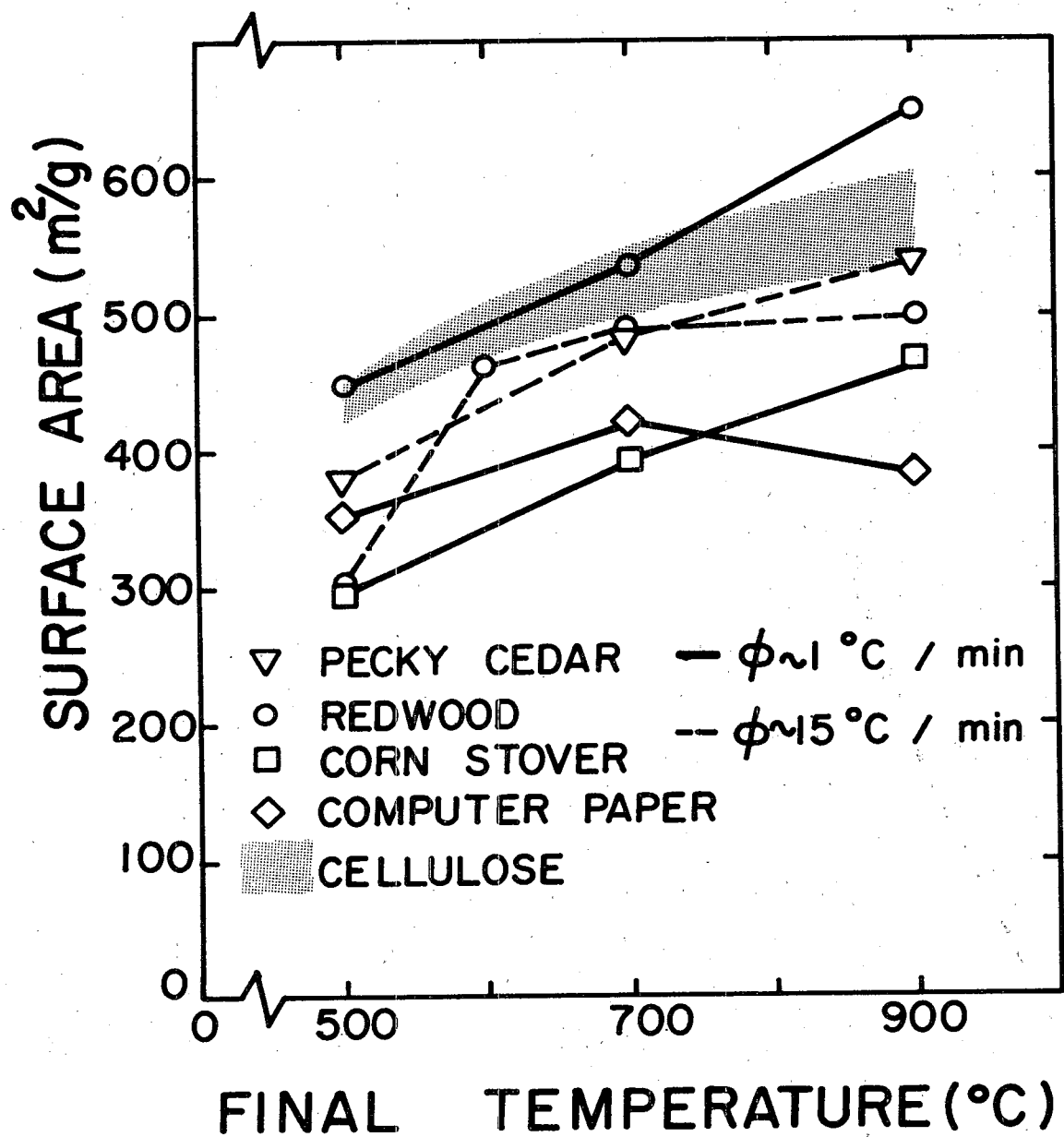


Figure 8. Surface area of char versus final temperature. Surface area determined by CO_2 adsorption at 195K.

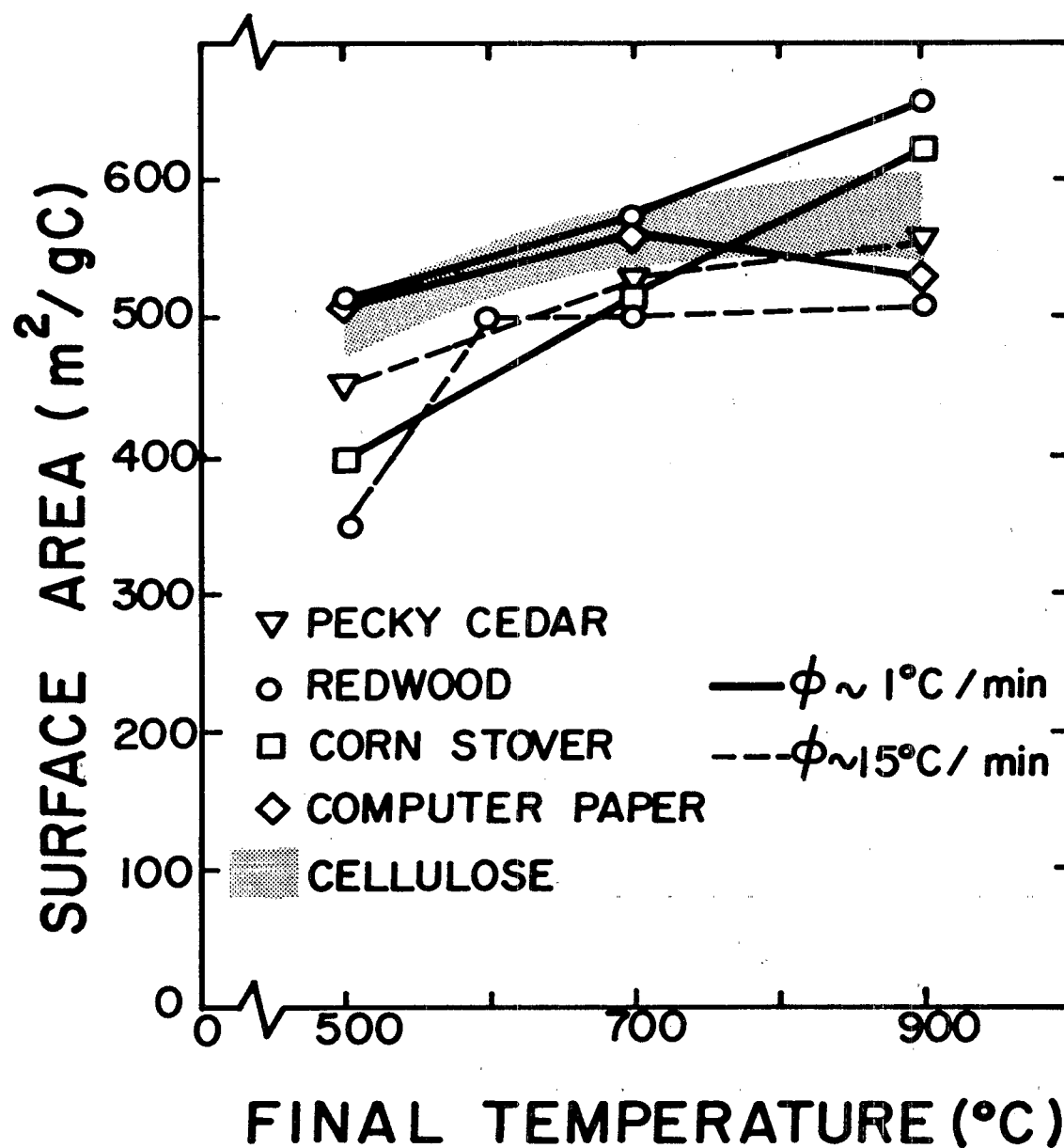


Figure 9. Surface area per gram carbon versus final temperature.

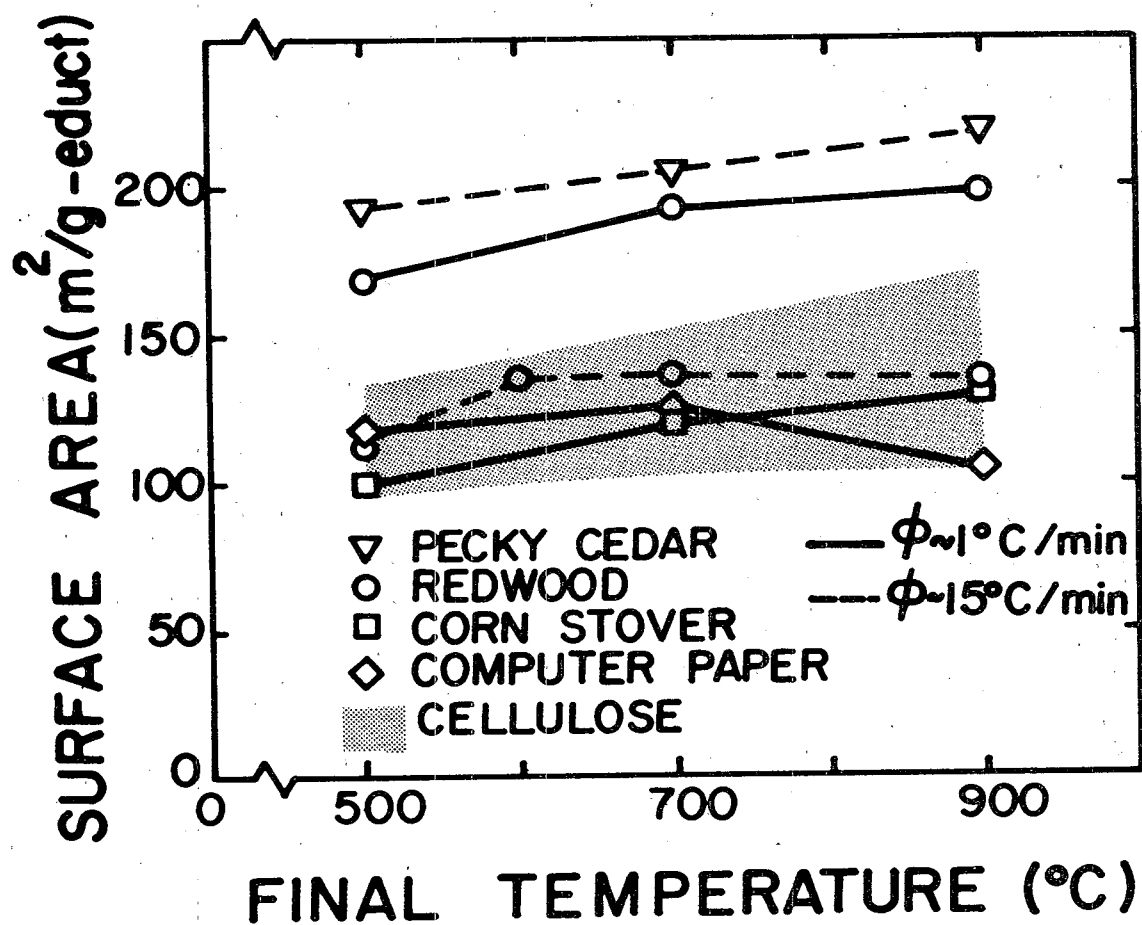


Figure 10. Surface area per gram educt versus final temperature.

thereby to prepare activated carbons of lignocellulosic origin for comparison to commercially available activated carbons on the basis of aqueous sorption performance. Our approach to the investigation of activation was to select an educt (prune pits) and activation conditions which would be expected to yield an activated carbon with favorable sorptive properties, based on studies of similar materials by Marsh et al. (2,3). The second phase of the investigation was to pyrolyze and activate RDF under the same conditions that yielded desirable activated carbons from prune pits. The second phase was intended to allow comparisons of the activation behavior of the very dissimilar educts and, further, to clarify the potential for the production of activated carbon from municipal waste.

Activation of Prune Pit Char

Prune pits which had a 0.62% ash content were first size-fractionated to 74-351 μm diameter (45 \times 200 mesh) and pyrolyzed as described above. The temperature in the furnace was raised from room temperature to 900°C at approximately 15°C/min. This resulted in a char yield of $25.02 \pm 0.11\%$.

This char was then activated in a controlled CO_2 environment at 900°C for times of 15, 30, 42, and 60 min (these will be designated henceforth as 15M, 30M, 42M, and 60M, respectively). Three to five samples were formed for each of these activation times. The percent mass loss during activation increased linearly with time of activation, as shown in Figure 11. Char activated for 15 min lost $21.65\% \pm 0.83\%$ of its mass whereas char activated for 60 min lost $67.22\% \pm 2.69\%$ of its mass. These values, along with N_2 -adsorption data, are summarized in Table 9.

The surface area and pore volume distribution of the activated prune pit chars were determined by N_2 -adsorption and mercury porosimetry.

N_2 -Adsorption Isotherms--

The N_2 -adsorption isotherms were measured in duplicate for 60M, 42M, 30M, and 15M (Figure 12). For comparison, N_2 -isotherms were also conducted on three commercially available activated carbons. Filtrasorb 400, Filtrasorb 100, and Aquanuchar A (F400, F100, and AN-A, respectively). These results are presented in Figure 13.

From the N_2 -isotherms and the BET equation (Eq. 1) was calculated surface area. Pore radius corresponds to relative pressure P/P_s as described by the Kelvin equation (Eq. 4). The volume in pores with radius less than a given value has been determined by the Cranston and Inkley method (12). The Kelvin equation can correctly measure the radius of only those pores with radius greater than 1 nm (7) (although it can incorporate the summation of pore volumes with smaller radii). Furthermore, above $P_2/P_s = 0.9$ (which corresponds to $r_p = 10$ nm), data are prone toward error and so cannot be quantitatively interpreted. This is because the value of P_s is very dependent on the temperature of the liquid nitrogen bath, which fluctuates slightly.

Included as ordinates in Figures 12 and 13 are both gaseous N_2 and liquid N_2 pore volumes. The gaseous N_2 volume measured at STP within the adsorption

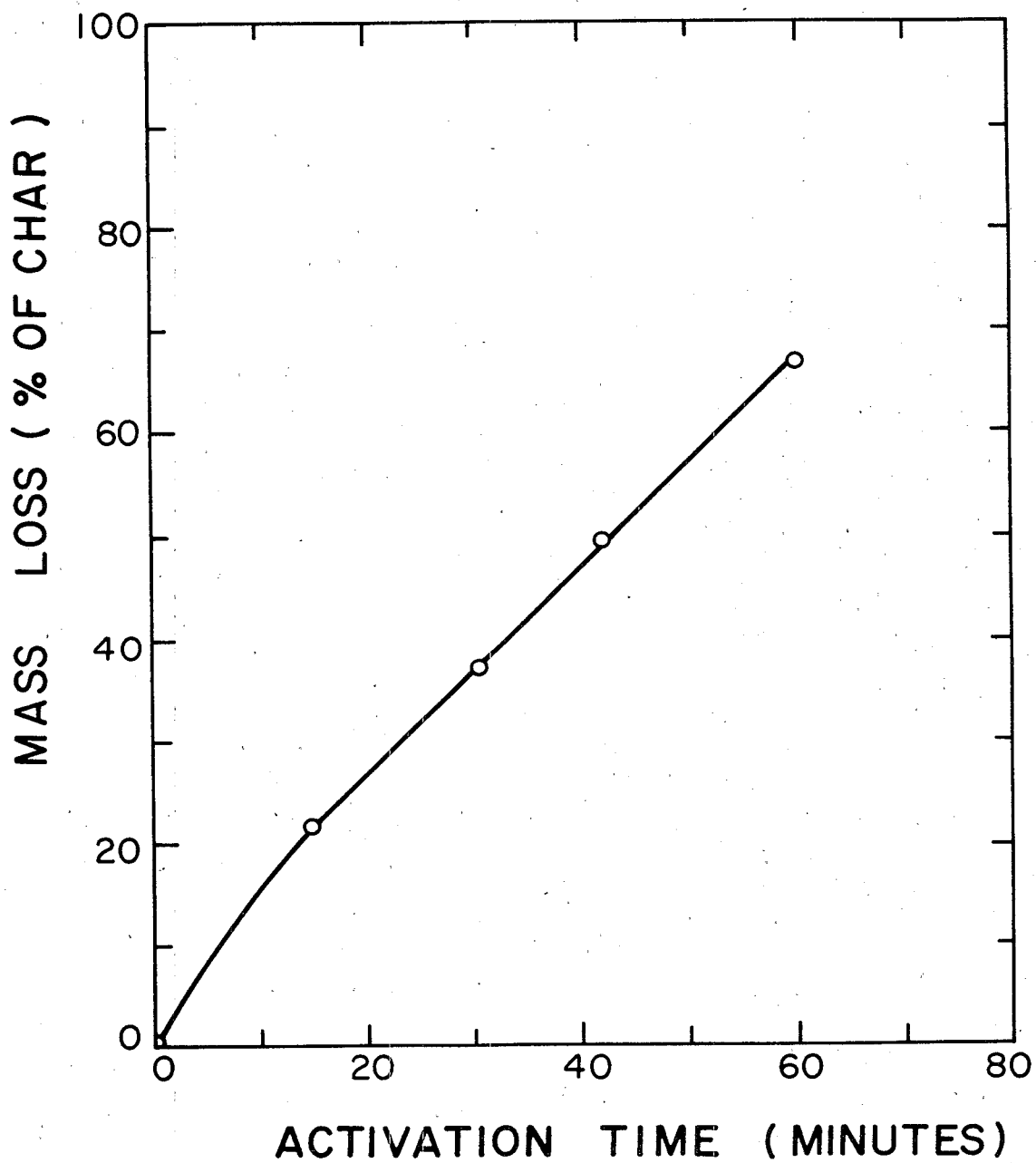


Figure 11. Mass loss versus activation time for prune pit char.

TABLE 9. PHYSICAL PROPERTIES OF ACTIVATED PRUNE PIT CHAR AND SEVERAL COMMERCIAL ACTIVATED CARBONS

Activation Time (minutes)	Number of Activation Samples	Percent Mass Loss ^b	N ₂ -BET ^a Surface Area (m ² /g)	N ₂ -BET Volume of Mono-layer Surface Coverage (cm ³ /g) ^c	N ₂ Liquid Pore Volume		Mercury Porosimetry Pore Volume with Radius 10nm<r<300nm	Total Pore Volume (cm ³ /g)	Percent of Pore Volume with r<3nm
					with Radius <3nm (cm ³ /g)	with Radius <10nm (cm ³ /g)			
Prune Pit Char									
0 ^d	-	0	(482) ^d						
15	3	21.65±0.83	663±10 (684)	0.237	0.275	0.291	0.072	0.363	75.8
30	4	37.08±1.69	927±3	0.332	0.376	0.410	0.104	0.514	73.2
42	4	49.73±1.26	1175±42	0.421	0.506	0.530	0.105	0.635	83.5
60	5	67.22±2.69	1692±8	0.606	0.746	0.802	0.128	0.930	80.2
Commercial Carbons									
Filtrasorb 400	-	-	998±30	0.357	0.440	0.481	0.160	0.641	68.6
Filtrasorb 100	-	-	897±5	0.321	0.395	0.436	0.160	0.596	66.3
Aquanuchar A	-	-	810.4±0.1	0.290	0.355	0.385	0.070	0.455	78.0

^aValues represent mean ± standard deviation for two or three replicates.^bValues represent mean ± standard deviation for number of activation samples.^cFrom the volume of monolayer surface coverage is calculated the N₂-BET specific surface area.^dValues in parentheses represent CO₂-BET calculations at 195K. It is not certain how to quantitatively compare CO₂-BET data with N₂-BET data.

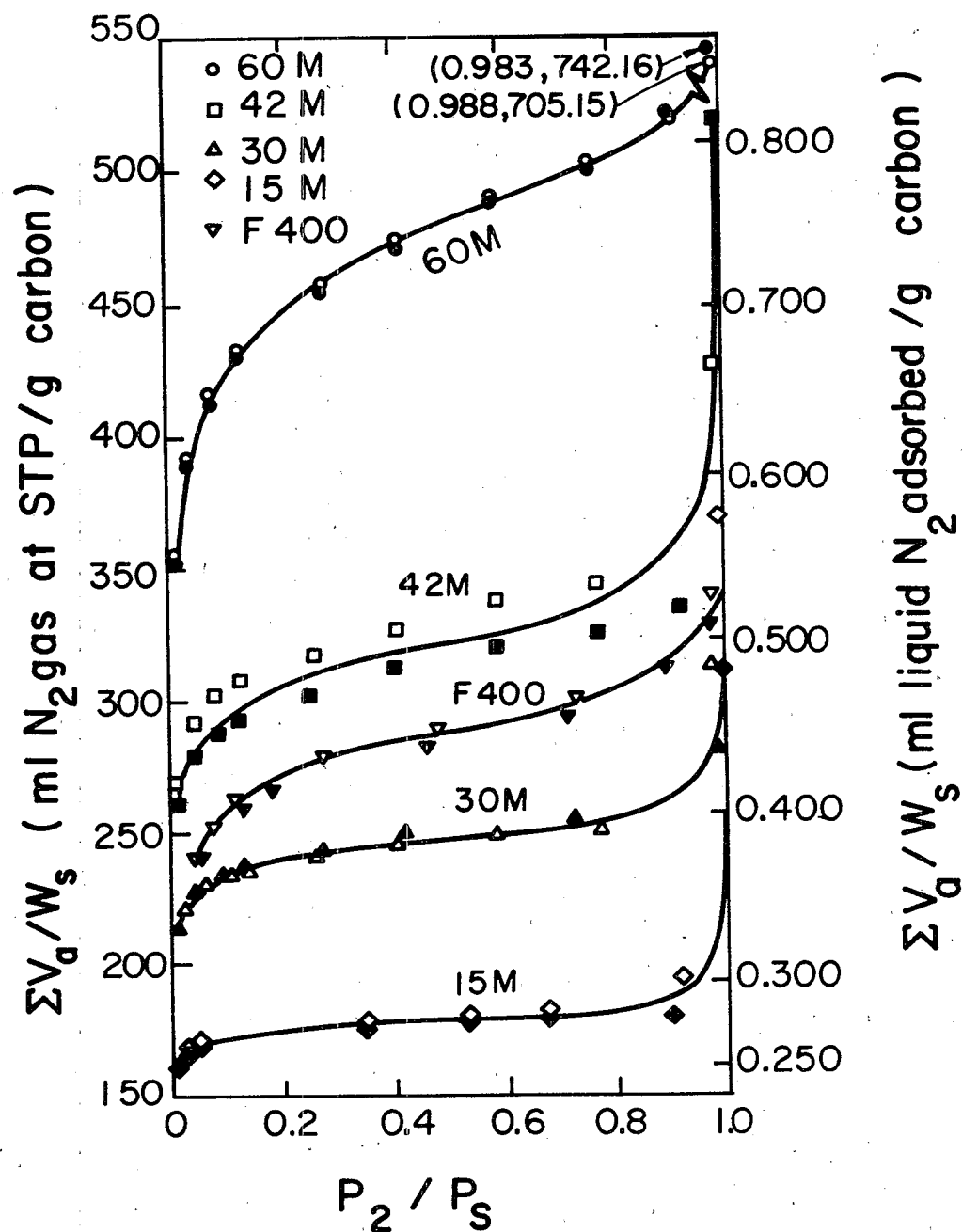


Figure 12. Nitrogen isotherms for 60M, 42M, 30M, 15M, and F400. Filled in and open symbols represent experiments 1 and 2, respectively.

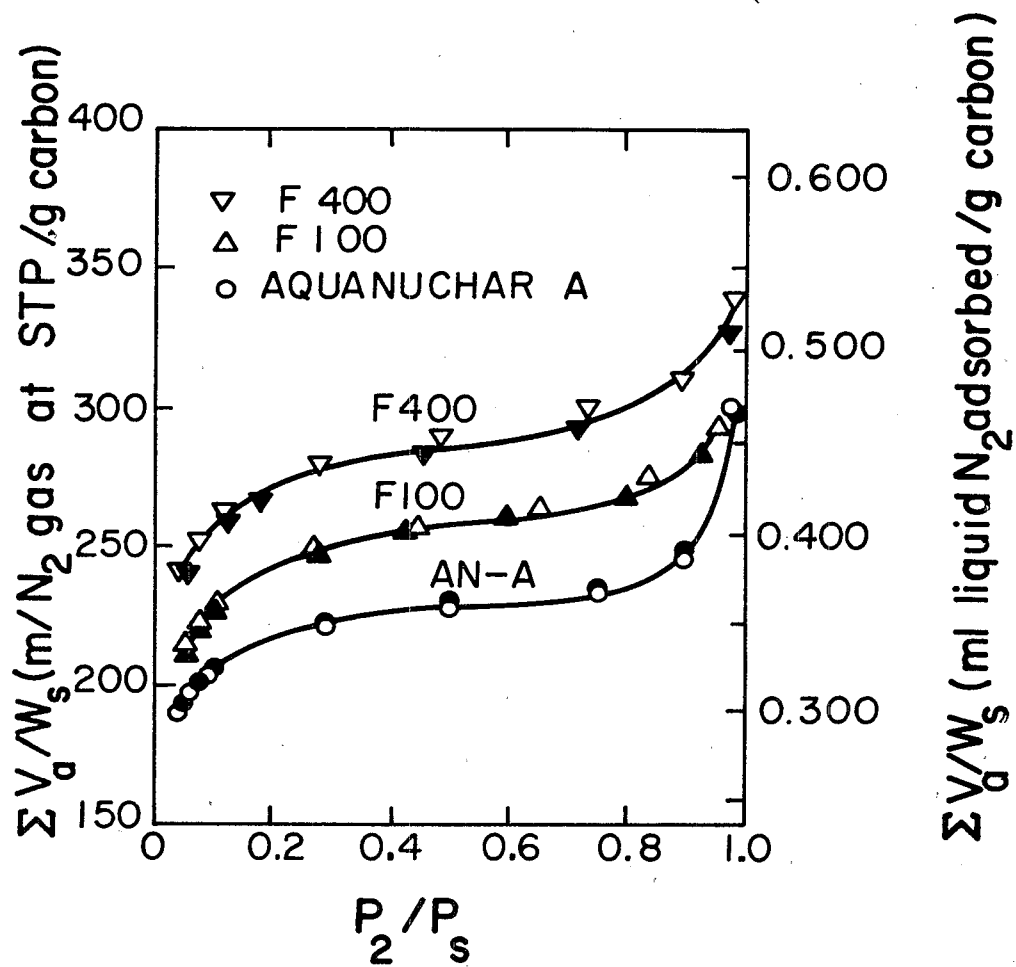


Figure 13. Nitrogen isotherms for F400, F100, and AN-A. Filled-in and opened symbols represent experiments 1 and 2, respectively.

equipment can be converted to the equivalent liquid N_2 volume at 77K by multiplying the former by 0.001558. The liquid N_2 volume corresponds closely to the true pore volume within the activated carbon. Pore volumes for $r_p < 3$ nm and $r_p < 10$ nm, along with surface areas, are shown in Table 9. N_2 -adsorption equilibrium times were generally about 10-30 min, although times of 90 min were required for the 15M carbon during the first several increments.

In the nitrogen-adsorption analysis of prune pit char (CHAR), however, adsorption equilibrium was not reached within 72 hours. This suggests that the diffusion of N_2 into the pores was extremely slow. CO_2 , however, could enter these pores more rapidly; equilibrium was reached within 30 min for adsorption at 195K. The difference in rate is due to a much higher activation energy for diffusion of nitrogen at 77K than for CO_2 at 195K (13). Based on CO_2 isotherms at 195K, the char's surface area was calculated by the BET equation (Eq. 1) as 482 m^2/g . The surface area estimated from CO_2 data at 195K should not be compared quantitatively to the estimate based on N_2 -adsorption.

To test the reproducibility of the activation experiments, N_2 -adsorption analyses were performed in duplicate for each of the three samples which were activated for 15 min. The percent variation in surface area should have been greatest at the shortest activation time since the timing error introduced by startup and shutdown would be the most significant under those conditions. If physical characteristics such as percent burnoff and surface area varied little among the samples activated for the shortest time, it would be reasonable to assume that they would vary even less among those samples with longer activation times. As can be seen in Table 10, variation in percent burnoff and surface area was indeed slight among the 15-min carbons. These results justified the mixing of carbons prepared by activation for a given time period to obtain adequate quantities for the aqueous sorption studies described later.

From the N_2 -adsorption isotherm data in Figures 12 and 13, it can be seen that the volume of pores measurable by N_2 adsorption ($r < 10$ nm) increased as activation time increased. Further, the corresponding values of the pore

TABLE 10. RELATION BETWEEN SURFACE AREA AND BURNOFF FOR CHARs ACTIVATED FOR 15 MINUTES

Experiment Number	Percent Burnoff	Surface Area m^2/g
1	22.50	674.6 \pm 0.4
2	21.59	660 \pm 5
3	20.85	654 \pm 8
Average	21.65 \pm 0.83	663 \pm 10

Note: Surface area values are mean \pm standard deviation for duplicate experiments on each sample.

volume ($r < 10$ nm) of Filtrasorb 400 and Filtrasorb 100 were intermediate between those of 42M and 30M. Filtrasorb 400 had slightly more small-pore volume than F100. AN-A had a small-pore volume similar to that of 30M. The 60M prune-pit-derived activated carbon had a small-pore volume more than 50% greater than any of the commercial products.

Likewise, specific surface area increased substantially both with activation time and with consequent increase in percent mass loss. Whereas the prune pit char activated for 15 min had a specific surface area of 663 ± 10 m²/g, the prune pit char activated for 60 min had a specific surface area of 1692 ± 8 m²/g, a value two-and-a-half times greater. Specific surface area is plotted as a function of percent mass loss in Figure 14.

The N₂-adsorption data in Table 9 reveals that the volume of monolayer surface coverage was a fairly consistent fraction (0.8) of the total pore volume with radius less than 3 nm. The volume of monolayer surface coverage (V_m) is used to calculate surface area (S), as described previously (Section 4). Including the appropriate constants for N₂ in Eq. 3 gives the following:

$$S(\text{m}^2/\text{g}) = 2792 V_m (\text{cm}^3/\text{g}) \quad (17)$$

Mercury Porosimetry--

Mercury porosimetry measurements, which describe the macro- and transitional-pores of a porous solid, were conducted on CHAR, 15M, 30M, 42M, 60M, F400, F100, and AN-A. The initial results for all of the carbons analyzed were of an S-shape similar to that for 60M in Figure 15. (The results for the other carbons are in Appendix B.) As can be seen in all of these curves, there is a great increase in penetration volume corresponding to a pore radius between 15,000 and 4,000 nm (or pressure of 8 to 20 psi). This increase is an artifact; it corresponds to the pore volume between the sample grains rather than within them and is not useful information for our purposes. Gan et al. (91) found that pressures below 60 psi ($r = 1500$ nm) corresponded to intraparticle voids for a 40×70 mesh fraction of both crushed glass and non-porous coals. Since the carbons we used were a factor of five smaller (200×400 mesh), it can be expected that the interparticle voids, which are assumed proportional in size to particle diameter, would occur down to a void radius of 300 nm (corresponding to 300 psi). This, then, was our assumed dividing line between intra- and interparticle porosity.

Indeed, a comparison of all of these penetration curves for the 200×400 mesh size reveals that if the penetration volume corresponding to 300 nm (300 psi) is subtracted from the penetration volumes corresponding to smaller pore radii, the data from the prune pit carbons appear reasonable, as shown in Figure 16, and the intraparticle voids no longer appear to be a significant factor.

The adjusted values of mercury penetration increase regularly with increasing activation time. The 15M activated carbon differs from the char only in the small transitional- and micropore range. The 30M, 42M, and 60M chars

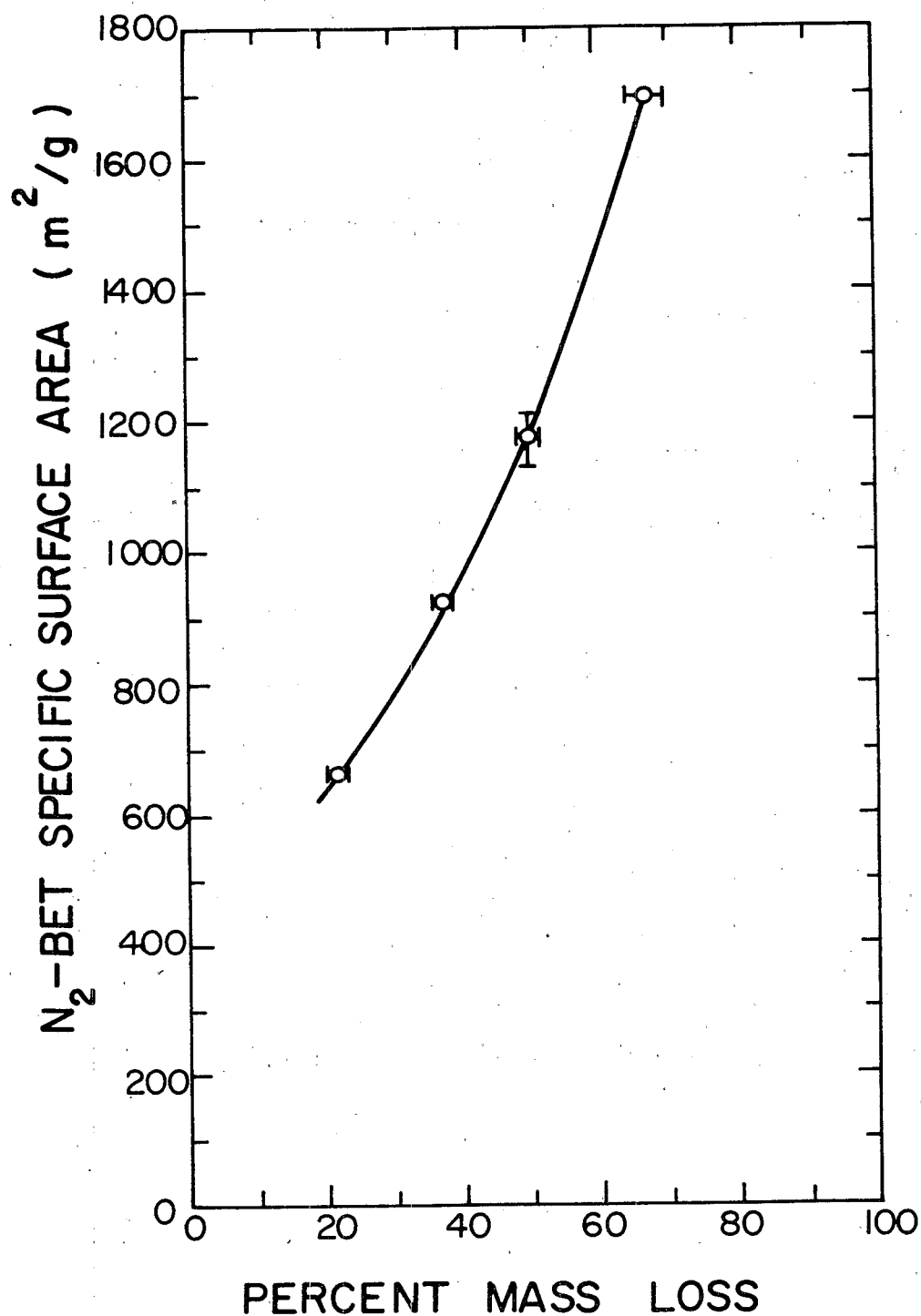


Figure 14. N₂-BET specific surface area versus percent mass loss for activated prune pit chars. Error bars are included to represent standard deviations when the standard deviation is greater than the magnitude of the corresponding symbol.

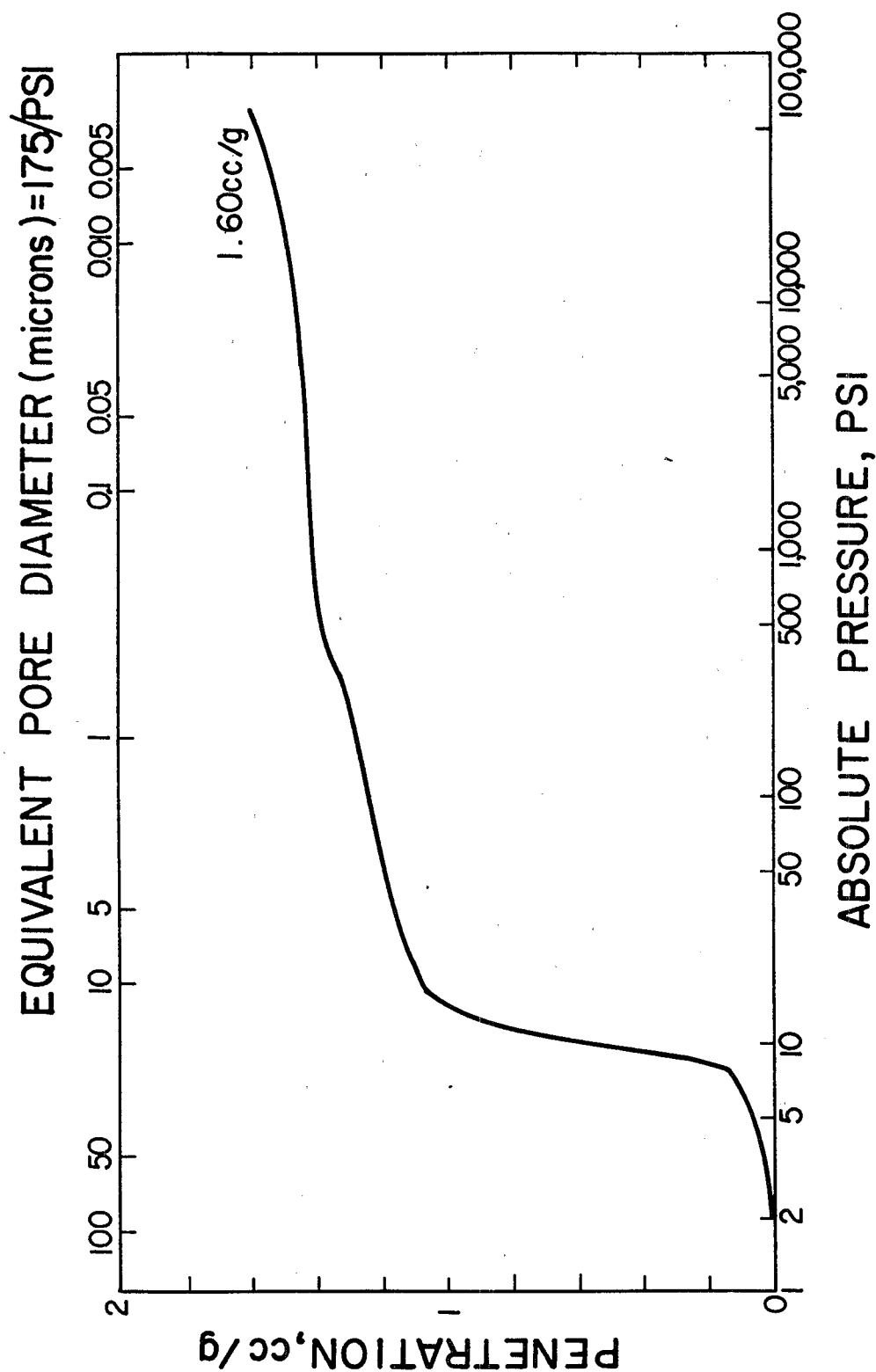


Figure 15. Mercury porosimetry: cumulative penetration volume versus pore diameter for 60M. The large jump in penetration for pressures below 300 psi corresponds to porosity external to the carbon grains. (1 psi = 6.89 kPa).

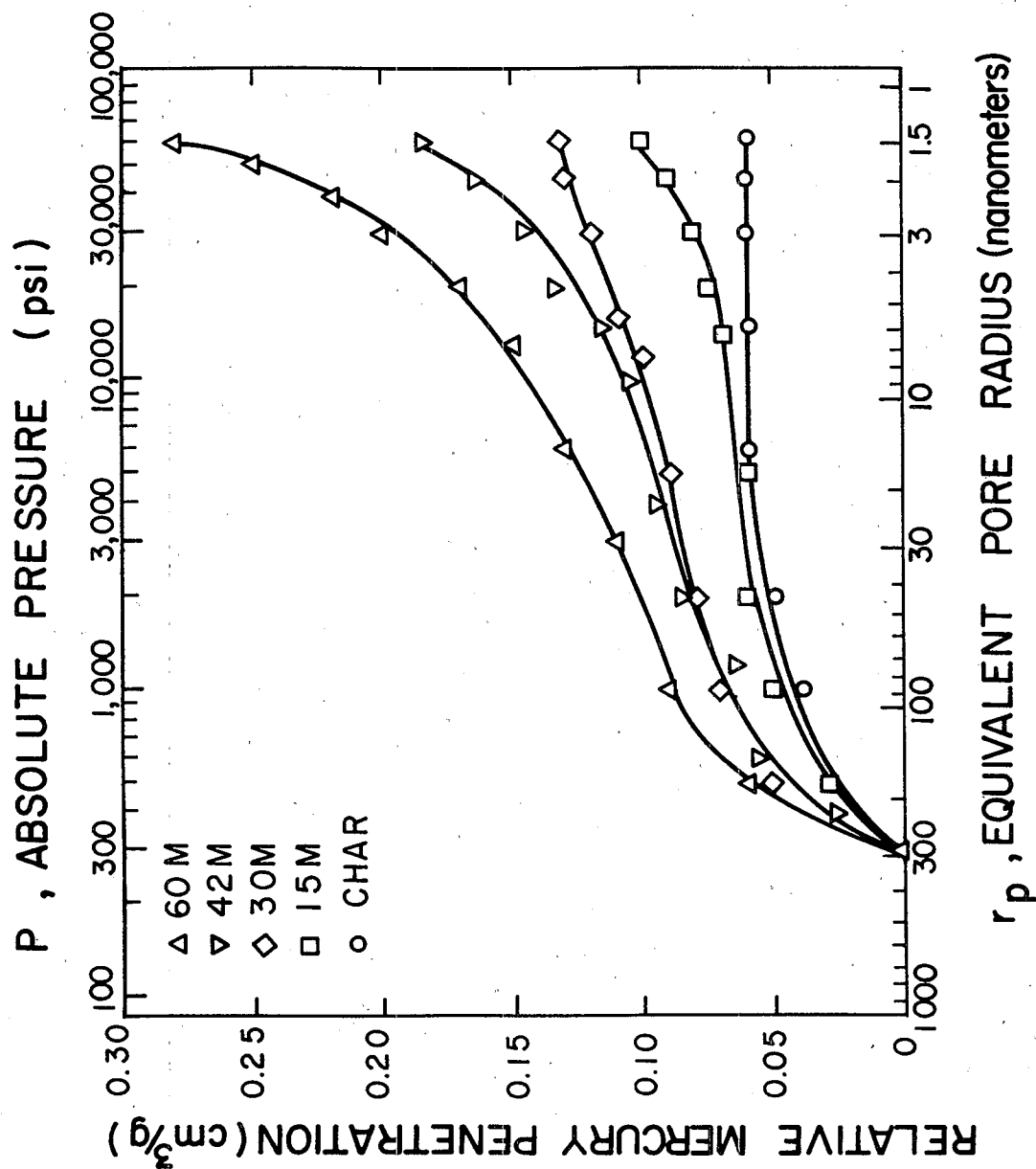


Figure 16. Mercury porosimetry: relative cumulative pore volume of mercury penetration versus equivalent pore radius for 60M, 42M, 30M, 15M, and CHAR. (1 psi = 6.89 kPa).

exhibit successively larger pore volumes in all size ranges, with the greatest increases occurring in the size range less than 10 nm.

The mercury porosimetry data for F400, F100, and AN-A, shown in Figure 17, reveal that F400 and F100 have much the same macro- and transitional-pore structure. The pore volume of AN-A is considerably less than those of F400 and F100.

Pore Volume Distribution--

Total pore volume including micro-, transitional-, and macropores was estimated for each of the activated carbons. This was achieved by summing the N_2 -adsorption and mercury porosimetry data; the total pore volumes are shown in Figures 18 and 19. The N_2 -adsorption data were used to determine pore volume up to a radius of 10 nm, and the mercury porosity data were used for pore volumes with a radius larger than this. The mercury porosimeter achieved pressures up to 60,000 psi, which corresponds to a pore radius of 1.5 nm. Ideally, then, the pore volume distributions as determined by mercury porosimetry should be equal to those calculated by N_2 -adsorption over the range for which both methods can be used for estimation, namely 1.5 nm to 10 nm (10 nm corresponds to a pressure of 8800 psi). Such a comparison, tabulated in Table 11, shows that pore volumes calculated by mercury porosimetry were not significantly higher than those calculated by N_2 -adsorption at these pore radii. This is somewhat surprising in light of the structural alteration that mercury porosimetry is often thought to cause in the analysis of carbonaceous materials (Section 4). Our results indicate that such alteration, which would have yielded artificially high values for pore volume, may not have occurred in the porosimetry analysis of prune pit char. However, the pore volume determined by N_2 -adsorption was considered to be the more accurate of the two methods for the region of pore radii less than 10 nm.

The data in Figure 18 show that the total pore volume with $r < 300$ nm increased with increased activation time and percent burnoff. Whereas the 60M carbon had a total pore volume of $0.930 \text{ cm}^3/\text{g}$, the 15M carbon had a total pore volume of only $0.363 \text{ cm}^3/\text{g}$. Figure 18 does not include char values because, as described above, N_2 -adsorption measurements of the char were not feasible.

TABLE 11. COMPARISON OF PORE VOLUMES DETERMINED BY N_2 -ISOTHERMS AND MERCURY POROSIMETRY FOR 60M, 42M, 30M, 15M, AND F400

Pore Radius Range (nm) ($1 < r < u$)	Pore Volume (cm^3/g)									
	60M		42M		30M		15M		F400	
	N_2	M.P.	N_2	M.P.	N_2	M.P.	N_2	M.P.	N_2	M.P.
$1.5 < r < 3$	0.070	0.080	0.044	0.040	0.015	0.010	0.007	0.020	0.022	0.070
$3 < r < 10$	0.053	0.060	0.030	0.030	0.029	0.023	0.011	0.015	0.047	0.050

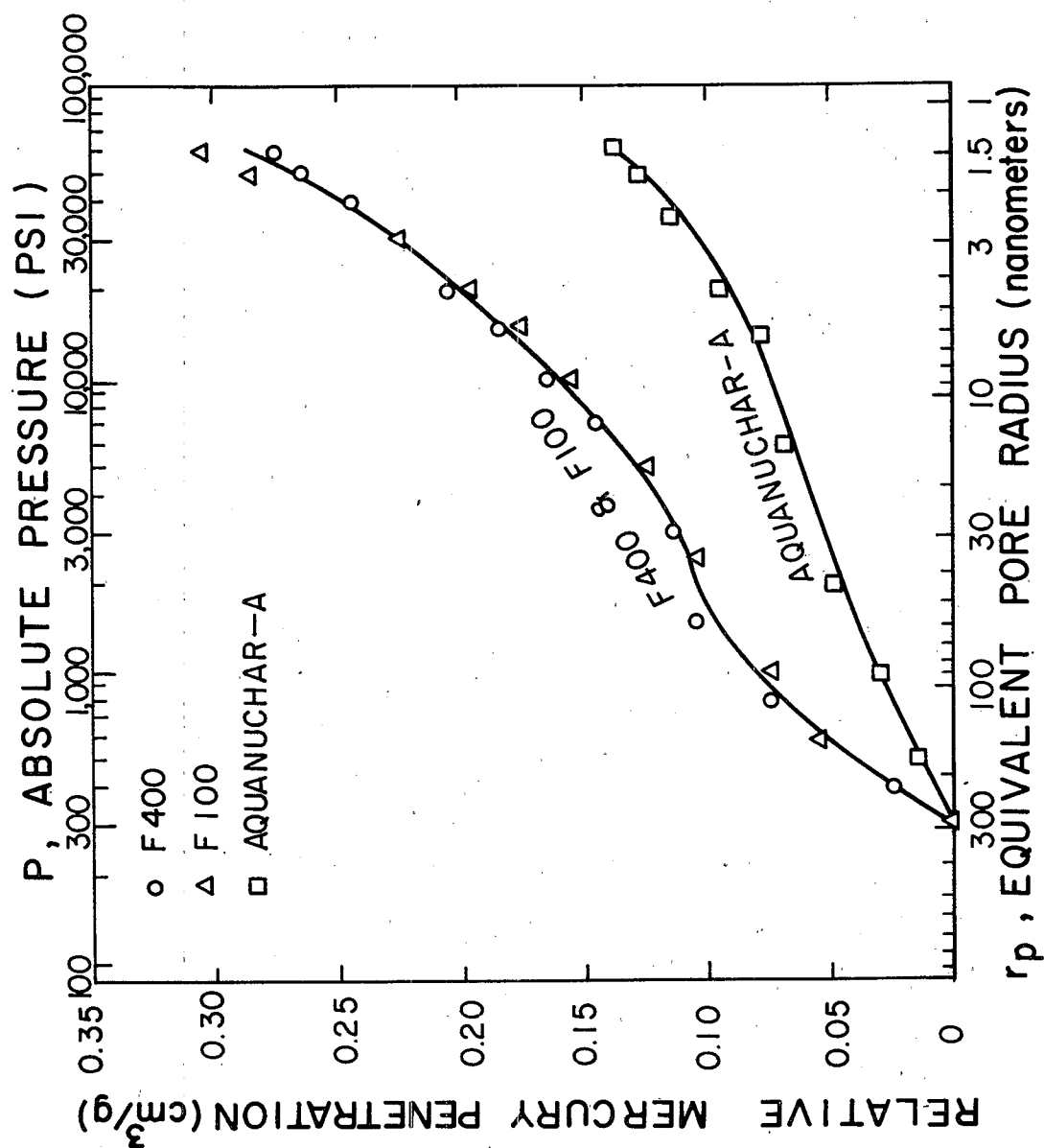


Figure 17. Mercury porosimetry: relative cumulative pore volume of mercury penetration versus equivalent pore radius for F400, F100, and AN-A.

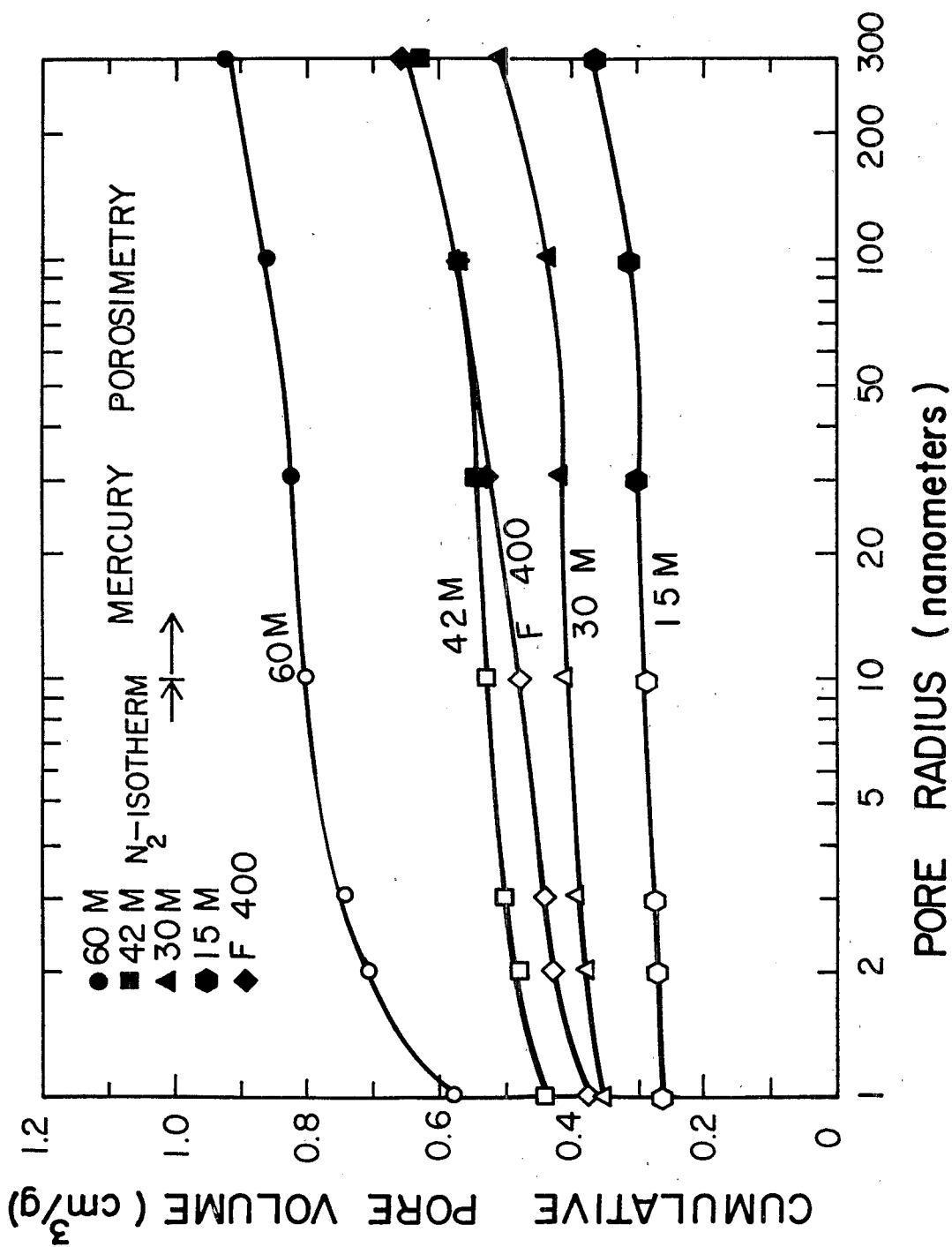


Figure 18. Pore volume versus pore radius as determined by N₂ adsorption isotherms and mercury porosimetry for 60M, 42M, 30M, 15M, and F400. Open symbols represent values determined by nitrogen-adsorption; filled-in symbols represent values determined by mercury porosimetry.

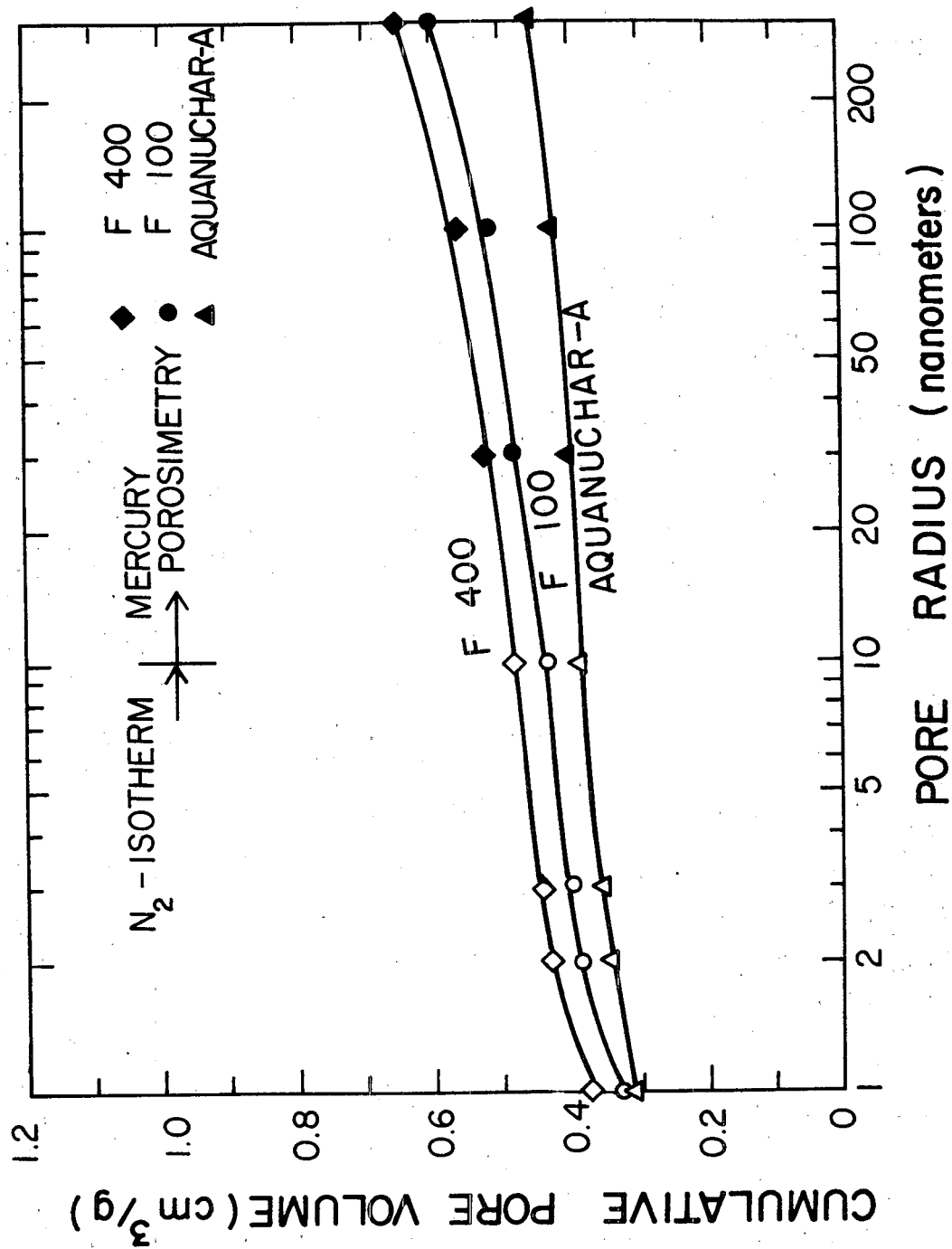


Figure 19. Pore volume versus pore radius as determined from N₂-adsorption isotherms and mercury porosimetry for F400, F100, and AN-A. Open symbols represent values determined by nitrogen-adsorption; filled-in symbols represent values determined by mercury porosimetry.

The F400 pore volume distribution was very similar to that of the 42M prune pit carbon; F100 had a micropore volume slightly less than F400 but otherwise similar. AN-A had a pore volume distribution between that of the 15M and 30M carbons.

The percent of the total pore volume that was of relatively small pore size ($r < 3$ nm) is shown in Table 9, along with various other pore volume data. The percent of pore volume within this arbitrarily chosen range ($r < 3$ nm) remained fairly constant at 73-83% (Table 9). Fundamental considerations would suggest that in the initial stage of gasification, formerly closed micropore volumes would be opened as key atoms blocking entrance to these pores are gasified. At the same time, the walls of the already opened pores would be gasified, causing an increase in the pore radius of any given pore. Initially, the effect of this process would be to increase both the specific surface area and the total pore volume (4). Moreover, if the volume of pores opened by gasification were greater than the volume increase from wall gasification, then the percent of total pore volume in the micropore range would increase. These exposed key atoms may gasify more readily than those along the wall surface because the exposed atoms probably have fewer and weaker bonds holding them in place (31).

Eventually, however, it is expected that the reservoir of closed pores would run out. At this point only those pores which had already been opened would be gasified. This would cause a net increase in the radius of all pores. At a further extent of gasification, the walls between pores would be completely gasified away, causing various formerly separated pores to merge into one large pore (4). The net effect of this process would be an eventual decrease in the specific surface area for a continued rise in total pore volume but decrease in percentage of pore volume within the micropore range.

For the gasification of the prune pit chars, however, such a decrease in surface area and percent small pore volume was not observed, even after 67% burnoff of the material.

Activation of Refuse-Derived Fuel

Refuse-derived fuel (RDF) char was prepared by pyrolysis under argon at approximately 15°C/min to a final temperature of 900°C. The RDF initially had an ash content of 11.68%; the complete composition was described earlier. The char yield for these pyrolysis conditions was 30.6% on a gross weight basis (standard deviation = 0.2%); the ash-free char yield, assuming no loss of inorganics, was 21.4%; the yield of carbon was calculated as 44.0%. As expected these results indicate a somewhat greater loss of carbonaceous material than was observed for prune pits pyrolyzed under the same conditions (ash-free char yield equal to 24.6%, carbon yield not determined). This expectation is based on the fact that, compared on the basis of organic material present in the educt, prune pits have a higher lignin content than RDF (approximately 35.7 versus 17.8%).

The RDF char was activated in a flow of CO₂ at 900°C. Due to the caking tendency of the char, a high CO₂ flow rate was necessary to effect even marginally homogeneous fluidization during activation. The flow rate (~ 3 l/min)

was significantly higher than that used in the activation of the prune pit char (~ 580 ml/min). To allow comparisons, activation of the RDF char was conducted for periods of time which resulted in burnoff (mass loss) based on carbon similar to the 42M and 60M prune pit activation experiments. Table 12 presents a summary of the results of the RDF activation, derived from Table 9. Table 12 also presents the results of surface area determinations of the activated carbons, using the BET equation (Eq. 1) to interpret N₂ adsorption at 77K. Since RDF char and activated carbons had such high ash contents, burnoff (mass loss) and surface area based on carbon are also presented to allow meaningful comparison with the prune pit results. Percent carbon values of the prune pit char and activated carbons were not determined. However, since the ash content of prune pits is on the same order as pecky cedar and redwood (i.e., < 1%), the carbon content of the char is reasonably estimated as similar to that of those materials pyrolyzed under similar conditions (i.e., 96.8% to 98.7% from Table 12). Thus the conversion of burnoff or surface area from gross weight basis to carbon basis would be small for the prune pit char and low-burnoff activated carbons (perhaps 5% higher surface area values, for example).

It is evident from Table 12 that mass loss for the RDF char occurs more rapidly than the prune pit char (approximately 65% carbon burnoff in 15 min versus 60 min). However, much more burnoff is required to produce a given surface area in the RDF char; e.g., 65% carbon burnoff of the RDF char yields a surface of approximately 930 m²/g carbon whereas only 37% burnoff of the prune pit char achieves the same specific surface per gram carbon. The RDF

TABLE 12. COMPARISON OF ACTIVATION OF PRUNE PIT CHAR AND RDF CHAR

Material	Time of Activation (min)	Carbon Content (%)	Mass Loss (%)		Surface Area ^a	
			Gross Wt. Basis	Carbon Basis ^b	m ² /g	m ² /g-Carbon ^c
Prune Pit Char	15	nd ^d	21.7	- ^e	663	-
"	30	nd	37.1	-	927	-
"	42	nd	49.7	-	1175	-
"	60	nd	67.2	-	1692	-
RDF Char	9	49.1	30.3	47.5	300	612
"	15	39.6	42.8	65.2	370	934

^aDetermined using BET equation on N₂ adsorption data (77K).

^bMass loss (carbon basis) = $100 - \frac{(\text{Carbon content of activated char})}{(\text{Carbon content of char})} (100 - \text{Gross Mass Loss})$.

^cSurface area (m²/g C) = surface area (m²/g)/carbon content of activated char.

^dnd = not determined.

^e(-) = cannot be calculated since percent carbon data not determined.

char loses mass more rapidly during activation with less development of surface area per unit mass lost. This comparison, however, is not general since the conditions of activation of the two chars are quite different (much higher CO_2 flow rate for RDF char activation).

In fact the different behavior of the RDF char in activation can be at least partly explained by the higher CO_2 flow rate and the much higher inorganic content of the char. It is thought that low flow rates of CO_2 allow retention of the gasification product CO at the char particle surface, resulting in inhibition of gasification of the surface and, therefore, greater development of microporosity per unit mass loss (50). Such was the case for prune pit char activation, which resulted in extensive microporosity and surface area development. The higher CO_2 flow rate in RDF char activation may have resulted in a higher percent of the observed mass loss occurring at the particle exterior at the expense of development of microporosity and therefore surface area. Furthermore, inorganic impurities are known to increase the rate of gasification (51) and are thought to concentrate on the particle surface (51), resulting in preferential development of macro- and transitional-pores (53). Hence, even for equivalent CO_2 flow conditions, RDF char would be expected to yield less microporosity and surface area per unit mass loss than prune pits or other low-ash materials.

These results are consistent with past work on RDF pyrolysis and activation (92), in which activated carbon made from RDF was found to have a large proportion of pore volume in the transitional-pore size range. In these studies the activated carbon prepared from RDF was found to have a low specific surface area ($350 \text{ m}^2/\text{g}$), similar to our results. The encouraging aspect about this past work, however, was that the waste-derived activated carbon, despite its low specific surface area, was equally effective as commercial activated carbon (AN-A) in reduction of organics (measured by chemical oxygen demand) in primary-treated municipal wastewater.

In conclusion our results and past work indicate that an activated carbon can be prepared from classified municipal solid waste (RDF) which, despite a low specific surface area and high ash content, may be a useful adsorbent for some applications such as wastewater treatment. Ash removal by washing (1), air-classification (92), or both might yield an activated carbon of generally acceptable quality. Finally, preparation of the char by pyrolysis to 900°C followed by activation with CO_2 at 900°C and lower flow rates than used in this study may result in an even more attractive activated carbon with more highly developed microporosity and surface area.

SORPTIVE PROPERTIES OF ACTIVATED LIGNOCELLULOSICS

Experiments were conducted both to determine the rate of approach to equilibrium for the various carbons and to determine an adsorption isotherm for the prune pit carbons and for F400. All DOC adsorption experiments were conducted with filter-sterilized unchlorinated secondary effluent from the Palo Alto Water Quality Control Plant.

Rate Experiments

F400, F100, and AN-A--

An experiment was conducted to compare F400, F100 and AN-A with respect to their rates of uptake of DOC from secondary effluent. In this experiment, a dose of 50 mg activated carbon/115 ml wastewater was used. Wastewater included 100 ml of secondary effluent plus 15 ml of Milli-Q water in which the activated carbon was presoaked overnight. The pH did not change significantly in this experiment, remaining in the range 7.5 to 8.0.

The kinetic behavior of Filtrasorb 400 and 100 were much alike in this experiment, as shown in Figure 20. Of an initial DOC concentration of 14.2 mg/l, only 9 mg/l remained after 20 min and 6.3 mg/l after 120 min. The AN-A adsorbed less rapidly; the residual concentration after 120 min was 8 mg/l.

Prune Pit Carbons and Filtrasorb 400--

Two adsorption experiments were conducted on 60M, 42M, 30M, and F400, with a dosage of 30 mg carbon/110 ml wastewater (runs 4 and 11). Coincidentally, the two secondary effluents used for these two experiments had virtually the same DOC of 10.04 ± 0.60 and 10.20 ± 0.55 mg/l for runs 4 and 11, respectively. In light of this similarity, the results of these two runs were averaged, and a 95% confidence interval was established for the average. In establishing a 95% confidence interval from two data sets, one must assume that the two data sets represent subgroups of the same population. Statistically, such a claim could not rigorously be made in this case; although the DOC of filtered secondary effluent on one day may by coincidence be the same as on another day, both the compounds which constitute this DOC and the properties of these compounds for the same two samples may vary considerably. Such problems are inherent when the complexity of secondary effluent is ignored by using a collective parameter such as DOC. The data from runs 4 and 11 are shown in Appendix C. The average of the two runs are in Figure 21. The 95% confidence interval for these averaged values are generally of a magnitude corresponding to the size of the symbols that are used to represent the data.

In run 4, the magnitude of adsorption at any given time increased with the magnitude of surface area. Adsorption is greatest for 60M, followed in order by 42M, F400, and 30M. In run 11, this same trend persisted with the exception that F400 and 42M behaved nearly the same. Moreover, for F400 the variation between the adsorption behavior of run 4 compared to run 11 was slightly greater than the variation experienced by any of the other activated carbons, especially at the longer times. For most of the carbons the variation in DOC at any given time, from run 4 to run 11 was on the order 0.5 to 1.0 mg/l. In comparison, the standard deviation varied from 0.10 to 0.65 mg/l for triplicate analyses for a given set of conditions.

Also included in run 11 are several data for 15M and Char at prolonged times, as can be seen in Appendix C. The 15M adsorbed less than did 30M, and the Char adsorbed less than did the 15M.

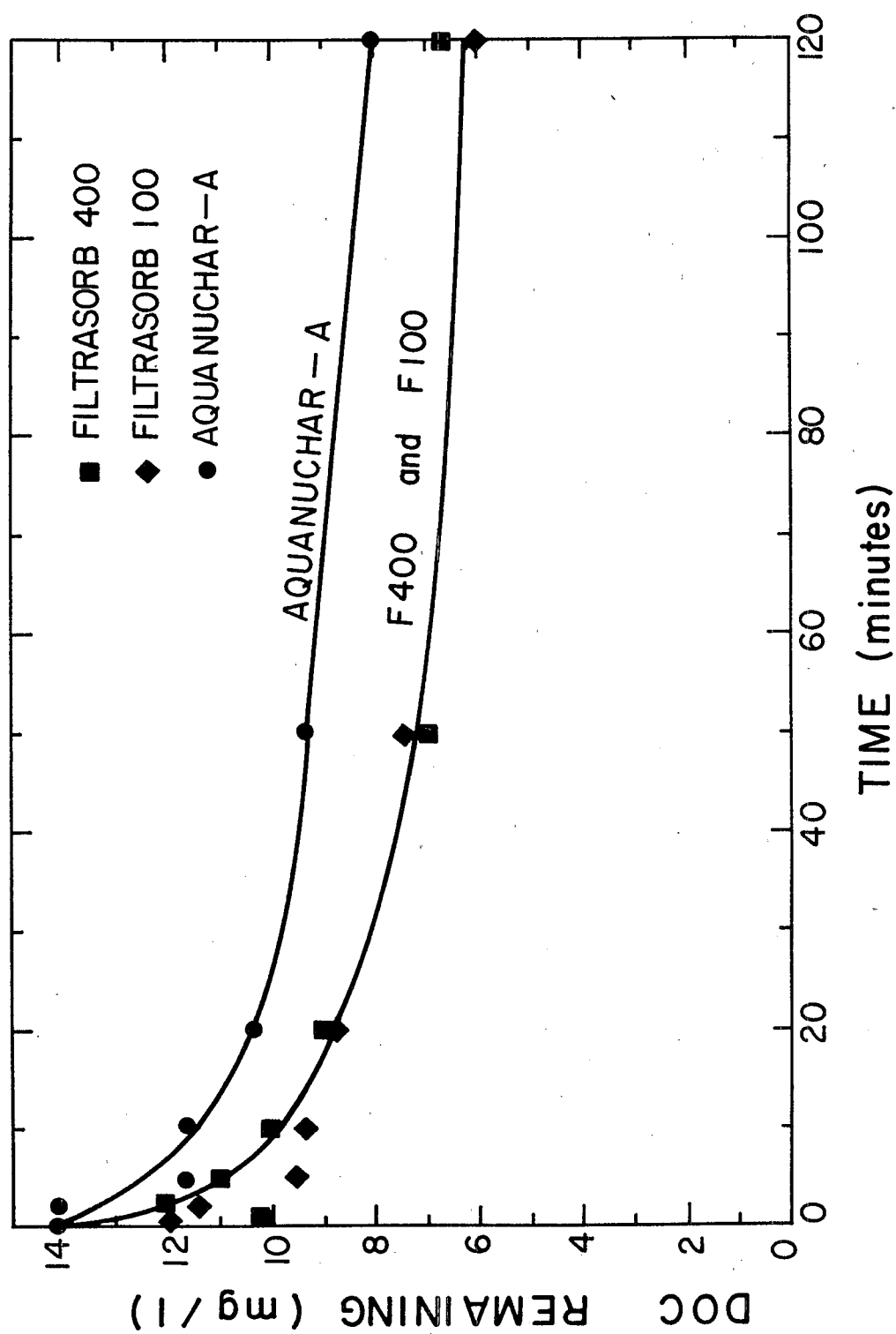


Figure 20. Kinetics of DOC adsorption for F400, F100, and AN-A (run 2) at a loading of 50 mg active carbon/110 ml wastewater

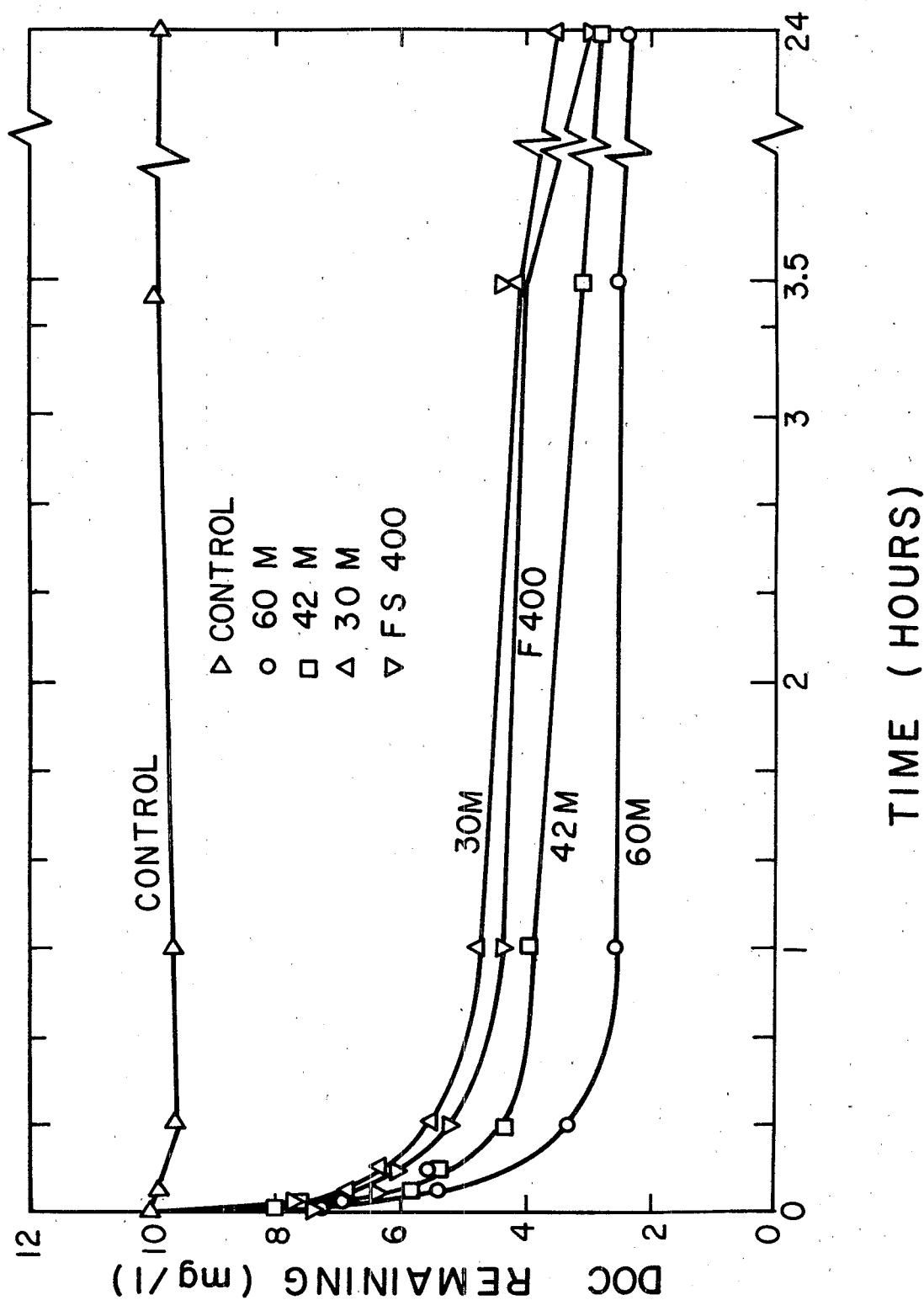


Figure 21. Kinetics of DOC adsorption for 60M, 42M, 30M, and F400 at a loading of 30 mg active carbon/110 ml wastewater. (Average of runs 4 and 11.) Error bars representing 95% confidence intervals are shown when they are not within the magnitude of the symbols. The bars are deleted for times less than 10 min to avoid confusion.

Adsorption Isotherms

Adsorption isotherms were conducted on 60M, 42M, 30M, and F400; the results of these experiments are plotted as q_e (mg DOC adsorbed/g carbon) versus C_e (mg DOC remaining/l) in Figure 22.

The development of adsorption isotherms required that the ratio of initial adsorbate (grams) to activated carbon (grams) be varied over a range of several orders of magnitude. In principle, this can be achieved by one of several methods. The first entails varying the concentration of the initial adsorbate over several orders of magnitude for a constant water volume and constant activated carbon mass. Alternatively, for a constant initial concentration of adsorbate, the ratio of activated carbon mass to water volume can be varied. The latter of these two is usually used, and was considerably more practical in our case in which the adsorbate consisted of the organic substance present in secondary effluent. It would not have been feasible to vary the concentration of residual organics over a wide range.

For these reasons, the ratio of activated carbon mass to wastewater volume was varied; the initial DOC concentration was maintained constant. In the experiments the carbon/wastewater ratio was varied from 0.990 g/25 ml to 0.015 g/200 ml, which represents a range of a factor of 500. It was found that the standard deviation in q_e (calculated as described below) was too great for carbon/wastewater ratios below the lower extreme of 0.015 g/200 ml. Although several experiments were conducted with lower ratios, the results were not statistically useful.

From the results of these experiments (designated as run 8), it can be seen in Figure 22 that 60M adsorbed the most DOC, followed closely by F400. Trailing behind these are 42M and then 30M. For the prune pit carbons, then, the magnitude of adsorption increased with increased activation.

The standard deviations for the data also are shown in Figure 22. The standard deviation of C_e was taken to be that of the triplicate analyses for a given sample; that of q_e was calculated as

$$s_{q_e} = \left[\frac{(S_{C_c})^2 + (S_{C_e})^2}{(C_c - C_e)^2} + \left(\frac{S_v}{V}\right)^2 + \left(\frac{S_m}{M}\right)^2 \right]^{1/2} \times q_e \quad (18)$$

where $C_c \pm S_{C_c}$ = the mean DOC concentration of the control \pm its standard deviation; $C_e \pm S_{C_e}$ = mean DOC concentration of the given sample at equilibrium \pm its standard deviation; $V \pm S_v$ = volume of wastewater \pm an expected experimental standard deviation taken to be 2%, and $M \pm S_m$ was the mass of the sample \pm the experimental standard deviation inherent in weighing. As can be seen in Figure 22, the standard deviation became great as C_e approached C_c . The value q_e was calculated as

$$q_e \text{ (mg/g)} = \frac{(C_c - C_e) \text{ (mg/l)} \times V \text{ (l)}}{M \text{ (g)}} \quad (19)$$

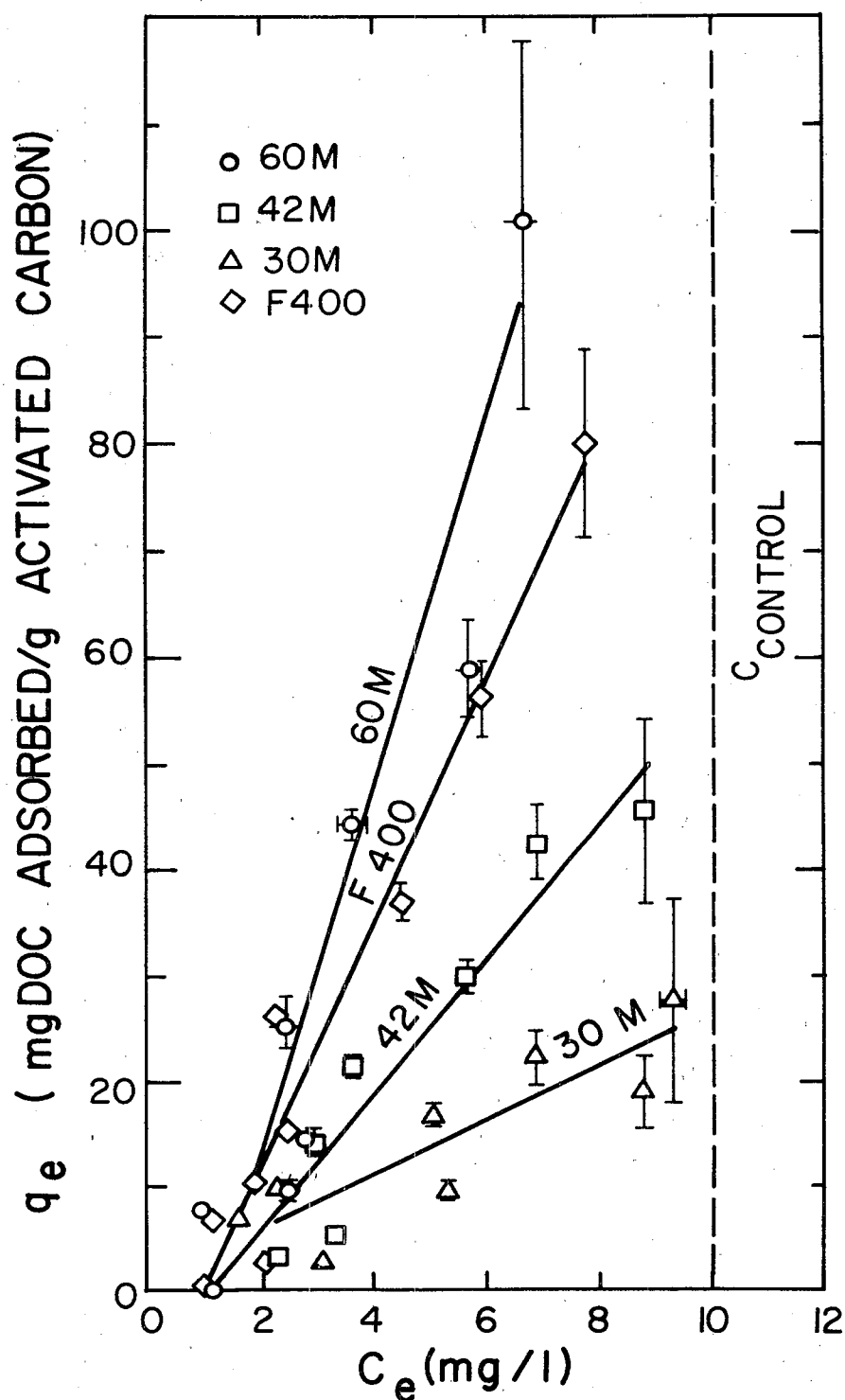


Figure 22. DOC adsorption isotherms: q_e versus C_e for 60M, 42M, 30M, and F400 (run 8). Error bars, representing standard deviation, are included when they exceed the magnitude of the corresponding symbol. Lines represent linear regression.

The control concentration C_c was used in the calculation of q_e rather than the initial concentration C_0 . The value C_c represents the DOC remaining in a controlled reaction flask which was subjected to the same conditions as was used for the samples. In the control flask, however, there was no activated carbon present.

It was the control concentration, rather than the initial concentration, with which adsorbed and bulk phases came into equilibrium.

Interestingly, linear isotherms most accurately fit the adsorption behavior of each of the activated carbons. Correlations with both Freundlich and linear isotherm relationships were investigated for these data; these models were not as successful in describing the data as were a linear isotherm. A plot with Langmuir coordinates ($1/q_e$ versus $1/C_e$) showed very little detectable pattern for any given carbon.

The Freundlich isotherm model fit all but the lower ranges of $\log q_e$ versus $\log C_e$ data. Experimental fluctuations in the data at these low ranges were exaggerated by the log-log type of a plot. The Freundlich equation is of the form:

$$q_e = K_F C_e^{1/n} \quad (9)$$

The values of n calculated from these data were generally close to 1 and a 95% confidence interval encompassed 1, as shown in Appendix D. This suggests that a linear isotherm could be as easily used to describe the data.

The linear isotherm was of the form:

$$q_e = b(C_e - C_n) \quad (10)$$

where C_n corresponded to the non-adsorbable portion of the DOC. The linear adsorption constants were determined by linear regression of the data in Figure 22. These constants, as well as the 95% confidence intervals are shown in Table 13.

TABLE 13. LINEAR ADSORPTION ISOTHERM COEFFICIENTS

Run No.	Activated Carbon Type	Calculated Nonadsorbable ^a DOC C_n (mg/l)	95% Confidence Interval of $b = q_e/(C_e - C_n)$ (liters/g)	Correlation Coefficient (r)	Number of Points
Run 8	60M	1.28	17.5 ± 7.3	0.9340	7
	42M	1.15	6.5 ± 2.0	0.9549	8
	30M	-0.44	2.5 ± 1.4	0.8683	8
	F400	0.95	11.4 ± 2.0	0.9763	10
Run 6	F400	0.97	5.4 ± 1.4	0.9333	13

^aDefined as the intercept on the abscissa of Figure 22.

The 95% confidence interval of b was computed as (93):

$$b \pm t(0.975, n-1) \cdot \left[\left(\frac{1}{n-2} \right) b^2 \left(\frac{1}{r^2} - 1 \right) \right]^{1/2} \quad (20)$$

where t is the t distribution, n is the number of data points, and r is the correlation coefficient.

The nonadsorbable concentration in these linear regressions was for most cases calculated to be about 1.0 mg/l. Indeed, in all the data collected in run 8, an equilibrium concentration of DOC never was achieved much below 1.0 mg/l, even at very high dosages of activated carbon. This fraction, then, could be considered to be the non-adsorbable portion of the DOC; it constituted about 10% of the total control concentration.

A second adsorption isotherm experiment was conducted with F400 (run 6); the results of this experiment are shown in Figure E-1 (Appendix E) along with the results of F400 in run 8 (the comparison isotherm experiment described above), and the adsorption isotherm data for F400 from the equilibrium conditions achieved in the kinetic experiments. As can be seen, the slope of the curve for run 6 is less steep than for run 8. Correspondingly, the control concentration for run 6 was nearly 2 mg/l higher (11.78 mg/l) than for run 8 (10.09 mg/l).

The isotherm data from the kinetic experiments agreed closely with the linear regression on the equilibrium isotherm results from run 8. The control concentrations in these kinetic experiments are shown in Appendix E, Fig. E-1.

The relationships between Γ_e (mg DOC adsorbed/m² specific surface area) and C_e was also investigated, and is presented for run 8 in Figure 23. As can be seen, F400 and 60M behaved much the same (within the statistical significance of the data). 42M adsorbed less organic carbon per N₂-BET specific surface area at a given equilibrium concentration C_e , and 30M still less. This would suggest that less of the specific surface area for 42M and 30M than for F400 and 60M was available for adsorbing some portion of organic compounds. The difference between the prune pit carbons was perhaps due to the size of the pores; the small pores may have excluded some of the larger organic molecules from reaching potential adsorption sites to a greater extent in the 30M carbon than in the 60M carbon.

The difference may also be due to variations in the functional groups which are present in the activated carbon at its surface. This question was not investigated in the present study.

Model for the Kinetics of Adsorption

The equation for diffusion into a spherical adsorbent grain for which a linear isotherm applies is of the form:

$$\frac{\partial C}{\partial t} = \frac{D}{(1+R)} \left(\frac{\partial^2 C}{\partial r^2} + \frac{2}{r} \frac{\partial C}{\partial r} \right) \quad (13)$$

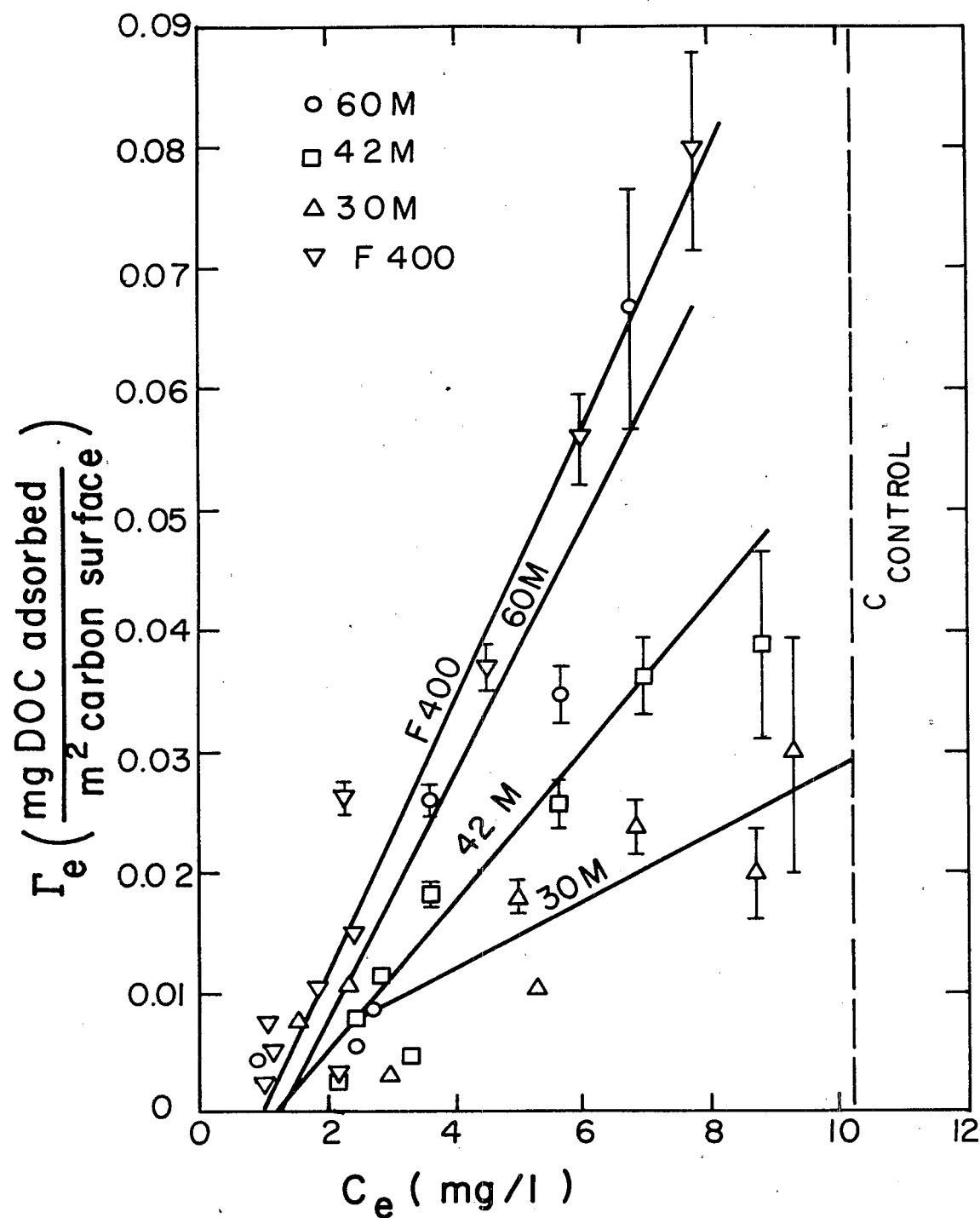


Figure 23. Γ_e (mg DOC adsorbed/m² surface area) versus C_e (mg/l DOC remaining in solution at equilibrium) for 60M, 42M, 30M, and F400 (run 8).

This was described in Section 5 of this report. For the case where the carbon is initially free of solute, and the bulk concentration decreases with time, this expression is numerically solved in the form given by Crank (68):

$$\frac{C_o - C_t}{C_o - C_\infty} = f = 1 - \sum_{n=1}^{\infty} \frac{6\alpha(\alpha + 1)e^{-\tau q_n^2}}{9 + 9\alpha + q_n^2 a^2} \quad (21)$$

where

- C_o = initial bulk solution concentration, (g/m³),
- C_t = concentration of bulk solution at time t, (g/m³),
- C_∞ = concentration of bulk solution at equilibrium, (g/m³),
- f = fractional approach to equilibrium,
- q_n = non-zero roots of $\tan q_n = 3q_n/(3+\alpha q_n)$ (Appendix F),
- $F = (C_o - C_\infty)/(C_o - C_n)$ = equilibrium fractional uptake,
- $\alpha = (1 - F)/F$,
- τ = dimensionless time parameter given by

$$\tau = \frac{Dt}{(1 + R)a^2} \quad (22)$$

where

- t = time, (s),
- D = diffusion coefficient, (m²/s),
- a = average grain diameter, (m), and
- R = partition coefficient between the adsorbed and bulk concentration of solute in a given activated carbon pore (dimensionless).

The diffusion equation can also be solved in another form that is more convenient for evaluation at small values of the time parameter (at small times the solution to Eq. 23 yields many roots). The alternative solution is of the form:

$$f = (1 + \alpha) \left[1 - \frac{\gamma_1}{\gamma_1 + \gamma_2} e^{\text{erfc}\left\{\frac{3\gamma_1}{\alpha} (\tau)^{1/2}\right\}} - \frac{\gamma_2}{\gamma_1 + \gamma_2} e^{\text{erfc}\left\{\frac{-3\gamma_2}{\alpha} (\tau)^{1/2}\right\}} \right] \quad (23)$$

In this notation:

$$\gamma_1 = \frac{1}{2} \{ (1 + 4/3\alpha)^{1/2} + 1 \} \quad (23a)$$

$$\gamma_2 = \gamma_1 - 1 \quad (23b)$$

$$e \operatorname{erfc} z \equiv \exp z^2 \operatorname{erfc} z$$

Both of these expressions were programmed on a Hewlett-Packard 97 calculator to be used in modeling the kinetic behavior of the DOC.

Several assumptions are required for the use of Eq. 13. The first of these is that diffusion occurs only in the bulk solution of the activated carbon pores, and that the portion of solute that is adsorbed is not free to diffuse along the surface of the pore. Moreover, it is assumed that the rate of adsorption and desorption is much faster than the rate of diffusion, so equilibrium between the pore bulk and adsorbed phase is considered to exist at all locations within the pores. The assumption of pore phase equilibrium is usually accepted in the literature (13,61,67,70). However, some of the literature indicates that surface diffusion does indeed occur (13,61,70) and often contributes more to overall mass flux within the pores than does bulk diffusion. In our experiments, using the collective parameter DOC, it was not possible to discriminate between surface diffusion and bulk diffusion, because the two cases are virtually identical mathematically when the equilibrium isotherm is linear.

The second group of assumptions relates to the calculation of F, the equilibrium fractional uptake. The quantity F equals the fraction of the total solute initially present that was eventually adsorbed by the activated carbon under the conditions of the experiment. It must be considered that the non-adsorbable portion of DOC, C_n , does not contribute to a diffusion driving force, and so should be subtracted from all values of concentration. The value F, then, is calculated as

$$F = \frac{([C_o - C_n] - [C_\infty - C_n])}{[C_o - C_n]} = \frac{C_o - C_\infty}{C_o - C_n} \quad (24)$$

The third group of assumptions relate to the calculation of R, the partition coefficient:

$$R = \left[\frac{\text{g solute adsorbed within the grain}}{\text{g solute in bulk solution within the grain}} \right]$$

$$R = \frac{\left(\frac{\text{g solute adsorbed}}{\text{g sorbent}} \times \frac{\text{g sorbent}}{\text{cm}^3 \text{ grain}} \right)}{\left(\frac{\text{g solute in pore solution}}{\text{cm}^3 \text{ pore volume}} \times \frac{\text{cm}^3 \text{ pore volume}}{\text{cm}^3 \text{ grain}} \right)}$$

$$R = \frac{[b \times 1000] \times \rho_b}{\epsilon_t} \quad (25)$$

where

b = the slope of the linear adsorption isotherm determined from run 8,
(mg solute/g carbon)/(mg solute/l solution)

ρ_b = (grams active carbon)/(cm³ carbon volume + cm³ void volume)

ϵ_t = (cm³ pore volume in the macro- and transitional-pore size range)/(cm³ total pore volume).

It is assumed that the interior void volume of the activated carbon can be determined as the summation of volumes calculated by N₂ isotherm and mercury porosimetry with radius < 300 nm. The bulk pore volume, representing the pore volume that contains a bulk solution phase (as opposed to only an adsorbed phase) is taken to be the interior pore volume which has a radius > 3 nm. It was further assumed that the true carbon density (excluding voids) was 2.1 g/cm³.

The values for b , ρ_b , ϵ_t , and R , based on these assumptions, are shown in Table 14 for 60M, 42M, 30M, and F400. The quantity of solute adsorbed, if these assumptions are correct, is more than four orders of magnitude greater than the quantity of solute in equilibrium with this in the bulk phase, as indicated by the values of R in Table 14.

Based on these assumptions, the averaged data from runs 4 and 11 were evaluated to see whether they exhibited behavior similar to that predicted by the model. Theoretical plots of $\log f$ versus $\log \tau$ could be made through the use of the two programmed numerical solutions (HP-97 calculator). Such plots were made for 60M, 42M, 30M, and F400 based on the fractional uptake (F) that was observed in each experiment. Of the two numerical solutions for the diffusion equation, the second, involving the error function, was the most convenient. In the first solution, the infinite series was truncated to six terms corresponding to the six roots for q_n that were provided and are shown here in

TABLE 14. ESTIMATION OF THE PARTITION PARAMETER R

Active Carbon Type	b ($\frac{\text{mg/g}}{\text{mg/l}}$)	ρ_b ($\frac{\text{g}}{\text{cm}^3}$)	ϵ_t ($\frac{\text{cm}^3 \text{ pores with } 3 \text{ nm} < r < 300 \text{ nm}}{\text{cm}^3 \text{ total volume}}$)	R ($\frac{\text{g adsorbed}}{\text{g in solution}}$)
60M	17.46	0.711	0.131	94,900
42M	6.48	0.900	0.1161	50,200
30M	2.53	1.010	0.139	18,300
F400	11.40	0.895	0.180	56,700

Appendix G (68). If the last of these terms is insignificantly small, then the model is accurate; however as τ becomes small, this last term becomes more significant. Likewise, the terms which were truncated out of the infinite series are also significant, and their exclusion from the infinite series causes the numerical solution to become inaccurate. This significant error occurs for values of τ less than 1×10^{-2} , corresponding to a time of 20 min in our experiments.

The second of the numerical solutions (Eq. 23), on the other hand, was useful throughout the range of times. Furthermore, it agreed with the first numerical solution to three significant digits for τ greater than 10^{-2} .

From the HP-97 programs were determined the diffusion coefficient D which resulted in the best fit between the experimental data and the theoretical model at any given time. These calculated diffusion coefficients were fairly consistent (within one order of magnitude, between 4×10^{-7} and 8×10^{-6} cm^2/sec) for all of the carbons studied. These are shown, along with τ and both the experimental f and calculated f , in Appendix G. The magnitude of diffusion coefficients for 60M were slightly larger than the others. Then, in descending order of D values came F400, 42M, and 30M. The difference between these, however, is not significant, especially in light of possible errors in estimating the several variables which were used to calculate the values of D .

For a given carbon, the diffusion coefficient was generally slightly higher at the early time of 1 min, and slightly lower at the latter times of 60 min and 210 min. This is consistent with what might be expected: at very short times, those compounds which diffuse the most rapidly tend to dominate. As time passes, these rapidly diffusing compounds will have already reached equilibrium, and those which diffuse more slowly will still be entering the carbon. The prominence of these slower molecules would tend to diminish the measured diffusion coefficient.

In a second approach to comparing the model to the experimental data, a median diffusion coefficient was chosen from the range of D values determined above for each of the carbons. This D usually corresponded to that measured at 5, 10, or 20 min. The value so chosen was designated the effective diffusivity D_e for the given experiment. Using this value D_e , corresponding values of τ were calculated. The plot of experimental values of f and τ (Figure 24) shows good agreement between the experimental data (represented by symbols) and the model (represented by the series of curves). These effective diffusion coefficients are tabulated in Table 15, along with the corresponding transitional- and macropore volumes.

These diffusion coefficients are compared (Table 16) with those predicted for bulk diffusion of high molecular weight compounds and various specific compounds (Reid and Sherwood (94)), and the pore and surface diffusion coefficients determined by several other investigators (61,70,79). As can be seen, the pore diffusion model and experimental data described in this report were successful in determining pore diffusion coefficients consistent with those expected for large molecules. Assuming a median molecular weight of 500 for organic constituents represented by DOC in secondary effluent (73,74,75), the expected value of the bulk diffusivity for DOC is on the order of $3 \times 10^{-10} \text{ m}^2/\text{s}$.

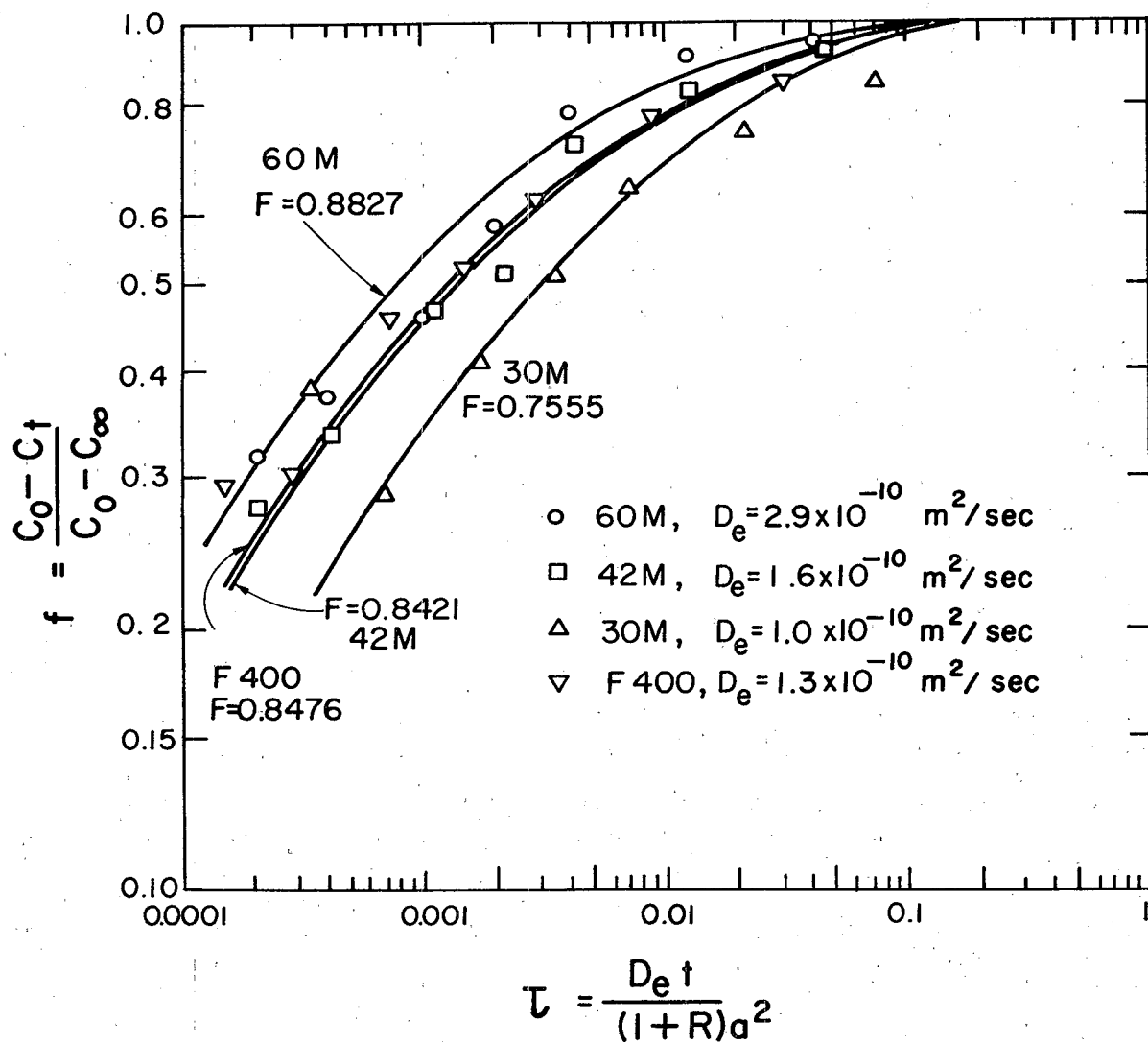


Figure 24. Pore diffusion model for kinetics of DOC adsorption by 60M, 42M, 30M, and F400. Values of D_e corresponding to best fit (runs 4 and 11). Curves represent the solution to pore diffusion model as f versus τ for the appropriate value of F , the total fractional uptake of DOC.

TABLE 15. MEDIAN DIFFUSION COEFFICIENT AND PORE VOLUME

Active Carbon Type	Average Effective Diffusivity (m^2/g)	Pore Volume (cm^3/g) with $3 \text{ nm} < r < 300 \text{ nm}$
60M	3.2×10^{-10}	0.128
42M	1.6×10^{-10}	0.105
30M	1.1×10^{-10}	0.104
F400	1.4×10^{-10}	0.160

The experimental values were in the range of 1×10^{-10} to $3 \times 10^{-10} \text{ m}^2/\text{s}$. Values of D_e slightly lower than the molecular diffusivity are justified by deviation of the pores from the ideal model of straight, cylindrical tubes (69). Frequently this deviation is expressed as

$$D_e = D/X \quad (26)$$

where

D_e = effective diffusivity for internal pore transport, m^2/s ,

D = molecular diffusivity, m^2/s , and

X = tortuosity factor, dimensionless, accounting for irregularities of pore shape.

Values of X have been reported in the range of 2 to 10 for porous solids such as catalyst grains (95).

Hence, the experimentally measured values of the effective diffusivity for activated carbons are consonant with a simple model assuming pore diffusion as the rate-limiting step. The good agreement between the measured rate data and form of the uptake curves based on the model (Figure 24) also strengthens confidence in the validity of the model as a means of interpreting our data. It appears unnecessary to consider surface diffusion as an important phenomenon contributing to the internal transport of the broad spectrum of organics measured by DOC. If surface diffusion were rate-controlling, the experimental pore diffusion coefficients would be substantially in excess of the molecular diffusivity.

The interpretation of the rate data in this work in terms of the pore diffusion model for internal transport should not be construed as a rejection of the surface diffusion model. Rather, it is intended simply to emphasize that transport by pore diffusion appears to be significant, and that the pore diffusion mechanism is sufficient to explain the observed rates, in view of the limitations of the data. This is not meant to imply that the interpretation of the rate data in terms of pore diffusion is the only correct approach to data analysis. Indeed, it is theoretically impossible to distinguish

TABLE 16. ESTIMATED DIFFUSION COEFFICIENTS

Diffusing Species	Molecular Weight	Adsorbent	Apparent Pore Diffusion Coefficient (m^2/sec)	Assumptions and Conditions for Measurement	Ref.
DOC	wide range, ~ 50% (w/w) > 500	60M 42M 30M F400	3.2×10^{-10} 1.6×10^{-10} 1.1×10^{-10} 1.4×10^{-10}	Pore diffusion, described in text.	Exptl. values from this work
"Typical" large molecules	500 5,000 50,000	(bulk diffusion)	3.5×10^{-10} 1.6×10^{-10} 0.74×10^{-10}	For very large unhydrated molecules in water at room temperature (Reid and Sherwood) $D = 2.74 \times 10^{-5} \text{M}^{-1/3}$.	(94)
Benzoic acid	122	(bulk diffusion)	12.1×10^{-10}	From table of diffusion coefficients in aqueous solutions at infinite dilution (Reid and Sherwood).	(94)
Oxalic acid	102		15.3×10^{-10}		
Iso Butyl alcohol	74		7.7×10^{-10}		
Phenol	94	F400	3.53×10^{-12}	Surface diffusion, based on the model of Crittenden, assuming that pore diffusion is insignificant.	(70)
Dodecyl benzene sulfonate	326		4.69×10^{-13}		
Phenol	94	Activated Carbon	$0.2-1.5 \times 10^{-10}$	Pore diffusion coefficient (Fritz).	(61)
Dodecyl benzene sulfonic acid	325	Activated Carbon	$1-2 \times 10^{-13}$	Solid diffusion coefficient (Fritz).	(61)
DOC	wide range	Activated Carbon	10^{-11} to 10^{-12}	Pore diffusion, based on model of Hsieh.	(79)

between the pore diffusion and surface diffusion for the case of linear equilibrium (61).

The apparent success of the pore diffusion model in simulating the rate of DOC uptake is surprising. Previous workers (61) studying the rate of uptake of model substances such as phenol and paranitrophenol by activated carbon have found internal transport to be more rapid than could be explained by pore diffusion, and hence have invoked the surface diffusion concept. The cause of the difference may lie in the different nature of the solutes: the model substances (phenol and p-nitrophenol) are more strongly sorbed than is the collective parameter DOC. Hence, the equilibrium isotherm for phenol and paranitrophenol is favorable ($n \gg 1$ in the Freundlich expression, Eq. 9) and the driving force for surface diffusion is greater than for pore diffusion. For DOC, the equilibrium isotherm is linear, and surface diffusion is less likely to be important.

SUMMARY

Results have been reported for experiments dealing with pyrolysis and activation of lignocellulosic materials, physical characterization of the resulting chars and activated carbons, and evaluation of the performance of activated carbon prepared from a lignocellulosic waste. Lignocellulosic materials were found to behave in pyrolysis according to their initial composition. The chars formed have a substantial microporous volume and specific surface, but no measurable pore volume in the size range essential for transport of large molecules. Activation in a CO_2 atmosphere at 900°C serves to enlarge the pores, and to create pore volume in a size range suitable as a diffusion network for organic substances of the sort encountered in water and wastewater. One such activated char prepared from prune pits demonstrated an adsorption capacity and transport rate coefficient (effective diffusivity) equal if not superior to the corresponding values for Filtrasorb 400, a commercially produced, coal-based activated carbon widely used for water and wastewater treatment. A simple model based on linear equilibrium and transport by pore diffusion proved useful in interpreting the data for DOC uptake by activated carbon.

REFERENCES

1. Hassler, J. W. Purification with Activated Carbon. Chemical Publishing Co., Inc., New York, New York, 1974. 390 pp.
2. Iley, M., H. Marsh, and F. R. Reinoso. The Adsorptive Properties of Carbonised Olive Stones. Carbon, 11:633-638, 1973.
3. Marsh, H., M. Iley, J. Berger, and T. Siemieniewska. The Adsorptive Properties of Activated Plum Stone Chars. Carbon, 13:103-109, 1975.
4. Mahajan, O. P., and P. L. Walker, Jr. Porosity of Coal and Coal Products In: Analytical Methods for Coal and Coal Products, Vol. I, C. Karr, Jr., ed. Academic Press, New York, New York, 1978. pp. 125-162.
5. Dubinin, M. M. Porous Structure and Adsorption Properties of Active Carbons. In: Chemistry and Physics of Carbon, Vol. 2, P. L. Walker, Jr., ed. Marcel Dekker, Inc., New York, New York, 1966. pp. 51-120.
6. Brunauer S., P. H. Emmett, and E. Teller. Adsorption of Gases in Multimolecular Layers. J. Am. Chem. Soc., 60:309-319, 1938.
7. Sutherland, J. W. The Usefulness of Measurements of the Physical Adsorption of Gases in Characterizing Carbons. In: Porous Carbon Solids, R. L. Bond, ed. Academic Press, New York, New York, 1967. pp. 1-64.
8. Lamond, T. G., J. E. Metcalfe, III, and P. L. Walker, Jr. 6Å Molecular Sieve Properties of Saran-Type Carbons. Carbon, 3:59-63, 1965.
9. Lamond, T. G., and H. Marsh. The Surface Properties of Carbon - II. The Effect of Capillary Condensation at Low Relative Pressures upon the Determination of Surface Area. Carbon, 1:281-292, 1964.
10. Atkins, J. A. Porosity and Surface Area of Carbon Black. Carbon, 3:299-303, 1965.
11. Chiche, P., S. Durif, and S. Prégermain. Development of the Internal Surface Area of Coals During Carbonization. Fuel, 44:5-28, 1964.
12. Cranston, R. W., and F. A. Inkley. The Determination of Pore Structures from Nitrogen Adsorption Isotherms. Advances in Catalysis, Vol. 9. Academic Press, New York, New York, 1957. pp. 143-155.

13. Walker, P. L., Jr., L. G. Austin, and S. P. Nandi. Activated Diffusion of Gases in Molecular-Sieve Materials. In: Chemistry and Physics of Carbon, Vol. 2, P. L. Walker, Jr., ed. Marcel Dekker, Inc., New York, New York, 1966. pp. 257-371.
14. Micromeritics Instrument Corporation. Instruction Manual for Model 2100 Orr Surface Area and Pore-Volume Analyzer. Norcross, Georgia, 1969. 55 pp.
15. El Tawil, M. M., and L. F. Brown. Changes in Pore Structure of a Devolatilized Coal Char upon Further Heating at Lower Temperature. Carbon, 14:132-133, 1976.
16. Marsh, H., and W. F. K. Wynne-Jones. The Surface Properties of Carbon - I. The Effect of Activated Diffusion in the Determination of Surface Area. Carbon, 1:269-279, 1964.
17. Scholten, J. J. F. Mercury Porosimetry and Allied Techniques. In: Porous Carbon Solids, R. L. Bond, ed. Academic Press, New York, New York, 1967. pp. 225-250.
18. Washburn, E. W. Note on a Method of Determining the Distribution of Pore Sizes in a Porous Material. Proc. Nat. Acad. Sci. U.S., 7:115-116, 1921.
19. Dickinson, J. M., and J. W. Shore. Observations Concerning the Determination of Porosities in Graphites. Carbon, 6:937-941, 1968.
20. Lehninger, A. L. Biochemistry, 2nd ed. Worth Publishers, Inc., New York, New York, 1975. 1104 pp.
21. Shafizadeh, F. Pyrolysis and Combustion of Cellulosic Materials. Advances in Carbohydrate Chemistry, 23:419-474, 1968.
22. Tang, M. M., and R. Bacon. Carbonization of Cellulose Fibers - I. Low Temperature Pyrolysis. Carbon, 2:211-220, 1964.
23. Bacon, R., and M. M. Tang. Carbonization of Cellulose Fibers - II. Physical Property Study. Carbon, 2:221-225, 1964.
24. Stamm, A. J. Thermal Degradation of Wood and Cellulose. Ind. Engr. Chem., 48:413-417, 1956.
25. Tang, W. K., and W. K. Neill. Effect of Flame Retardants on Pyrolysis and Combustion of α -Cellulose. J. Polym. Sci: Part C, 6:65-81, 1964.
26. Brunner, P. H. Examination of the Pyrolysis of Cellulose for the Production of Activated Carbon from Wastes. Internat. Solid Wastes Assoc. Bull., 23:2-10, 1977.
27. Broido, A. Thermogravimetric and Differential Thermal Analysis of Potassium Bicarbonate Contaminated Cellulose. Pyrodynamics, 4:243-251, 1966.

28. Hawkins, W. L. Polymer Stabilization. Wiley Interscience, New York, New York, 1972.
29. Brunner, P. H., and P. V. Roberts. The Significance of Heating Rate on Char Yield and Char Properties in the Pyrolysis of Cellulose. Carbon (in press).
30. Masters, K. J., and B. McEnaney. The Structural Evolution of a Microporous Carbon with Heat Treatment. Paper presented at 14th Biennial Conference on Carbon sponsored by the American Carbon Society, The Pennsylvania State University, 1979. (Proceedings in press.)
31. Freeman, E. M., and H. Marsh. Selective Structural Gasification from Paracrystalline Carbon - A Critical Assessment and Gas-Phase Adsorption Investigation. Carbon, 8:19-30, 1970.
32. Sarkanen, K. V., and C. H. Ludwig. Lignins. Wiley-Interscience, New York, New York, 1971. 916 pp.
33. Shafizadeh, F., and G. P. McGinnis. Chemical Composition and Thermal Analysis of Cottonwood. Carbohydr. Res., 16:273-277, 1971.
34. Shafizadeh, F., and P. P. S. Chin. Thermal Deterioration of Wood. In: Wood Technology: Chemical Aspects, I. S. Goldstein, ed., A.C.S. Symposium Series 43. American Chemical Society, Washington, D.C., 1977.
35. Philpot, C. W. Influence of Mineral Content on the Pyrolysis of Plant Materials. Forest Science, 16:461-471, 1970.
36. George, C. W., and R. A. Susott. Effects of Ammonium Phosphate and Sulfate on the Pyrolysis and Combustion of Cellulose. USDA Forest Service Research Paper INT-90. Intermountain Forest and Range Experiment Station, Ogden, Utah, 1971.
37. Rothermel, R. C. Forest Fires and the Chemistry of Forest Fuels. In: Thermal Uses and Properties of Carbohydrates and Lignins. F. Shafizadeh, K. V. Sarkanen, and D. A. Tillman, eds. Academic Press, New York, New York, 1976. pp. 245-258.
38. Susott, C. W., W. F. DeGroot, and F. Shafizadeh. Heat Content of Natural Fuels. J. Fire Flammability, 6:311-315, 1975.
39. Fass, S. M., G. V. Desai, L. F. Brown, and R. E. West. The Consequences of Different Temperatures on Pore Structure Development in Carbon. Carbon, 12:619-631, 1974.
40. Lamond, T. G., and H. Marsh. The Surface Properties of Carbons - III. The Process of Activation of Carbons. Carbon, 1:293-307, 1964.
41. Dubinin, M. M., G. M. Plavnik, and E. D. Zaverina. Integrated Study of the Porous Structure of Activated Carbons from Carbonized Sucrose. Carbon, 2:261-268, 1964.

42. Yousef, A. M. Fine Structure of Lignituous Coals. Carbon, 13:1-6, 1975.
43. Miura, S., P. L. Silveston, and K. Hashimoto. Analysis of Pore Development Processes During Gasification of a Carbon Char. Carbon, 13:391-400, 1975.
44. Mahajan, O. P., R. Yarzab, and P. L. Walker, Jr. Unification of Coal-Char Gasification Reaction Mechanisms. Fuel, 57:643-646, 1978.
45. Jüntgen, H. Manufacture and Properties of Activated Carbon. In: Translation of Reports on Special Problems of Water Technology, H. Sontheimer, ed. EPA-600/9-76-030, U.S. Environmental Protection Agency, Cincinnati, Ohio, 1976.
46. Dutta, S., Y. Wen, and R. J. Belt. Reactivity of Coal and Char - 1. In Carbon Dioxide Atmosphere. Ind. Engr. Chem., Proc. Des. Div., 16(1):20-30, 1977.
47. McEnaney, B., and N. Dovaston. The Development of Porosity in Heat-Treated Polymer Carbons upon Activation by Carbon Dioxide. Carbon, 13:515-519, 1975.
48. Tomkow, K., T. Siemieniewska, F. Czechowski, and A. Jankowska. Formation of Porous Structures in Activated Brown-Coal Chars Using O_2 , CO_2 and H_2O as Activating Agents. Fuel, 56:121-124, 1977.
49. Turkdogan, E. T., and J. V. Vintners. Effect of Carbon Monoxide on the Rate of Oxidation of Charcoal, Graphite and Coke in Carbon Dioxide. Carbon, 8:39-53, 1970.
50. Rand, B., and H. Marsh. The Process of Activation of Carbons by Gasification with CO_2 - III. Uniformity of Gasification. Carbon, 9:79-85, 1971.
51. Walker, P. L., Jr., M. Shelef, and R. A. Anderson. Catalysis of Carbon Gasification. In: Chemistry and Physics of Carbon, Vol. 4, P. L. Walker, Jr., ed. Marcel Dekker, Inc., New York, New York, 1968.
52. Walker, P. L., Jr., L. Pentz, D. L. Biederman, and F. J. Vastoka. The Influence of "Inert" Diluent Gases on the Rate of Carbon Gasification. Carbon, 15:165-168, 1977.
53. Marsh, H., and B. Rand. The Process of Activation of Carbons by Gasification with CO_2 - II. The Role of Catalytic Impurities. Carbon, 9:63-77, 1971.
54. Hennig, G. R. Catalytic Oxidation of Graphite. J. Inorg. Nucl. Chem., 24:1129-1137, 1962.
55. Langmuir, I. The Adsorption of Gases on Plane Surfaces of Glass, Mica and Platinum. J. Am. Chem. Soc., 40:1361, 1918.

56. Hiemenz, P. C. Principles of Colloid and Surface Chemistry. Marcel Dekker, Inc., New York, New York, 1977. 516 pp.
57. Jain, J. S., and V. L. Snoeyink. Adsorption from Bislute Systems on Active Carbon. J. Water Poll. Control Fed., 45:2463-2479, 1973.
58. Weber, W. J., and J. C. Morris. Equilibria and Capacities for Adsorption on Carbon. ASCE, J. San. Engr. Div., 90:79-107, 1964.
59. Weber, W. J. Physicochemical Processes for Water Quality Control. Wiley-Interscience, New York, New York, 1972. 640 pp.
60. Mattson, J. S., and H.B. Mark. Activated Carbon Surface Chemistry and Adsorption from Solution. Marcel Dekker, Inc., New York, New York, 1971. 237 pp.
61. Fritz, W., W. Merk, and E. U. Schlünder. Competitive Adsorption of Two Dissolved Organics onto Activated Carbon. Part II: Adsorption Kinetics in Batch Reactors. In: Proceedings on Practical Applications of Adsorption Techniques in Drinking Water, NATO Committee on Challenges of Modern Society and U.S. Environmental Protection Agency, Reston, Virginia, Apr. 30-May 2, 1979. (Proceedings in press.)
62. Freundlich, H. Colloid and Capillary Chemistry. Methuen and Co., Ltd., London, 1926
63. Sontheimer, H. Basic Principles of Adsorption Process Techniques. In: Translation of Reports on Special Problems of Water Technology, Volume 9 - Adsorption. EPA-600/9-76-030, U.S. Environmental Protection Agency, Cincinnati, Ohio, 1976. pp. 29-66.
64. Dobbs, R. A., R. J. Middendorf, and J. M. Cohen. Carbon Adsorption Isotherms for Toxic Organics. Municipal Environmental Research Laboratory, Office of Research and Development, EPA-600/880-023, U.S. Environmental Protection Agency, Cincinnati, Ohio, 1980. 321 pp.
65. Radke, C. J., and J. M. Prausnitz. Thermodynamics of Multi-Solute Adsorption from Dilute Liquid Solutions. Journal AIChE, 18(4):761-768, 1972.
66. Fritz, W., and E. U. Schlünder. Competitive Adsorption of Two Dissolved Organics onto Activated Carbon, Part I: Adsorption Equilibria. In: Proceedings on Practical Applications of Adsorption Techniques in Drinking Water, sponsored by NATO Committee on Challenges of Modern Society and U.S. Environmental Protection Agency, Reston, Virginia, Apr. 30-May 2, 1979. (Proceedings in press.)
67. DiGiano, F. A., G. Baldauf, B. Frick, and H. Sontheimer. A Simplified Competitive Equilibrium Adsorption Model. Chem. Eng. Sci., 33(12):1667-1673, 1978.

68. Crank, J. The Mathematics of Diffusion. Oxford University Press, Amen House, London, 1957. 347 pp.
69. Roberts, P. V. The Adsorption of Normal Paraffins from Binary Liquid Solutions by Molecular Sieve SA Adsorbent. Ph.D. Thesis, Cornell University, Ithaca, New York, 1966. 230 pp.
70. Crittenden, J. C., and W. J. Weber. Predictive Model for Design of Fixed-Bed Adsorbers: Parameter Estimation and Model Development. ASCE, Jour. of Env. Eng. Div., 104(EE2):185-197, 1978.
71. Crittenden, J. C., and W. J. Weber. Model for Design of Multicomponent Adsorption Systems. ASCE, Jour. of Env. Eng. Div., 104(EE6):1175-1195, 1978.
72. Weber, W. J., and J. C. Morris. Kinetics of Adsorption on Carbon from Solution. ASCE, San. Eng. Div., 89(31):31-59, 1963.
73. DeWalle, F. B., and E. S. K. Chian. Removal of Organic Matter by Activated Carbon Columns. ASCE, Jour. Env. Eng. Div., 100(EE5):1089-1105, 1974.
74. Parkin, G. F. Sources and Characteristics of Soluble Organic Nitrogen in Activated-Sludge Effluents. Ph.D. Thesis, Stanford University, Stanford, California, 1977. 245 pp.
75. Keller, J. V. Activated Carbon Adsorption of Soluble Organic Nitrogen Compounds in Municipal Secondary Effluent. Engineer's Thesis, Stanford University, Stanford, California, 1976. 55 pp.
76. McCarty, P. L., D. G. Argo, and M. Reinhard. Reliability of Advanced Wastewater Treatment. In: Proceedings of Water Reuse--From Research to Application. Amer. Water Works Assoc. Research Foundation, Denver, Colorado, 1979. pp. 1249-1275.
77. Sontheimer, H., E. Heilker, M. P. Jekel, H. Nolte, and F. H. Vollmer. The Mülheim Process. J. Am. Water Works Assoc., 70:393-396, 1978.
78. Frick, B. Prediction of Multicomponent Adsorption Behavior in Activated Carbon Adsorbers--Equilibrium Aspects. In: Proceedings on Practical Applications of Adsorption Techniques in Drinking Water, sponsored by NATO Committee on Challenges of Modern Society and U.S. Environmental Protection Agency, Reston, Virginia, Apr. 30-May 2, 1979. (Proceedings in press)
79. Hsieh, J. S., R. M. Turian, and C. Tien. Batch Adsorption Kinetics in Sewage-Activated Carbon. J. ASCE, San. Eng. Div., 97(SA4):505-521, 1971.
80. Levy, S. J. San Diego Demonstrates Pyrolysis of Solid Waste. EPA-SW80d.2, U.S. Environmental Protection Agency, 1975.

81. Klumb, D. L., and P. R. Brendel. Union Electric's Solid Waste Utilization System. In: Energy and Resource Recovery from Industrial and Municipal Solid Wastes, G. F. Kroneberger, ed. AIChE Symposium Series #162, Vol. 73. American Institute of Chemical Engineers, New York, New York, 1977. pp. 160-167.
82. Moore, W. E., and D. B. Johnson. Procedures for the Chemical Analysis of Wood and Wood Products. Forest Products Laboratory, Forest Service, U.S. Department of Agriculture, 1967.
83. The Chemical Rubber Company. Handbook of Chemistry and Physics, 48th Edition, R. C. Weast, ed. Cleveland, Ohio, 1967-1968.
84. Dohrmann Division of Envirotech Corporation. Dohrmann DC-50/52 Series Total Organic Carbon Analyzers Equipment Manual. Santa Clara, California, 1977.
85. Pacheco, L., D. S. Yan, and H. Marsh. Activated Carbon from Sport Coffee Grounds. Paper presented at 14th Biennial Conference on Carbon, sponsored by the American Carbon Society and The Pennsylvania State University, 1979. (Proceedings in press.)
86. Boucher, F. B., E. W. Knell, G. T. Preston, and G. M. Mallan. Pyrolysis of Industrial Wastes for Oil and Activated Carbon Recovery. EPA-600/2-77-091, U.S. Environmental Protection Agency, Cincinnati, Ohio, 1977. 170 pp.
87. Dandy, A. J. Production and Characterization of Activated Carbons from Agricultural Waste Products and Wood Charcoal. New Zealand J. of Science, 20:291-294, 1977.
88. General Electric Company. Solid Waste Management Technology Assessment. Van Nostrand Reinhold Company, New York, New York, 1975.
89. Mackay, H. A. The Influence of Polymer Structure on the Conversion of Synthetic Resins to Carbon Coke. Carbon, 8:517-526, 1970.
90. Sawyer, C. N., and P. L. McCarty. Chemistry for Sanitary Engineers. McGraw-Hill Book Company, New York, New York, 1967. 518 pp.
91. Gan, H., S. P. Nandi, and P. L. Walker, Jr. Nature of the Porosity in American Coals. Fuel, 51:272-277, 1972.
92. Roberts, P. V., J. O. Leckie, and P. H. Brunner. Pyrolysis for the Production of Activated Carbon from Cellulosic Solid Wastes. In: Solid Wastes and Residues, Conversion by Advanced Thermal Processes, J. L. Jones and S. B. Radding, eds. ACS Symposium Series 76. American Chemical Society, Washington, D.C., 1978. pp. 392-410.
93. Dixon, W. J., and F. J. Massey. Introduction to Statistical Analysis. McGraw-Hill Book Co., Inc., New York, New York, 1957. 488 pp.

94. Reid, R. C., and T. K. Sherwood. The Properties of Gases and Liquids. McGraw-Hill Book Co., Inc., San Francisco, California, 1966. 646 pp.
95. Satterfield, C. N., and T. K. Sherwood. The Role of Diffusion in Catalysis. Addison-Wesley Company, Reading, Massachusetts, 1963. pp. 20-23.

APPENDIX A

USE OF LINEAR REGRESSIONS FOR DATA PLOTTING

In this appendix the justification is presented for reporting ash-free char yield versus T_F and carbon yield versus T_F as linear regressions of the experimental data.

Figures A-1 and A-2 are plots of average ash-free yield versus T_F for the lignocellulosics discussed in the body of this report. Data points are connected by smooth lines, resulting in curvilinear plots. Table A-1 is a summary of linear regressions of the data plotted in Figures A-1 and A-2. Figure A-3 is a plot for four of the least linear (lowest r^2) ash-free yield versus T_F linear regression relationships along with the data points and their 90% confidence intervals (standard deviations having been estimated as footnoted in Table 3 of the report). Data at 600°C were not duplicated, and hence no confidence intervals are shown though it is reasonable to expect confidence intervals of roughly the same magnitude as the other data for the given material. From Figure A-3 it is clear that statistically the data do not differ significantly from the linear regression. Thus only the linear regressions are used for comparative purposes in the report.

The case is similar for carbon yield versus T_F . Table A-2 lists the results of linear regression of the data. Figure A-4 displays the linear regressions, data points and confidence intervals for two of the materials. Again the data do not differ in a statistically significant way from the regression, and therefore only the regressions are used in the report for comparison.

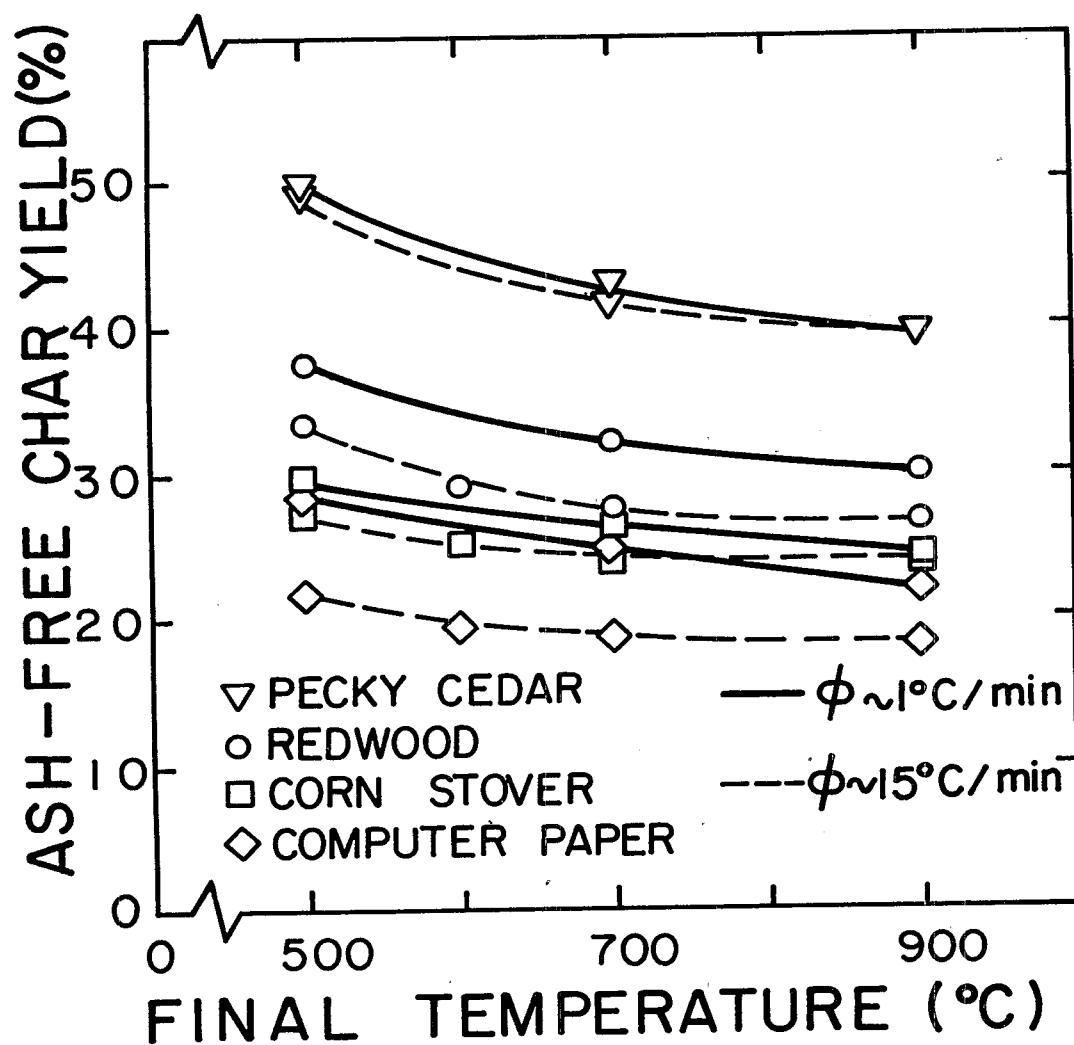


Figure A-1. Ash-free char yield versus final temperature: low and medium heating rates

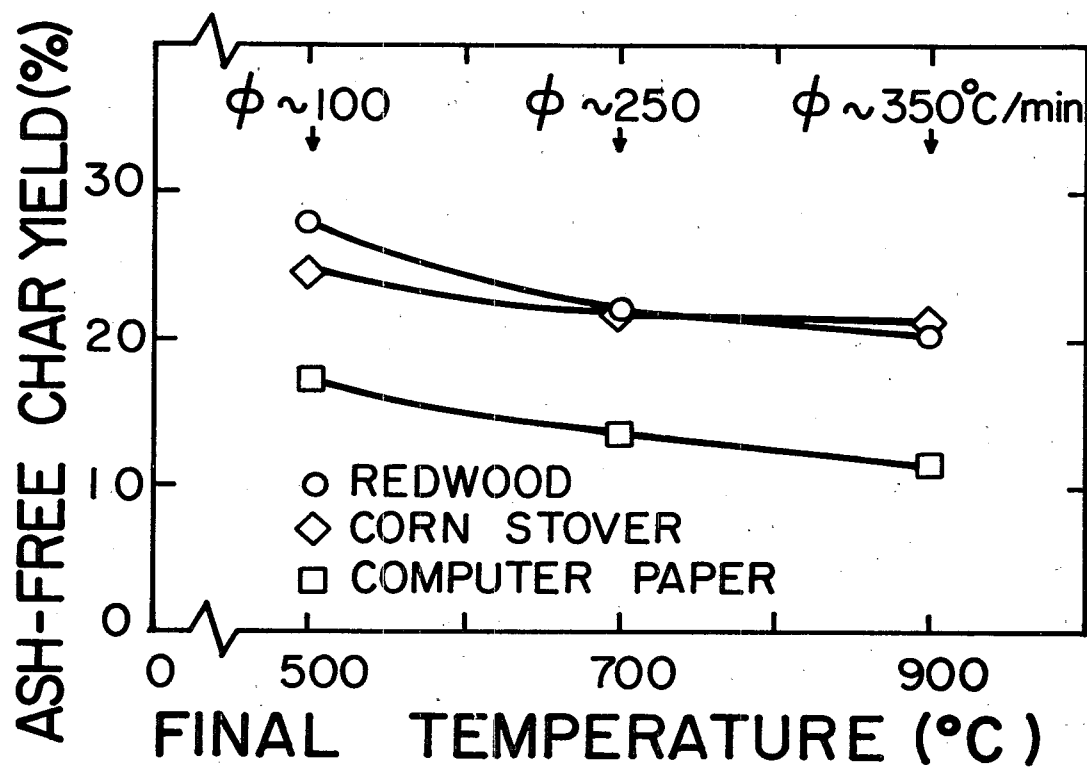


Figure A-2. Ash-free char yield versus final temperature: high heating rates.

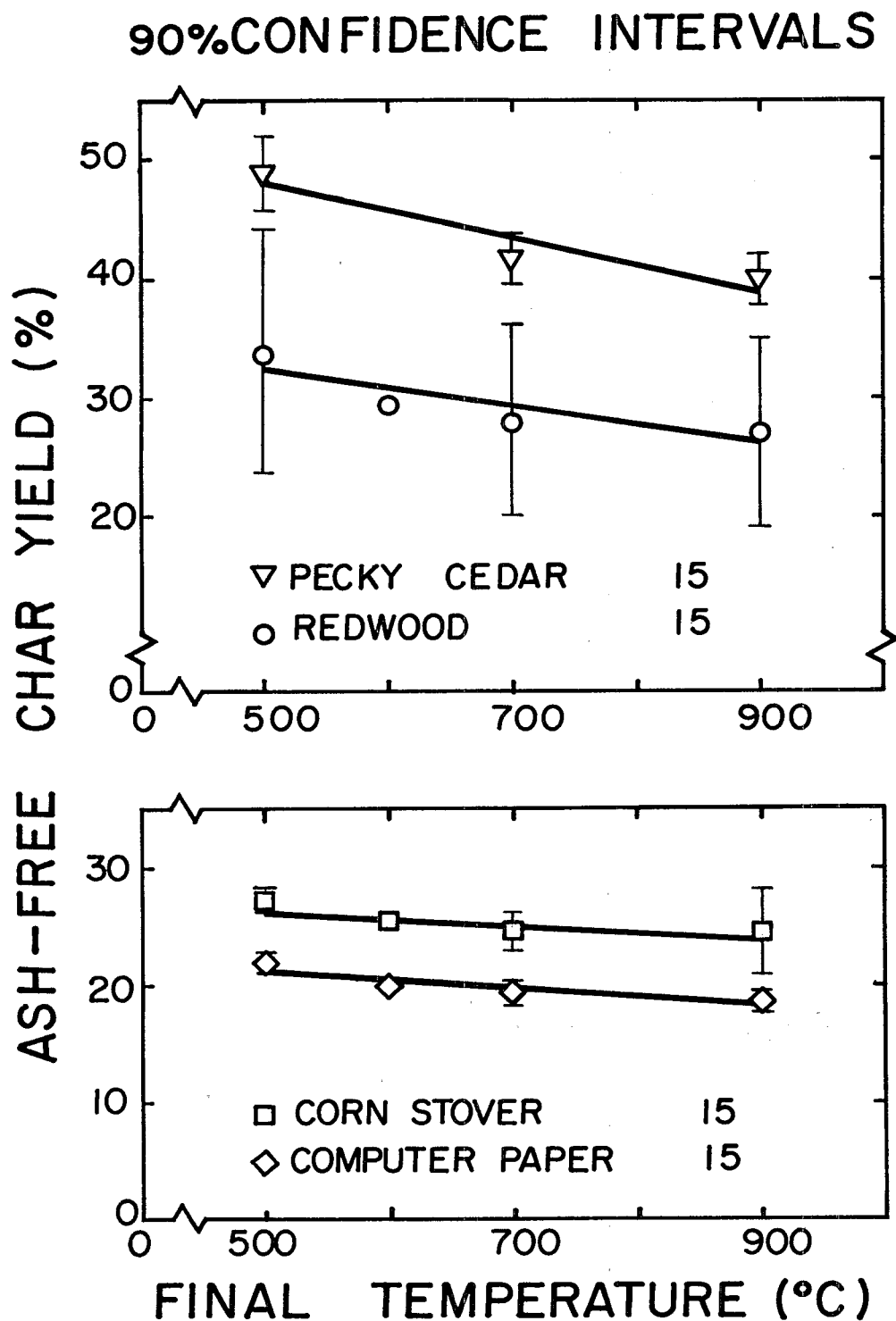


Figure A-3. Linearity of the plots of ash-free yield versus final temperature for pyrolysis at 15°C/min

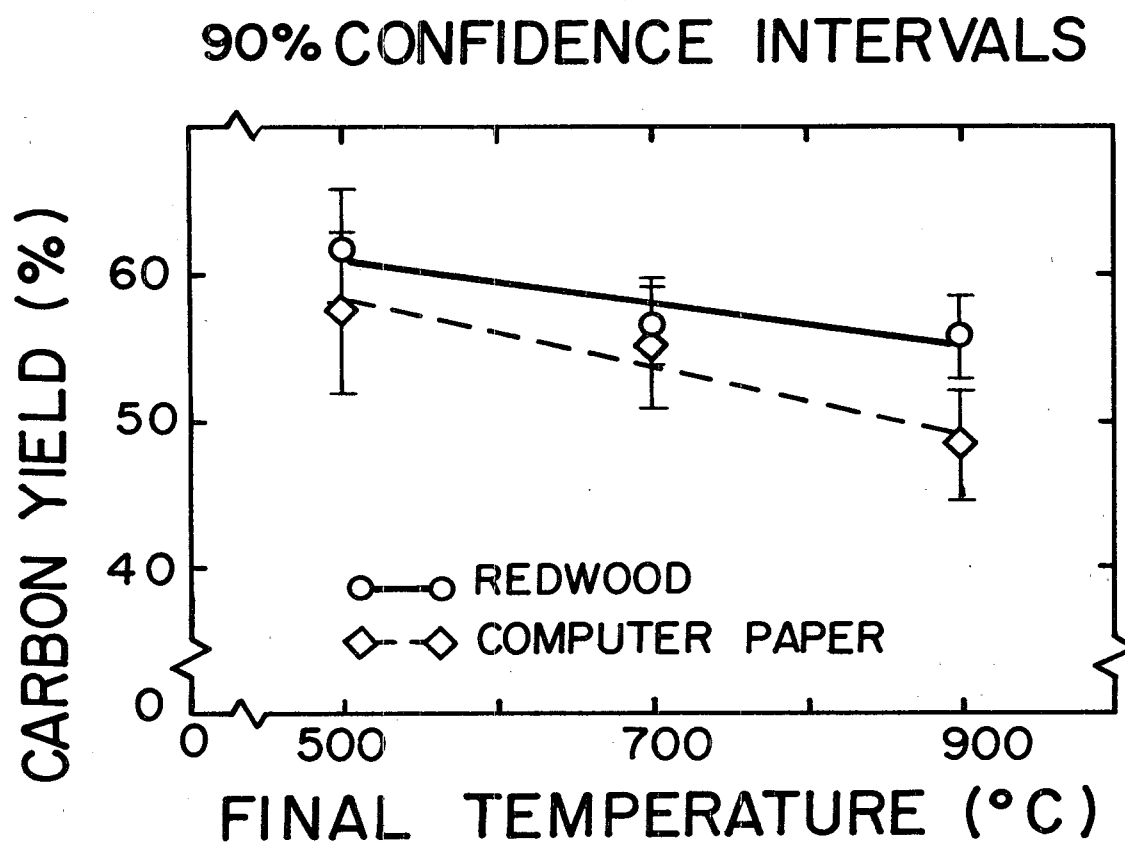


Figure A-4. Linearity of the plots of ash-free yield versus final temperature for pyrolysis at 1°C/min

TABLE A-1. SUMMARY OF LINEAR REGRESSIONS OF ASH-FREE CHAR YIELD
VERSUS FINAL PYROLYSIS TEMPERATURE FOR SELECTED LIGNOCELLULOSICS

Material	ϕ , °C/min	Regression Constants ^a		
		a_1	a_0	r^2
Pecky Cedar	1	-0.03	62.50	0.96
	15	-0.02	58.89	0.89
Redwood	1	-0.02	46.32	0.95
	15	-0.02	40.09	0.76
	Max	-0.02	36.50	0.90
Corn Stover	1	-0.01	35.80	0.98
	15	-0.01	30.30	0.77
	Max	-0.01	29.15	0.90
Computer Paper	1	-0.02	37.35	1.00
	15	-0.01	25.59	0.85
	Max	-0.01	24.00	0.97

^aRegression Equation: Ash-Free Char Yield (%) = $a_1 T_F + a_0$, where T_F is expressed in °C.

TABLE A-2. SUMMARY OF LINEAR REGRESSIONS OF CARBON YIELD
VERSUS FINAL PYROLYSIS TEMPERATURE FOR SELECTED LIGNOCELLULOSICS

Material	ϕ , °C/min	Regression Constants ^a		
		a_1	a_0	r^2
Pecky Cedar	1	-0.021	85.5	1.00 ^b
	15	-0.009	74.8	0.69
Redwood	1	-0.015	68.3	0.84
	15	-0.010	58.4	0.70
Corn Stover	1	-0.022	67.1	0.99
	15	-0.004	51.0	0.76
Computer Paper	1	-0.023	69.7	0.91
	15	-0.011	50.1	0.92

^aRegression equation: Carbon Yield (%) = $a_1 T_F + a_0$, where T_F is expressed in °C.

^bOnly two points (500, 700°C) available for "regression."

APPENDIX B

MERCURY POROSIMETRY MEASUREMENTS

The mercury porosimetry measurements, as determined by American Instrument Company, are shown in the following Figures B-1 through B-7 for 42M, 30M, 15M, CHAR, F400, F100, and AN-A. These have not been corrected for the effect of external porosity.

POROSITY DETERMINATION

AMINCO FORM
CATALOG 5-713A

SAMPLE 42M

SAMPLE WEIGHT 0.0311 grams

DATE 11-2-79 ORDER No. K9-4156

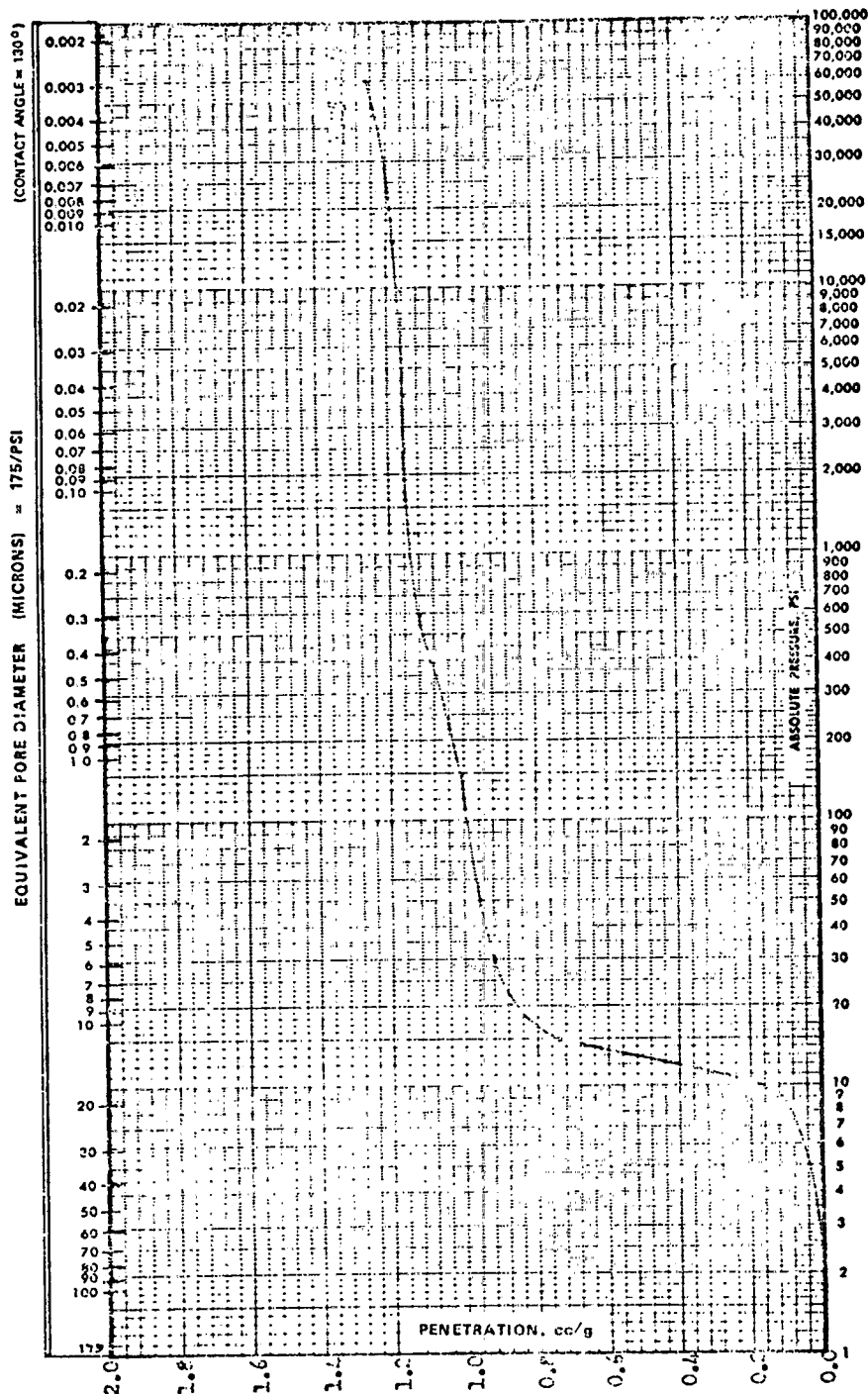


Figure B-1. Mercury porosimetry: cumulative penetration volume versus pore diameter for 42M.

POROSITY DETERMINATION

AMINCO FORM
Cat. No. 6-7136 A

SAMPLE 30 M
SAMPLE WEIGHT 0.1072 grams
DATE 10-31-79 ORDER No. K9-4156

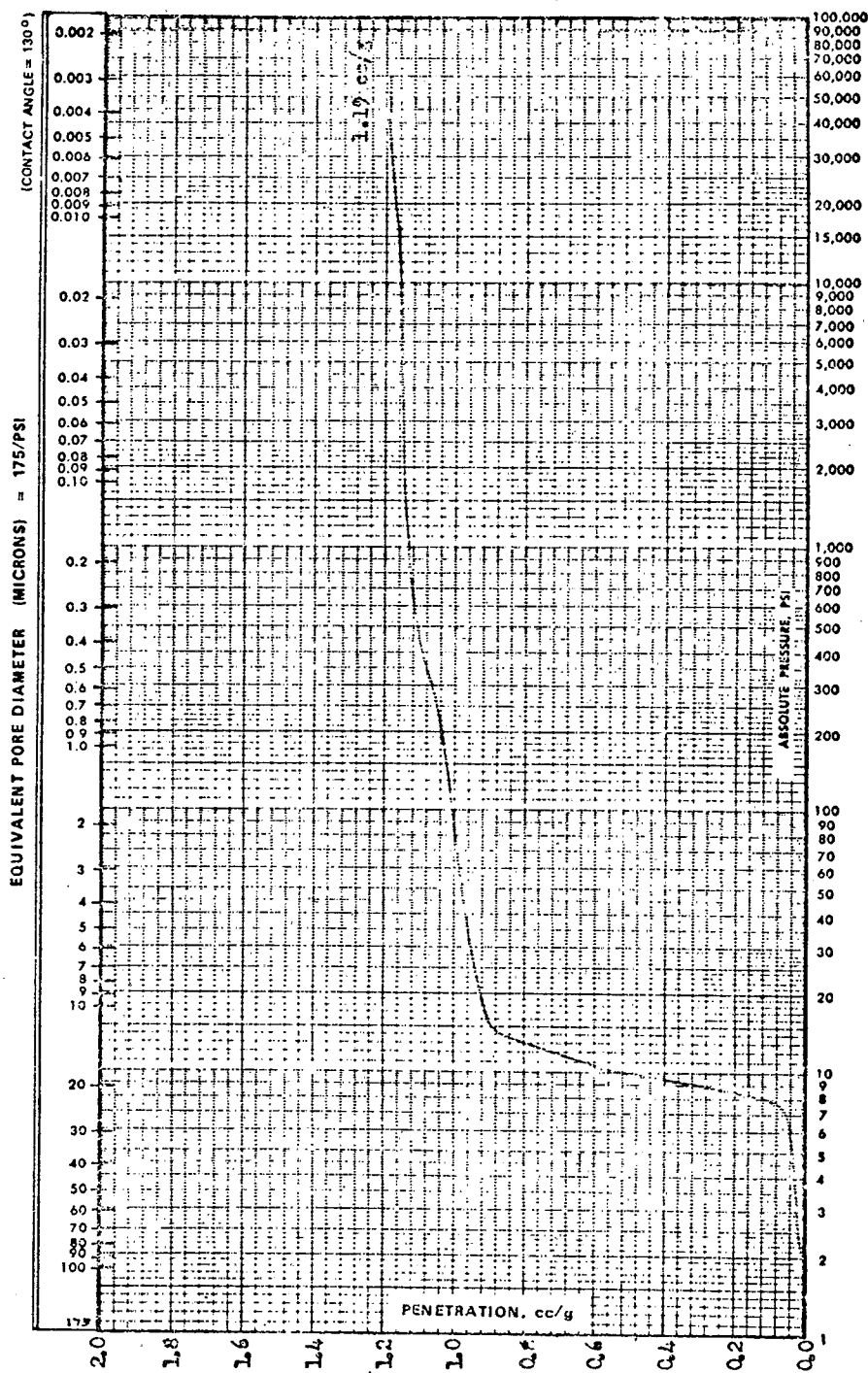


Figure B-2. Mercury porosimetry: cumulative penetration volume versus pore diameter for 30M.

POROSITY DETERMINATION

SAMPLE 151

SAMPLE WEIGHT 0.1532 grams

DATE 10-31-79 ORDER No. 89-4156

AMINCO FORHL
CALING. F-7135A

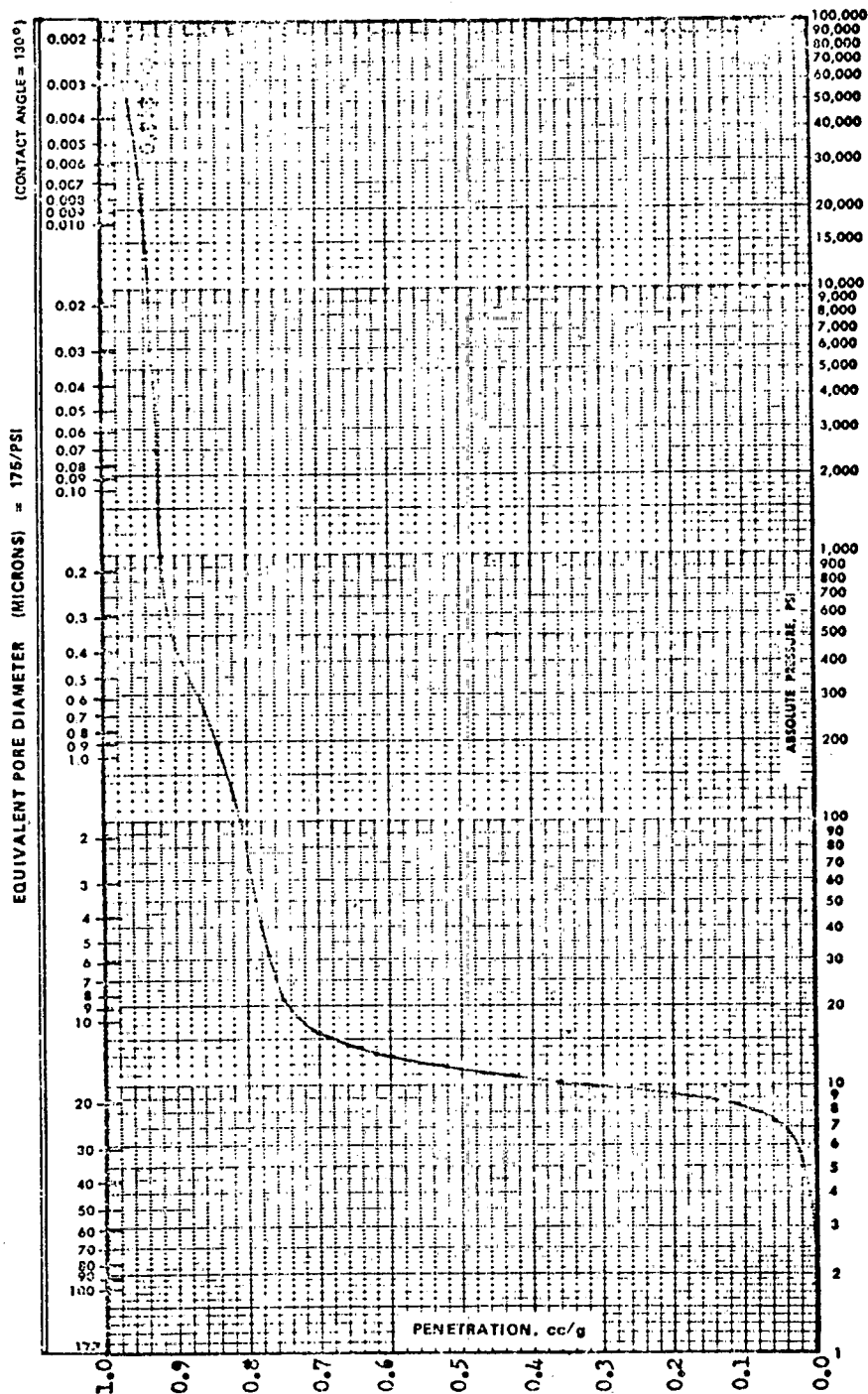


Figure B-3. Mercury porosimetry: cumulative penetration volume versus pore diameter for 15M.

AMINCO FORM
Cat. No. 6-7135 A

POROSITY DETERMINATION

SAMPLE Char
SAMPLE WEIGHT 0.1053 grams
DATE 11-1-79 K9-4156 ORDER No. _____

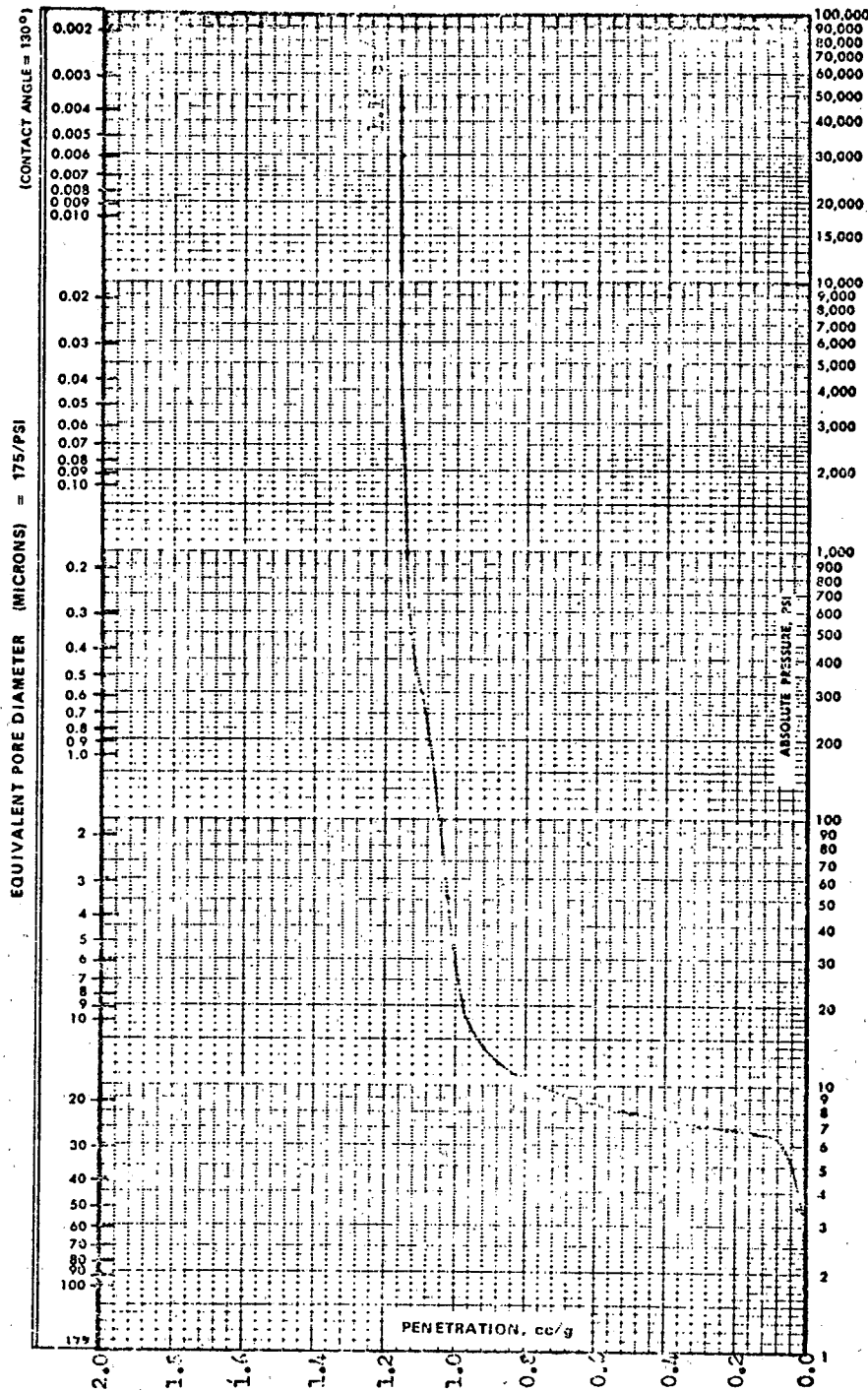


Figure B-4. Mercury porosimetry: cumulative penetration volume versus pore diameter for CHAR.

POROSITY DETERMINATION

SAMPLE Filtrisorb 400
 SAMPLE WEIGHT 0.1118 grams
 DATE 11-26-78 ORDER No. K6-3478

AMINCO FORM
 CAL. No. 6-7135A

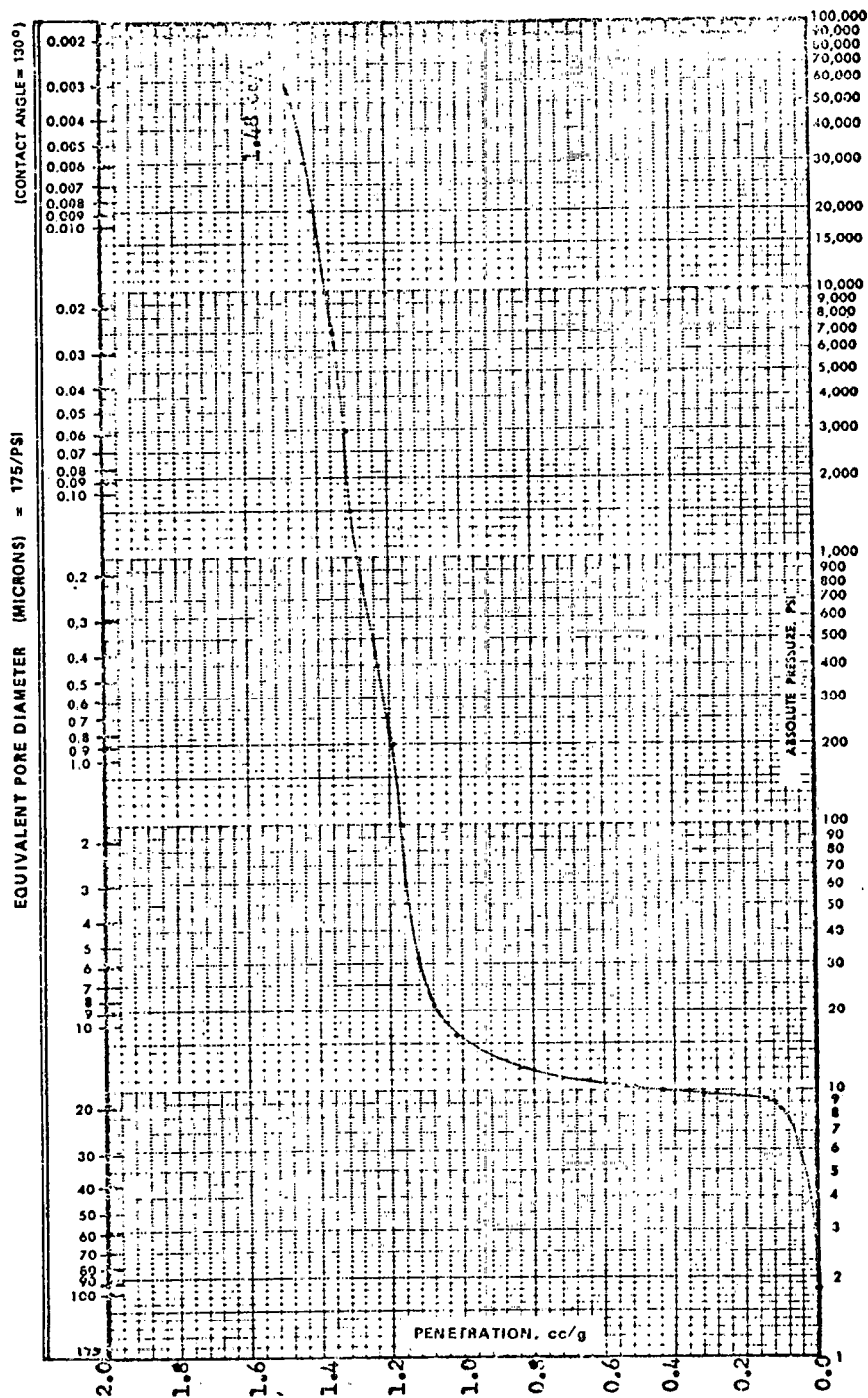


Figure B-5. Mercury porosimetry: cumulative penetration volume versus pore diameter for F400.

POROSITY DETERMINATION

AMINCO FORM
CAL. No. 5-7135 A

SAMPLE Filtrisorb 100 34-75M
 SAMPLE WEIGHT 0.1413 grams
 DATE 11-26-75 ORDER No. K8-3478

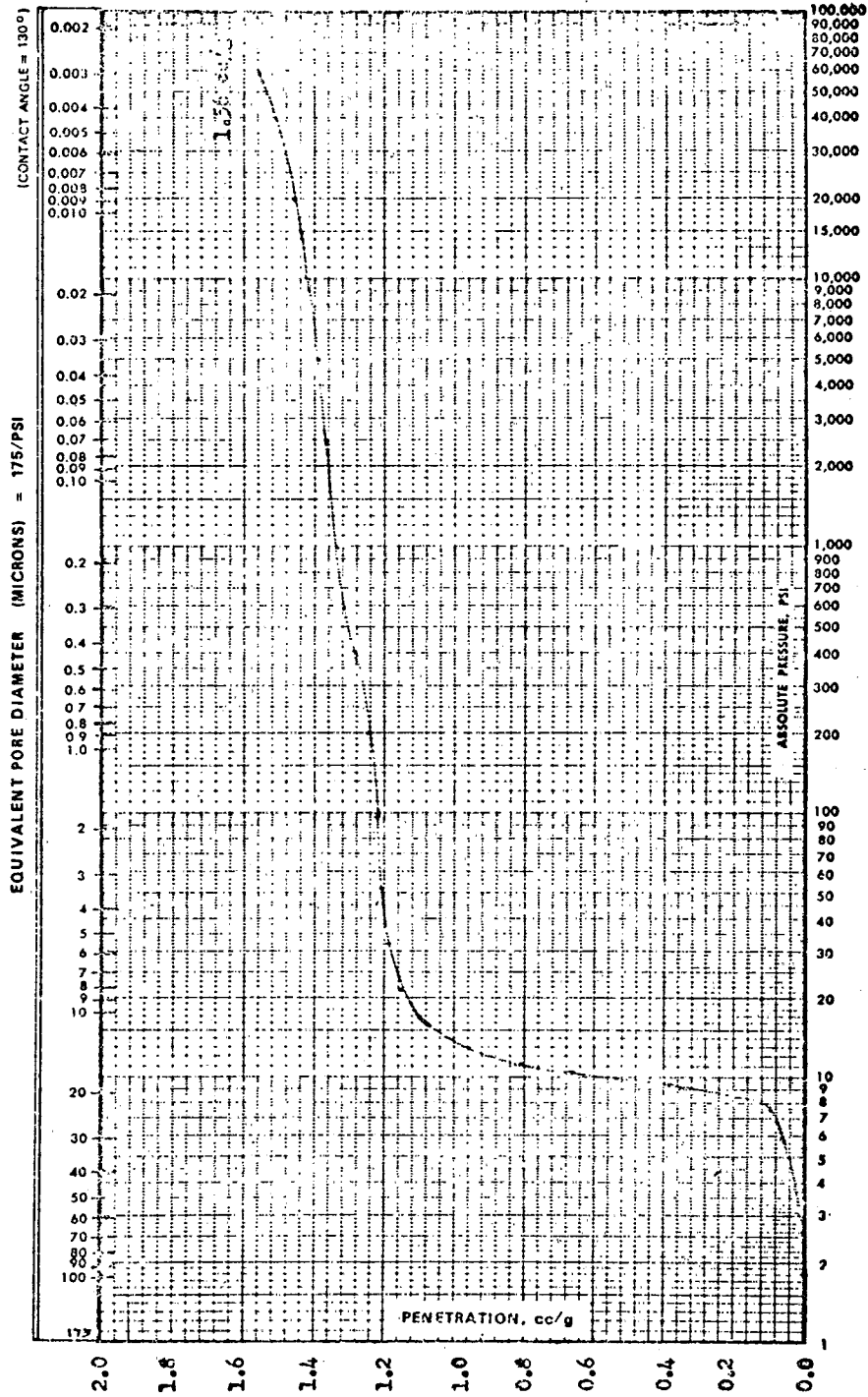


Figure B-6. Mercury porosimetry: cumulative penetration volume versus pore diameter for F100.

POROSITY DETERMINATION

SAMPLE Aqua Nuchar A 34-75 microns
 SAMPLE WEIGHT 0.1214 grams
 DATE 11-28-78 ORDER No. X8-3478

AMINCO FORM
 Cst. No. 6-7136A

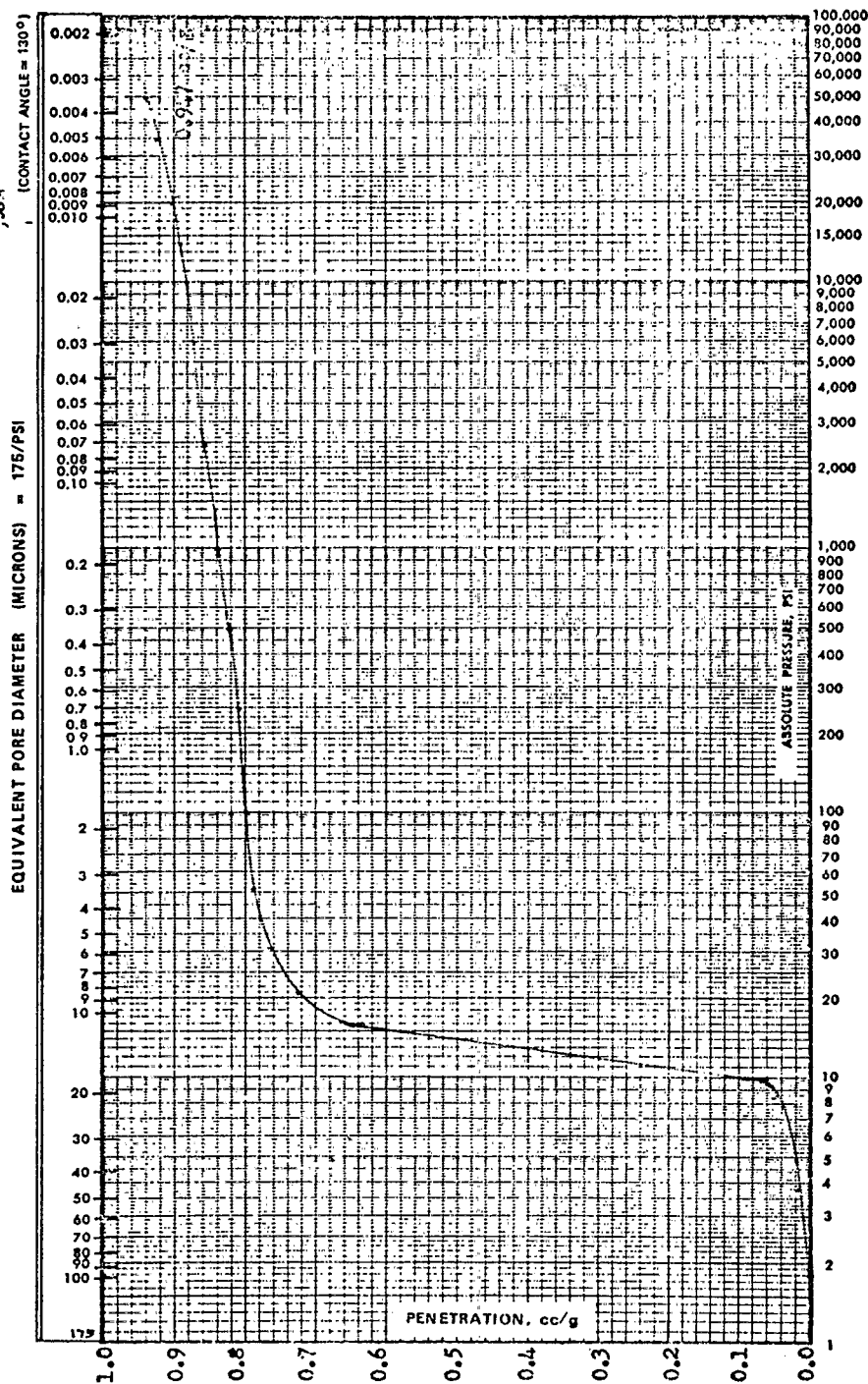


Figure B-7. Mercury porosimetry: cumulative penetration volume versus pore diameter for AN-A.

APPENDIX C

DOC RATE OF ADSORPTION EXPERIMENTS

Kinetics of DOC adsorption were evaluated in two experiments: run 4 and run 11. These are shown as follows in Figures C-1 and C-2. The results of these and an average of the two are discussed in the text.

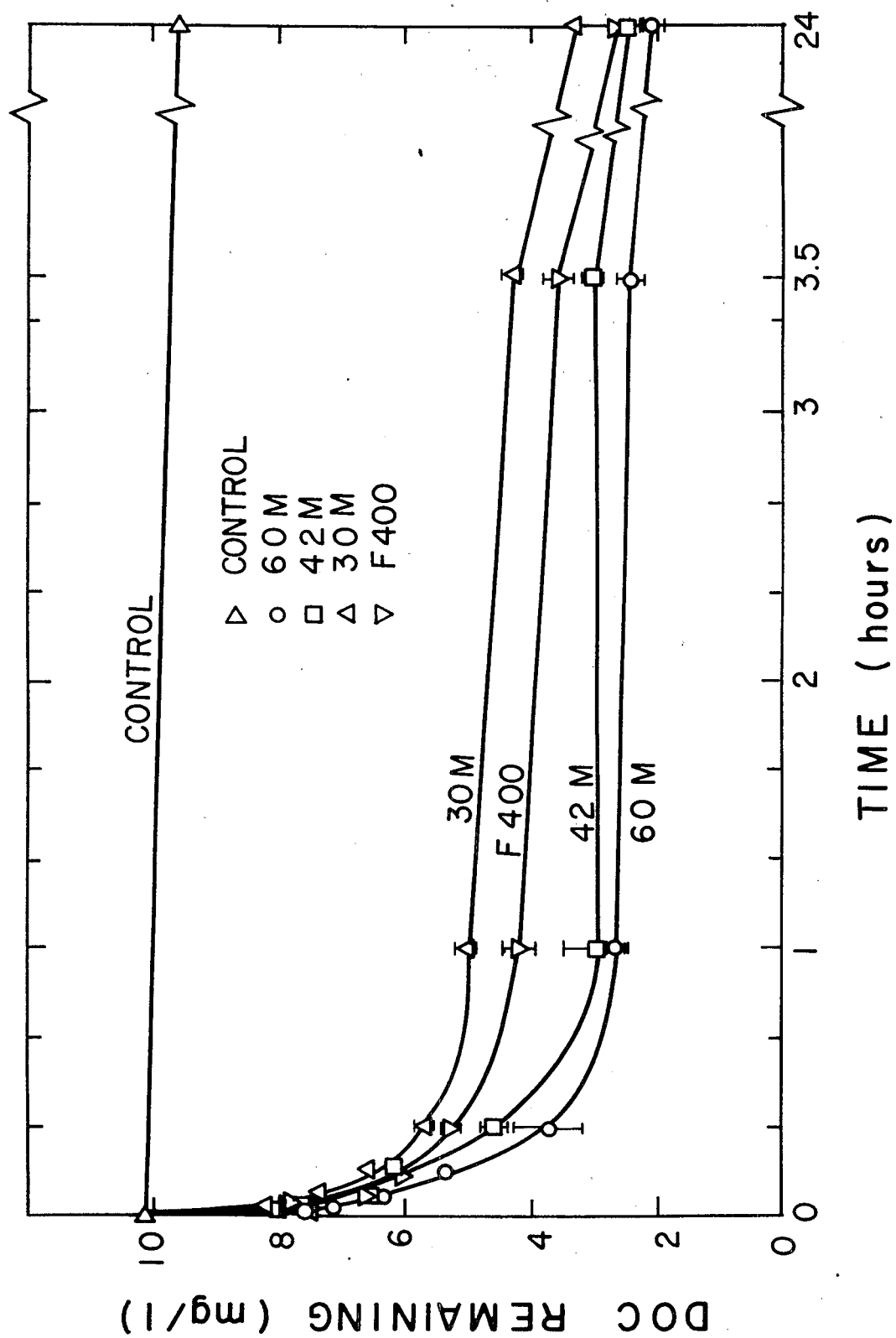


Figure C-1. Kinetics of DOC adsorption for 60M, 42M, 30M, and F400 (run 4) at a loading of 30 mg activated carbon/110 ml wastewater

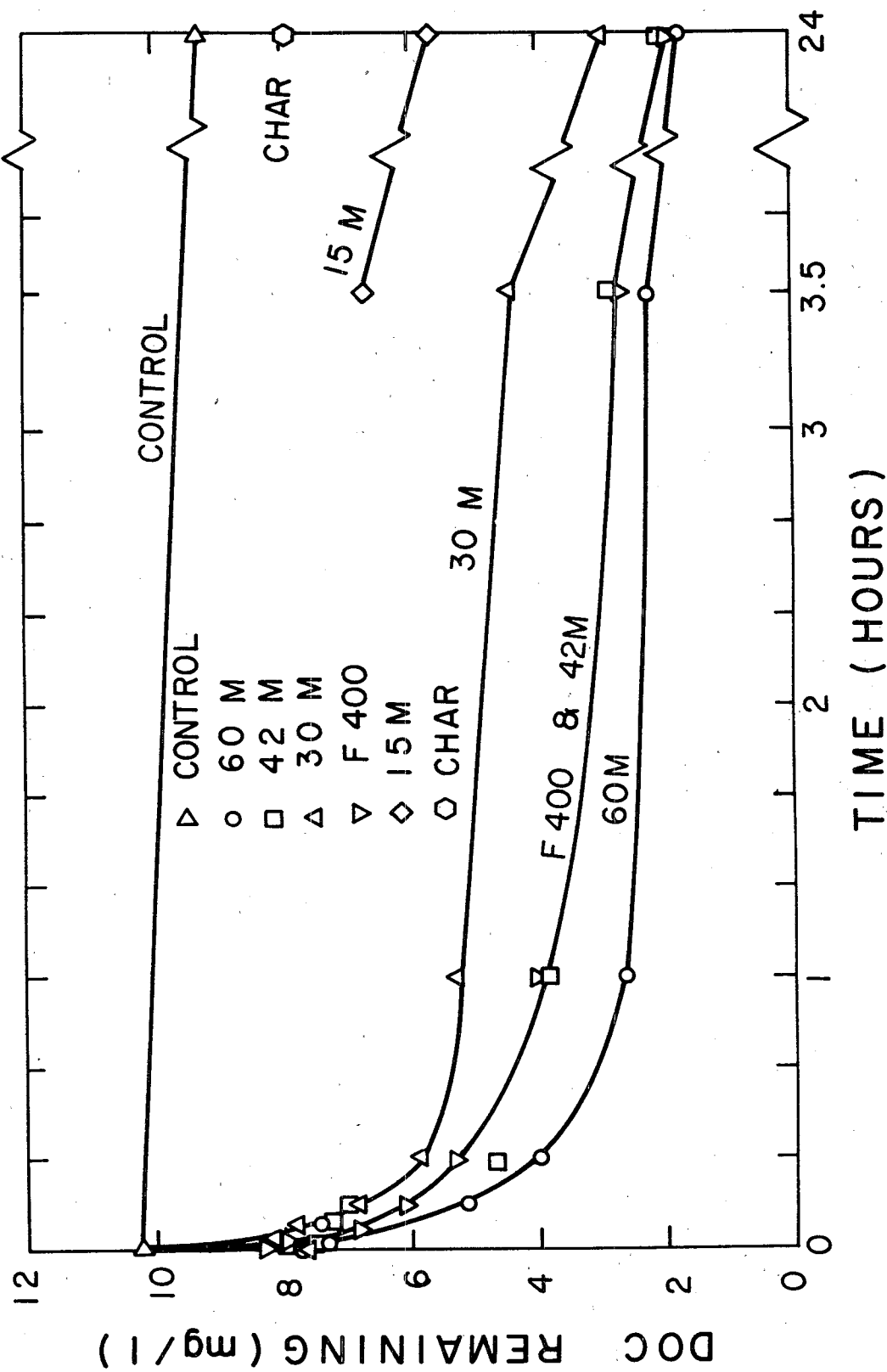


Figure C-2. Kinetics of DOC adsorption for 60M, 42M, 30M, and F400 (run 11) at a loading of 30 mg activated carbon/110 ml wastewater. Several data for 15M and CHAR are also included.

APPENDIX D

FREUNDLICH ISOTHERM COEFFICIENTS

The Freundlich isotherm coefficients were calculated as follows. As can be seen, the 95% confidence interval in most cases included unity (1.0), indicating that a linear isotherm would be an acceptable model for the data.

TABLE D-1. FREUNDLICH ISOTHERM COEFFICIENTS

Run Number	Carbon Type	Subtracting C_n (mg/l) as Non-Adsorbable	K_F	n	95% Confidence Interval of $b = 1/n$	r^2	Points Included (All with $C_e > x$)	Number of Points
Run 6	F400	0.73	6.57	1.2531	0.7980±0.1470	0.9345	$C_e > 0.98$	12
Run 8	F400	1.00	8.95	0.8737	1.1445±0.8129	0.7036	$C_e > 1.87$	7
	60M	1.00	8.85	0.7221	1.3848±0.8275	0.8223	$C_e > 2.43$	6
	42M	1.00	4.27	0.8076	1.2383±0.5926	0.8028	(all)	8
	30M	1.00	6.40	1.8560	0.5388±0.5430	0.4786	(all)	8

APPENDIX E

LINEAR ISOTHERMS FOR F400 FOR VARIOUS EXPERIMENTS

Two linear isotherm experiments were conducted on F400 (runs 6 and 8); these were conducted at two different wastewaters, which had different concentrations of DOC. The concentrations of the controls for these are included in Figure E-1. In run 6, a higher control concentration existed than for run 8, and correspondingly, the equilibrium concentrations (C_e) were higher for a given q_e in run 6 than in run 8.

Further, the equilibrium data for various kinetic experiments with F400 are also included. These are discussed in the text.

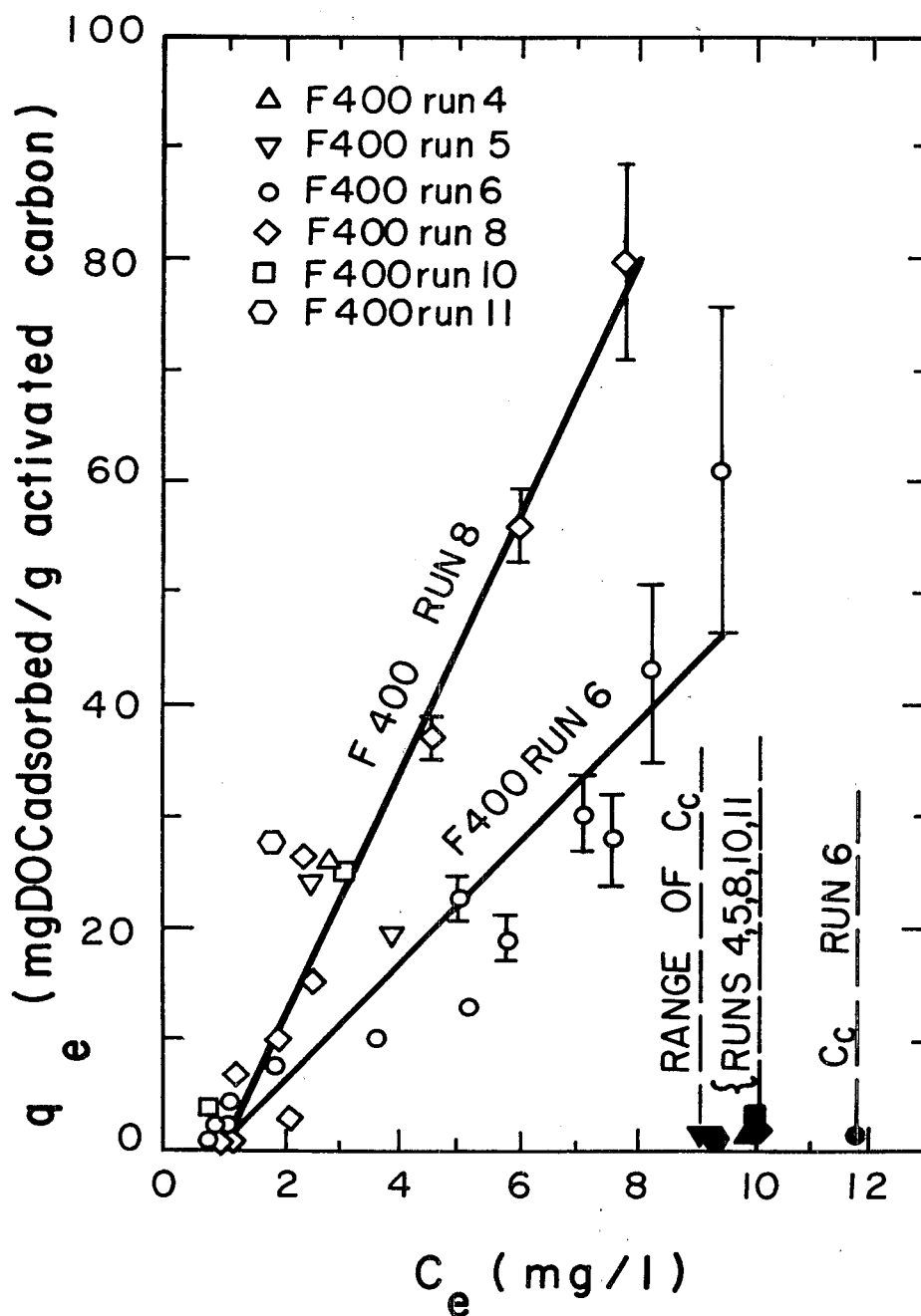


Figure E-1. Linear DOC adsorption isotherms for F400 for runs 6 and 8. Also included are the equilibrium values of q_e versus C_e from various kinetic experiments. Error bars represent standard deviation when the standard deviation is greater than the magnitude of the symbols. Lines represent linear regressions for runs 6 and 8, respectively. The concentration of controls are represented by filled-in symbols at the lower right-hand corner of the figure.

APPENDIX F

ROOTS OF $\tan q_n$ IN ANALYTIC SOLUTION TO DIFFUSIVITY

The roots of $\tan q_n$ for the expression

$$\tan q_n = 3q_n / (3 + \alpha q_n^2)$$

which are essential in solving Eq. 21 are as follows:

TABLE F-1. ROOTS OF $\tan q_n = 3q_n / (3 + \alpha q_n^2)$ (Ref. 68)

Fractional							
Uptake	α	q_1	q_2	q_3	q_4	q_5	q_6
0	∞	3.1416	6.2832	9.4248	12.5664	15.7080	18.8496
0.1	9.0000	3.2410	6.3353	9.4599	12.5928	15.7292	18.8671
0.2	4.0000	3.3485	6.3979	9.5029	12.6254	15.7554	18.8891
0.3	2.3333	3.4650	6.4736	9.5567	12.6668	15.7888	18.9172
0.4	1.5000	3.5909	6.5665	9.6255	12.7205	15.8326	18.9541
0.5	1.0000	3.7264	6.6814	9.7156	12.7928	15.8924	19.0048
0.6	0.6667	3.8711	6.8246	9.8369	12.8940	15.9779	19.0784
0.7	0.4286	4.0236	7.0019	10.0039	13.0424	16.1082	19.1932
0.8	0.2500	4.1811	7.2169	10.2355	13.2689	16.3211	19.3898
0.9	0.1111	4.3395	7.4645	10.5437	13.6133	16.6831	19.7564
1.0	0	4.4934	7.7253	10.9041	14.0662	17.2208	20.3713

APPENDIX G

COMPUTATION OF DIFFUSION COEFFICIENTS

TABLE G-1. COMPUTATION OF DIFFUSION COEFFICIENTS FOR 60M, 42M, 30M, F400

60M F = 0.8827 R = 94,900				
Time	D_e (m^2/sec)	τ (unitless)	f (calc.) (unitless)	f (experiment) (unitless)
1 min.	2.9×10^{-10}	2.08×10^{-4}	0.3141	0.3180
2 min.	2.3×10^{-10}	3.24×10^{-4}	0.3692	0.3702
5 min.	1.8×10^{-10}	6.36×10^{-4}	0.4626	0.4547
10 min.	2.1×10^{-10}	1.50×10^{-3}	0.5902	0.5876
20 min.	4.9×10^{-10}	6.94×10^{-3}	0.7988	0.7963
1 hr.	8.2×10^{-10}	3.47×10^{-2}	0.9392	0.9329
3.5 hr.	3.3×10^{-10}	4.86×10^{-2}	0.9572	0.9565
24 hr.				1.0000
42M F = 0.8421 R = 50,200				
Time	D_e (m^2/sec)	τ (unitless)	f (calc.) (unitless)	f (experiment) (unitless)
min.	1.99×10^{-10}	2.65×10^{-4}	0.2784	0.2734
2 min.	1.64×10^{-10}	4.34×10^{-4}	0.3364	0.3359
5 min.	1.64×10^{-10}	1.08×10^{-3}	0.4621	0.4635
10 min.	1.13×10^{-10}	1.52×10^{-3}	0.5125	0.5117
20 min.	2.36×10^{-10}	6.26×10^{-3}	0.7258	0.7279
1 hr.	1.47×10^{-10}	1.17×10^{-2}	0.8082	0.8073
3.5 hr.	1.45×10^{-10}	4.05×10^{-2}	0.9295	0.9297
24 hr.				1.0000

TABLE G-1 cont.

TABLE G-1 cont.

30M

F = 0.7555

R = 18,300

Time	D_e (m^2/sec)	τ (unitless)	f (calc.) (unitless)	f (experiment) (unitless)
1 min.	0.38×10^{-10}	1.38×10^{-3}	0.3798	0.3788
2 min.	0.97×10^{-10}	7.10×10^{-4}	0.2921	0.2888
5 min.	0.97×10^{-10}	1.77×10^{-3}	0.4120	0.4093
10 min.	0.97×10^{-10}	3.55×10^{-3}	0.5178	0.5109
20 min.	1.1×10^{-10}	8.11×10^{-3}	0.6517	0.6488
1 hr.	0.65×10^{-10}	1.42×10^{-2}	0.7401	0.7460
3.5 hr.	0.44×10^{-10}	3.31×10^{-2}	0.8576	0.8505
24 hr.				1.0000

F400 (Runs 4, 11)

F = 0.8476

R = 60,300

Time	D_e (m^2/sec)	τ (unitless)	f (calc.) (unitless)	f (experiment) (unitless)
1 min.	2.5×10^{-10}	2.92×10^{-4}	0.2971	0.2950
2 min.	1.3×10^{-10}	3.02×10^{-4}	0.3009	0.3014
5 min.	1.3×10^{-10}	9.73×10^{-4}	0.4560	0.4580
10 min.	1.3×10^{-10}	1.53×10^{-3}	0.5232	0.5226
20 min.	1.3×10^{-10}	3.02×10^{-3}	0.6275	0.6274
1 hr.	1.1×10^{-10}	8.08×10^{-3}	0.7683	0.7684
3.5 hr.	0.67×10^{-10}	1.64×10^{-2}	0.8522	0.8525
24 hr.				1.0000

TABLE G-2. COMPUTATION FOR PORE DIFFUSION MODEL BASED ON
AN ASSUMED MEDIAN D FOR 60M, 42M, 30M, F400

F400 (Run 4, 11)		F = 0.8476	R = 56,700	Median D = 1.29×10^{-10}	
Time	D (m^2/sec)	τ (unitless)	f (calc.) (unitless)	f (experiment) (unitless)	
1 min.	1.29×10^{-10}	1.52×10^{-4}	0.2283	0.2950	
2 min.		3.03×10^{-4}	0.3015	0.3014	
5 min.		7.58×10^{-4}	0.4201	0.4580	
10 min.		1.52×10^{-3}	0.5223	0.5226	
20 min.		3.03×10^{-3}	0.6282	0.6274	
1 hr.		9.10×10^{-3}	0.7837	0.7684	
3.5 hr.		3.18×10^{-2}	0.9143	0.8525	
24 hr.		2.18×10^{-1}	0.9942	1.0000	

TABLE G-2 cont.

TABLE G-2 cont.

60M $F = 0.8827$ $R = 94,900$ Median $D = 3.96 \times 10^{-10}$

Time	D (m^2/sec)	τ (unitless)	f (calc.) (unitless)	f (experiment) (unitless)
1 min.	3.96×10^{-10}	2.08×10^{-4}	0.3168	0.3180
2 min.		4.16×10^{-4}	0.4060	0.3702
5 min.		1.04×10^{-3}	0.5387	0.4547
10 min.		2.08×10^{-3}	0.6418	0.5876
20 min.		4.16×10^{-3}	0.7384	0.7963
1 hr.		1.25×10^{-2}	0.8631	0.9329
3.5 hr.		4.37×10^{-2}	0.9532	0.9565
24 hr.		2.99×10^{-1}	0.9919	1.0000

42M $F = 0.8421$ $R = 50,200$ Median $D = 1.64 \times 10^{-10}$

Time	D (m^2/sec)	τ (unitless)	f (calc.) (unitless)	f (experiment) (unitless)
1 min.	1.64×10^{-10}	2.17×10^{-4}	0.2571	0.2734
2 min.		4.35×10^{-4}	0.3366	0.3359
5 min.		1.09×10^{-3}	0.4624	0.4635
10 min.		2.17×10^{-3}	0.5674	0.5117
20 min.		4.35×10^{-3}	0.6729	0.7279
1 hr.		1.30×10^{-2}	0.8211	0.8073
3.5 hr.		4.56×10^{-2}	0.9380	0.9297
24 hr.		3.13×10^{-1}	0.9903	1.0000

30M $F = 0.7555$ $R = 18,300$ Median $D = 0.97 \times 10^{-10}$

Time	D (m^2/sec)	τ (unitless)	f (calc.) (unitless)	f (experiment) (unitless)
1 min.	0.97×10^{-10}	3.54×10^{-4}	0.2215	0.3788
2 min.		7.08×10^{-4}	0.2945	0.2888
5 min.		1.77×10^{-3}	0.4150	0.4093
10 min.		3.54×10^{-3}	0.5211	0.5109
20 min.		7.08×10^{-3}	0.6336	0.6488
1 hr.		2.13×10^{-2}	0.8025	0.7460
3.5 hr.		7.43×10^{-2}	0.9429	0.8505
24 hr.		5.09×10^{-1}	0.9560	1.0000

TECHNICAL REPORT DATA
(Please read Instructions on the reverse before completing)

1. REPORT NO. EPA-600/2-80-123		2.		3. RECIPIENT'S ACCESSION NO.	
4. TITLE AND SUBTITLE PREPARATION AND EVALUATION OF POWDERED ACTIVATED CARBON FROM LIGNOCELLULOSIC MATERIALS				5. REPORT DATE August 1980 (Issuing Date)	
				6. PERFORMING ORGANIZATION CODE	
7. AUTHOR(S) Paul V. Roberts, Douglas M. Mackay, and Fred S. Cannon				8. PERFORMING ORGANIZATION REPORT NO.	
9. PERFORMING ORGANIZATION NAME AND ADDRESS Department of Civil Engineering Stanford University Stanford, California 94305				10. PROGRAM ELEMENT NO. A36B1C	
				11. CONTRACT/GRANT NO. Grant No. EPA-R-803188	
12. SPONSORING AGENCY NAME AND ADDRESS Municipal Environmental Research Laboratory, Cinti, OH Office of Research and Development U.S. Environmental Protection Agency Cincinnati, Ohio 45268				13. TYPE OF REPORT AND PERIOD COVERED Final Nov. 1976 - Oct. 1979	
				14. SPONSORING AGENCY CODE EPA/600/14	
15. SUPPLEMENTARY NOTES Project Officer - Dr. Richard A. Dobbs (513/684-7649)					
16. ABSTRACT <p>This research project was conceived as a preliminary evaluation of the technical feasibility of converting solid wastes into adsorbents suitable for wastewater treatment. The work emphasized the pyrolysis of solid wastes rich in organic constituents, mainly agricultural wastes. The char prepared from one of these materials (prune pits) was subsequently activated for comparison with activated carbons that are widely used in water and wastewater treatment.</p> <p>The chars so prepared showed specific surface areas of 300 to 650 m²/g, measured by CO₂-BET adsorption (195K), but the pores were so small that the solids were penetrated only slowly by N₂. Pyrolysis at 700° to 900°C resulted in a greater char specific surface than did pyrolysis at 500°C. The activated carbons made from prune pits demonstrated favorable adsorption performance, when compared with an activated carbon widely used in water and wastewater treatment. The prune pit char activated at 60 min. demonstrated a higher adsorption capacity and superior adsorption kinetics compared to the commercial product (Filtrisorb 400), when judged according to the uptake of dissolved organic carbon (DOC) from secondary effluent. This difference coincided with a greater surface area and macro- and transitional (3 to 300 nm) pore volume for the activated carbon made from prune pits. An adsorbent made by activation of prune pit char for 42 min. was approximately equivalent to Filtrisorb 400 in every respect.</p>					
17. KEY WORDS AND DOCUMENT ANALYSIS					
a. DESCRIPTORS		b. IDENTIFIERS/OPEN ENDED TERMS		c. COSATI Field/Group	
Sewage treatment; Chemical Removal; Activated Carbon Treatment		Physical Chemical Treatment		13B	
18. DISTRIBUTION STATEMENT Release to Public		19. SECURITY CLASS (This Report) Unclassified		21. NO. OF PAGES 139	
		20. SECURITY CLASS (This page) Unclassified		22. PRICE	

